INVESTIGATING THE ROLE OF HIP1/PDGFβR IN LEUKEMOGENESIS AND IMATINIB SENSITIVITY

by

Steven Thomas Philips

A dissertation submitted in partial fulfillment
of the requirements for the degree of
Doctor of Philosophy
(Cellular and Molecular Biology)
in The University of Michigan
2010

Doctoral Committee:

Associate Professor Theodora S. Ross, Chair
Associate Professor Kathleen Collins
Professor Andrzej Dlugosz
Associate Professor Nicholas Donato
Professor Gary Hammer
Professor Benjamin Margolis

ACKNOWLEDGEMENTS

I would like to thank my mentor, Theodora Ross, for her guidance and enthusiasm over the past four years. Dr. Ross' passion for science and medicine has been an inspiration to me. I would also like to thank the members of my thesis committee, Andrzej Dlugosz, Kathy Collins, Nick Donato, Ben Margolis and Gary Hammer for their scientific and technical advice during this work. Scientific contributions to this thesis have come from many members of the Ross laboratory and other collaborators. In particular, I would like to acknowledge the work done by Chiron Graves, Katherine Oravecz-Wilson, Sarah Bradley, Alice Gauvin, Heather Ames, Lina Li, Brendan Crawford and Grace Liu. Ömer Yilmaz, Sean Morrison and Ivan Maillard provided knowledge and reagents for hematopoietic analysis. Thank you to the Day, Macoska and Zhang labs for use of equipment and reagents.

As the submission of this dissertation, chapters 2 and 3 have been published in modified form:

> Graves, C. W.*, S. T. Philips*, et al. (2008). "Use of a cryptic splice site for the expression of huntingtin interacting protein 1 in select normal and neoplastic tissues." Cancer Res **68**(4): 1064-73. *These authors contributed equally
>
> Oravecz-Wilson, K. I.*, S. T. Philips*, O. H. Yilmaz*, et al. (2009). "Persistence of leukemia-initiating cells in a conditional knockin model of an imatinib-responsive myeloproliferative disorder." Cancer Cell **16**(2): 137-48. *These authors contributed equally

Chapter 4 is in preparation for submission:

Philips, S. T., Oravecz-Wilson, K. I., , Ross, T. S. (2010) “Leukemia Initiating Cells Revert to Hematopoeitic Stem Cell Functionality in the Presence of Imatinib.” (manuscript in preparation)

This work was supported by the National Cancer Institute grants CBTG CA009676 (S.T.P.), R01 CA82363-03 (T.S.R.), and R01 CA098730-01 (T.S.R.), a Burroughs Wellcome Fund Clinical Scientist Award in Translational Research (T.S.R.), and the Howard Hughes Medical Institute (S.J.M.). T.S.R. is a Leukemia and Lymphoma Society Scholar. I have received academic and financial support from the Cancer Biology Training Grant, the Medical Scientist Training Program (MSTP), the Graduate Program in Cellular and Molecular Biology (CMB) and Rackham Graduate School. In particular, I would like to thank Ronald Koenig, Penny Morris, Ellen Elkin, Hilkka Ketola and Laurie Koivupalo at the MSTP, and Jessica Schwartz, Claire Kolman and Cathy Mitchell at CMB for all of their help.

Finally, I would like to thank my family and friends for their emotional and intellectual support over the years. I am especially indebted to my parents, Tom and Wilsy, and my brother, Justin. I would also like to thank all of my medical and graduate school friends who have reminded me of life outside the lab. Most of all, I would like to thank my fiancé, Jillian, for her patience and encouragement.

TABLE OF CONTENTS

LIST OF FIGURES

LIST OF TABLES

ABSTRACT

The Huntingtin interacting protein 1 (HIP1)-platelet-derived growth factor beta receptor (PDGFβR) fusion oncogene (H/P), resulting from a somatic t(5;7) translocation, causes expression of a constitutively active tyrosine kinase and is associated with myelomonocytic leukemia. To gain an understanding of the mechanism of leukemogenesis, we generated a mouse model with a conditional H/P knockin allele. We found that activation of this allele *in vivo* in hematopoietic cells of adult mice was not sufficient to induce leukemia. However, co-induction with a conditional human t(8;21) AML1-ETO (A/E) knockin allele resulted in a fully penetrant, rapid onset aggressive myeloproliferative disease. The leukemic cells were completely recombined and were uniformly Gr-1 positive. This leukemia was associated with a decreased frequency of hematopoietic stem cells (HSC) in the bone marrow and was sensitive to tyrosine kinase inhibition by imatinib. Imatinib treatment normalized white blood cell counts and restored bone marrow stem cell frequency but unexpectedly increased the ability of the leukemia to be transferred to syngeneic recipients. We show that a leukemia-initiating cell (LIC) persists *in vivo* during imatinib therapy, shares phenotypic characteristics with HSCs, and does not depend on H/P signaling for survival. Mobilization of the LIC was unable to enhance sensitivity to imatinib. This first example of a conditional knockin mouse model of a leukemogenic tyrosine kinase has facilitated the identification of an A/E cooperating mutation and has shed surprising light on the differential response of

different leukemia cells to imatinib targeted therapy. The persistence of an LIC corroborates clinical data and provides a model system for testing of novel therapies. The disparity between different cancer cells in the same tumor is an issue that needs to be resolved and from such models as that described here the resolution of this issue is now more tractable.

CHAPTER 1

INTRODUCTION

Summary

Constitutively activated receptor tyrosine kinases have been discovered in many forms of cancer, most predominantly hematopoietic neoplasms. One such mutation is the t(5;7) reciprocal translocation discovered in patients with chronic myelomonocytic leukemia (CMML)[1]. This translocation fuses the majority of the *Hip1* gene to the transmembrane and tyrosine kinase coding-domains of the *Pdgfβr* gene. This chapter summarizes the information known about the HIP1 family and its role in cancer, the transforming properties of the HIP1/PDGFβR fusion protein, mouse modeling of chronic myeloid leukemia, and therapeutic challenges in CML.

HIP1

Huntingtin interacting protein 1 (HIP1), the mammalian homologue of yeast Sla2p, was discovered by yeast two-hybrid screen as an interacting partner with huntingtin (htt), the protein that is mutated in Huntington's disease (HD)[2]. The interaction between HIP1 and htt was found to be inversely correlated with the polyglutamine length in htt and this decreased interaction is hypothesized to play a

role in HD pathogenesis. *Hip1* encodes a 116-kDa cytoplasmic protein that is expressed in select mouse tissues, specifically brain and lung[3]. HIP1 contains phosphoinositide, AP2, clathrin and actin binding domains and has been implicated as a co-factor in clathrin-mediated endocytosis of membrane bound receptors (**Figure 1.1A**)[4-8]. Previous work in our laboratory has demonstrated that HIP1 binds to and stabilizes epidermal growth factor receptor (EGFR), increasing downstream signaling[9]. Moreover, overexpression of HIP1 transforms 3T3 mouse fibroblasts to grow in an anchorage-independent fashion and form tumors in nude mice[9]. HIP1 has also been found to associate with c-Kit, PDGFβR, FGFR4, AMPARs, and NMDARs but the precise role of HIP1 in clathrin-mediated endocytosis remains unclear (unpublished data)[4,10,11]. We have shown that HIP1 is expressed at high levels in many human cancers including those derived from the prostate, lung, ovary, colon, breast, brain and lymphoid tissue[12-14]. Moreover, HIP1 expression was found to be a negative prognostic factor in prostate cancer[12]. HIP1 has also been shown to be necessary for prostate and breast tumorigenesis in mouse model systems[15,16]. Adult *Hip1* null mice display a complex degenerative phenotype characterized by kypholordosis, shortened lifespan, testicular degeneration, micro-opthalmia and cataracts[3,17]. The phenotype of this mouse clearly demonstrates that *Hip1* has an important role in normal cellular homeostasis. Chapter 2 of this thesis describes the discovery and characterization of a cryptic splicing event that occurs in a targeted *Hip1* mutant mouse that partially restores HIP1 protein functions as well as breast and prostate tumorigenesis in models of these cancers that are inhibited by HIP1 deficiency.

HIP1/PDGFβR

Prior to the discovery that HIP1 expression is altered in solid tumors, *Hip1* was cloned as the chromosome 7 locus in a t(5;7)(q33;q11.2) translocation with the platelet-derived growth factor β receptor (PDGFβR) gene in a patient with CMML[1]. This in-frame chromosomal translocation fuses amino acids 1-950 of HIP1 with the transmembrane and tyrosine kinase domains of the type III receptor tyrosine kinase PDGFβR (**Figure 1.1B**). Only 18 C-terminal amino acids of HIP1 are excluded from the fusion protein. Seventeen other translocations involving the *Pdgfβr* gene have been identified in CMML and most patients demonstrate the common clinical features of leukocytosis, eosinophilia, variable dysplastic monocytosis and splenomegaly[18]. The other fusion partners of *Pdgfβr,* including TEL(ETV6), H4/D10S170, Rabaptin-5 and CEV14, are unrelated in function but share in common motifs which are thought to facilitate ligand-independent oligomerization of the fusion proteins[19]. HIP1 contains a leucine zipper motif, a domain that has been shown to mediate homodimerization[20]. The reciprocal PDGFβR/HIP1 fusion protein or transcript was not identified in the original patient and the other reciprocal translocations are not thought to play a role in leukemic transformation[1].

The fusion protein HIP1/PDGFβR (H/P) is cytoplasmic, constitutively phosphorylated and causes IL3-independent growth of the pro-B cell line Ba/F3[21]. These transformed cells have constitutively activated STAT5 and tyrosine phosphorylation of an as yet unidentified protein, p130. Interestingly, the leucine zipper domain was not found to be necessary for H/P oligomerization but rather, the terminal 55 amino acids of the HIP1 portion (corresponding to the actin-binding

TALIN homology domain) were necessary for oligomerization. In contrast to findings with other X/P fusions, additional HIP1 sequences were found to be necessary for transformation of Ba/F3 cells. Specifically, deletion of amino acids 690-752 of HIP1 led to abrogation of transforming ability in Ba/F3 cells and this was associated with the loss of association with and tyrosine phosphorylation of p130. There are no known functional motifs with sequence homology in this region. It is unclear whether these residues are necessary for transformation of hematopoietic cells *in vivo*. Other PDGFβR fusions such as TEL/PDGFβR (T/P) have been shown to rely on STAT5 activation for transforming properties *in vitro* and *in vivo* [22,23]. While there is clearly a role for the 5' fusion partner in X/P translocations, most of the available data suggests that these oncogenic fusion proteins induce CMML via hyperactivity of the PDGFβR downstream signaling pathways [21,23]. The principal pathways that have been shown to play a role in X/P mediated transformation are Ras/MAPK, PI3K, PLCγ and STAT5a/b.

Modeling CML in mice

Modeling hematopoietic neoplasms in mice, specifically the chronic myeloid forms, has been challenging for various reasons. One of the first approaches that gained popularity was transplantation of bone marrow cells that have been retrovirally transduced with the oncogene of interest [24,25]. This approach utilizes the MSCV LTR promoter to express high levels of oncogene in immature hematopoietic progenitors. Hematopoietic cells are isolated from donor mice that have been pre-

treated with the chemotherapeutic agent 5-flurouracil (5FU) and then cultured in cytokine-enriched media short term. Some of the known X/PDGFβR (X/P) fusions (Tel/P, Rabaptin-5/P) have been tested by this bone marrow transduction/transplantation assay (BTT) and these have all resulted in fatal myeloproliferative disease (MPD) closely resembling human CML and/or CMML[26,27]. Chapter 3 describes our use of the H/P oncogene in the BTT assay and the induction of a similar MPD.

Despite the success of the BTT method in validating the leukemogenic potential of fusion tyrosine kinases, the system has multiple flaws that prevent its usefulness for evaluating the complexities of disease progression or measuring responsiveness to therapies. First, the MSCV LTR promoter does not restrict oncogene expression levels and supraphysiologic levels of the oncoproteins are almost always detected in recipient mice. In fact, transplant mice often develop a fatal myeloproliferative disease so rapidly after transplant that blastic transformation or investigation of therapeutic benefits cannot be observed before the mice die. Second, due to the random nature of retroviral integration, additional mutations are introduced into the genome. Third, short-term culture of hematopoietic cells during retroviral transduction may select for the most "leukemic" clones prior to transplant. Fourth, while the 5FU pretreatment does enrich for hematopoietic stem cells, the exact identity of the infected cell/cells is often unclear. While the 5' fusion partners' are not believed to play a critical role in the functionality of fusion RTKs, their regulatory elements would presumably affect expression of the novel gene (i.e. *Tel* regulatory

elements would control the T/P expression profile, *Hip1* regulatory elements would control the H/P expression profile).

To improve on these drawbacks, recent reports have used a gene "knockin" strategy to express fusion oncogenes under the spatial and temporal control of endogenous mouse promoters[28]. Loxp-flanked transcriptional stop cassettes are introduced upstream of the knocked-in oncogene, and Cre transgenic mice can then be used to limit expression to specific subsets of cells. The mouse hematopoietic system follows a hierarchical model driven by a rare, pluripotent stem cell (**Figure 1.2**, HSC) which gives rise to all blood cell types[29]. Many cell types in the hematopoietic system, including the HSC, can be prospectively isolated based on the expression of unique surface marker combinations. These "phenotypically" identified cells can be "functionally" validated by transplant and cell culture assays. The conditional knockin system is a powerful approach that combines the comprehensive knowledge of mouse hematopoiesis with gene targeting. Chapter 3 describes the generation and analysis of a conditional knockin of H/P into the mouse *Hip1* locus. Importantly, we and others have found striking differences between the phenotypes generated by the BTT system and conditional knockin mice.

Tyrosine kinase inhibitor therapy in CML

Most cases of chronic myeloid leukemia (CML) are the result of a somatic t(9;22) translocation that produces the fusion oncogene BCR/ABL. Similar to the X/P fusions in CMML, BCR/ABL has constitutive kinase activity and causes hyper-production of mature myeloid cells that manifests clinically as splenomegaly and

leukocytosis. The advent of the molecularly targeted small molecule imatinib mesylate (IM) has revolutionized CML treatment[30]. Imatinib mesylate is a 2-phenylaminopyrimidine derivative that competitively binds to the ATP-binding site of ABL, c-KIT, PDGFαR, and PDGFβR thus inhibiting kinase signaling. The use of IM as first-line therapy for new diagnosis CML with the t(9;22) translocation has improved the 5-year survival rate to 89%[31]. Nevertheless, with the passage of time, problems such as kinase domain drug resistance mutations and BCR/ABL transcript persistence have prevented the proclamation of "cure". *In vitro* evidence suggests that the primitive "CML stem cell" is refractory to tyrosine kinase inhibitor (TKI) therapy[32] and patients who stop therapy invariably relapse[33,34]. Eradication of CML necessarily requires eradication of the "CML stem cell" and concerted efforts are being taken to identify and characterize this malignant population.

The goal of this thesis was to investigate the mechanisms by which H/P induces chronic myelomonocytic leukemia with a focus on therapeutic strategies targeting H/P signaling. In Chapter 2, we describe our characterization of an unexpected splicing phenomenon that circumvented a gene targeting event to conditionally knockout *Hip1*. This information led to a better understanding of the complex *Hip1* genetic locus that was used for the work that followed. In Chapter 3, we describe a novel mouse model of MPD induced by expression of the human tyrosine kinase oncogene H/P and the human transcription factor oncogene AML1/ETO (A/E) from their endogenous loci. We further demonstrate persistence of a leukemia-initiating cell (LIC) despite hematologic response to tyrosine kinase

inhibition. In Chapter 4, we further characterize the H/P;A/E-driven MPD and investigate the potential mechanisms of LIC persistence.

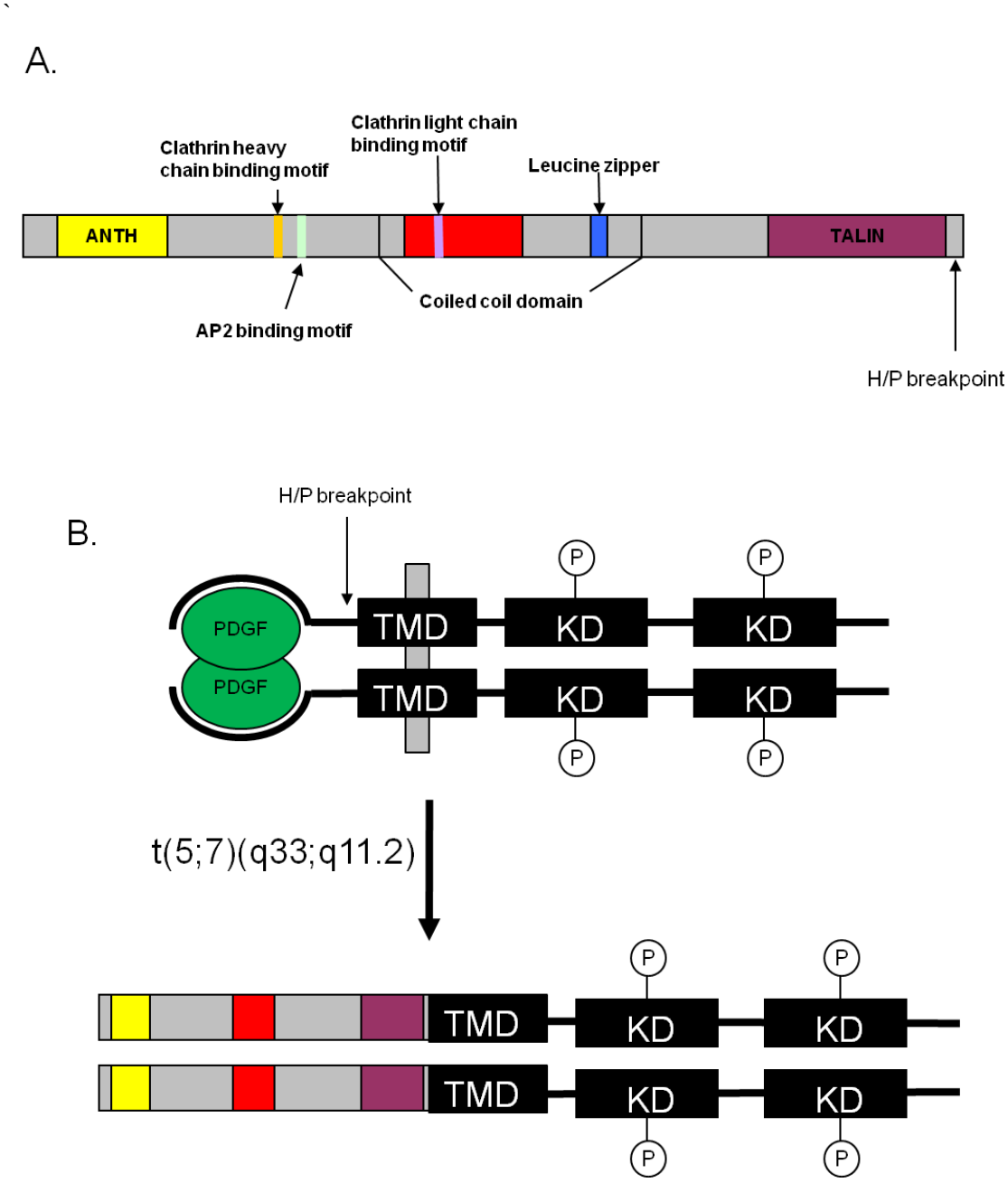

Figure 1.1: Huntingtin Interacting Protein 1 (HIP1) and the HIP1/PDGFβR fusion protein

A. Structure of mammalian HIP1 depicting the binding domains for lipids (ANTH), AP2, clathrin and actin (TALIN). Also depicted are the coiled coil and leucine zipper domains and the breakpoint in the t(5;7) translocation.

B. Top, Platelet-derived growth factor β receptor (PDGFβR) structure depicting extracellular PDGF binding domain, transmembrane domain (TMD) and split kinase domain (KD). PDGF binding induces dimerization and kinase activity. *Bottom,* HIP1/PDGFβR fusion protein dimerizes independently of ligand stimulation, leading to constitutive kinase activity.

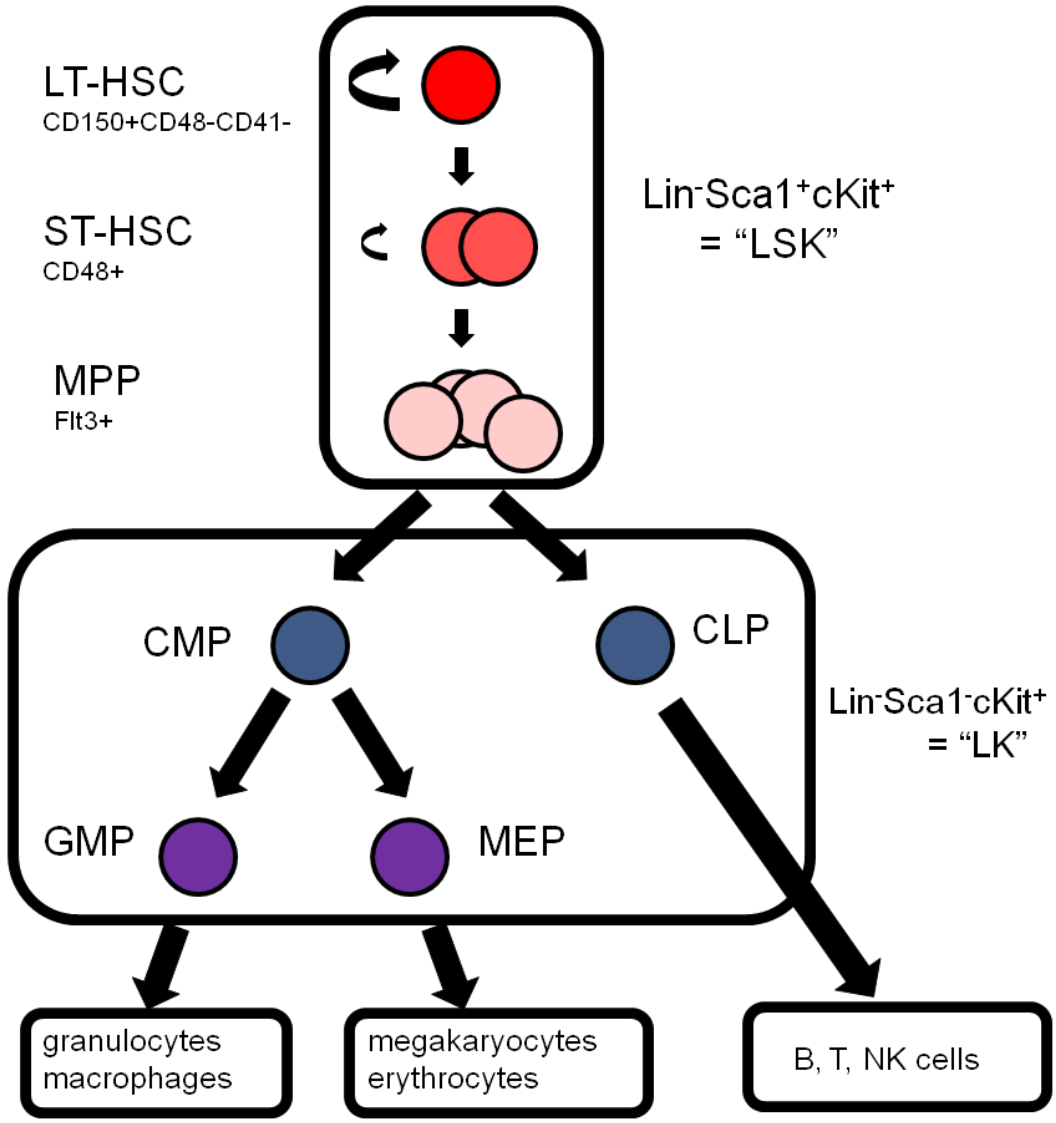

Figure 1.2: Simplified schematic model of normal hematopoietic development.
Rare, pluripotent, self-renewing hematopoietic stem cells (red) differentiate into committed myeloid and lymphoid progenitors (blue) which differentiate into all mature blood cell types. Abbreviations: LT-HSC - Long-term HSC, ST-HSC - Short-term HSC, MPP – multipotent progenitor, CMP – committed myeloid progenitor, CLP – committed lymphoid progenitor. GMP – granulocyte/macrophage progenitor, MEP – megakaryocyte/erythrocyte progenitor. See text and methods for surface marker combinations

References

1. Ross, T. S., Bernard, O. A., Berger, R. & Gilliland, D. G. Fusion of Huntingtin interacting protein 1 to platelet-derived growth factor beta receptor (PDGFbetaR) in chronic myelomonocytic leukemia with t(5;7)(q33;q11.2). *Blood* **91**, 4419-26 (1998).
2. Kalchman, M. A. et al. HIP1, a human homologue of S. cerevisiae Sla2p, interacts with membrane-associated huntingtin in the brain. *Nat Genet* **16**, 44-53 (1997).
3. Oravecz-Wilson, K. I. et al. Huntingtin Interacting Protein 1 mutations lead to abnormal hematopoiesis, spinal defects and cataracts. *Hum Mol Genet* **13**, 851-67 (2004).
4. Hyun, T. S. et al. HIP1 and HIP1r stabilize receptor tyrosine kinases and bind 3-phosphoinositides via epsin N-terminal homology domains. *J Biol Chem* **279**, 14294-306 (2004).
5. Engqvist-Goldstein, A. E. et al. The actin-binding protein Hip1R associates with clathrin during early stages of endocytosis and promotes clathrin assembly in vitro. *J Cell Biol* **154**, 1209-23 (2001).
6. Metzler, M. et al. HIP1 functions in clathrin-mediated endocytosis through binding to clathrin and adaptor protein 2. *J Biol Chem* **276**, 39271-6 (2001).
7. Mishra, S. K. et al. Clathrin- and AP-2-binding sites in HIP1 uncover a general assembly role for endocytic accessory proteins. *J Biol Chem* **276**, 46230-6 (2001).
8. Waelter, S. et al. The huntingtin interacting protein HIP1 is a clathrin and alpha-adaptin-binding protein involved in receptor-mediated endocytosis. *Hum Mol Genet* **10**, 1807-17 (2001).
9. Rao, D. S. et al. Altered receptor trafficking in Huntingtin Interacting Protein 1-transformed cells. *Cancer Cell* **3**, 471-82 (2003).
10. Wang, J., Yu, W., Cai, Y., Ren, C. & Ittmann, M. M. Altered fibroblast growth factor receptor 4 stability promotes prostate cancer progression. *Neoplasia* **10**, 847-56 (2008).
11. Metzler, M. et al. Disruption of the endocytic protein HIP1 results in neurological deficits and decreased AMPA receptor trafficking. *EMBO J* **22**, 3254-66 (2003).
12. Rao, D. S. et al. Huntingtin-interacting protein 1 is overexpressed in prostate and colon cancer and is critical for cellular survival. *J Clin Invest* **110**, 351-60 (2002).
13. Bradley, S. V. et al. Huntingtin interacting protein 1 is a novel brain tumor marker that associates with epidermal growth factor receptor. *Cancer Res* **67**, 3609-15 (2007).
14. Bradley, S. V. et al. Aberrant Huntingtin interacting protein 1 in lymphoid malignancies. *Cancer Res* **67**, 8923-31 (2007).
15. Bradley, S. V. et al. Serum antibodies to huntingtin interacting protein-1: a new blood test for prostate cancer. *Cancer Res* **65**, 4126-33 (2005).
16. Graves, C. W. et al. Use of a cryptic splice site for the expression of huntingtin interacting protein 1 in select normal and neoplastic tissues. *Cancer Res* **68**, 1064-73 (2008).
17. Rao, D. S. et al. Huntingtin interacting protein 1 Is a clathrin coat binding protein required for differentiation of late spermatogenic progenitors. *Mol Cell Biol* **21**, 7796-806 (2001).
18. Matsumura, I., Mizuki, M. & Kanakura, Y. Roles for deregulated receptor tyrosine kinases and their downstream signaling molecules in hematologic malignancies. *Cancer Sci* **99**, 479-85 (2008).
19. Cross, N. C. & Reiter, A. Fibroblast growth factor receptor and platelet-derived growth factor receptor abnormalities in eosinophilic myeloproliferative disorders. *Acta Haematol* **119**, 199-206 (2008).
20. Landschulz, W. H., Johnson, P. F. & McKnight, S. L. The leucine zipper: a hypothetical structure common to a new class of DNA binding proteins. *Science* **240**, 1759-64 (1988).
21. Ross, T. S. & Gilliland, D. G. Transforming properties of the Huntingtin interacting protein 1/ platelet-derived growth factor beta receptor fusion protein. *J Biol Chem* **274**, 22328-36 (1999).
22. Cain, J. A. et al. Myeloproliferative disease induced by TEL-PDGFRB displays dynamic range sensitivity to Stat5 gene dosage. *Blood* **109**, 3906-14 (2007).

23. Sternberg, D. W. et al. The TEL/PDGFbetaR fusion in chronic myelomonocytic leukemia signals through STAT5-dependent and STAT5-independent pathways. *Blood* **98**, 3390-7 (2001).
24. Wong, S. & Witte, O. N. Modeling Philadelphia chromosome positive leukemias. *Oncogene* **20**, 5644-59 (2001).
25. Van Etten, R. A. Models of chronic myeloid leukemia. *Curr Oncol Rep* **3**, 228-37 (2001).
26. Tomasson, M. H. et al. Fatal myeloproliferation, induced in mice by TEL/PDGFbetaR expression, depends on PDGFbetaR tyrosines 579/581. *J Clin Invest* **105**, 423-32 (2000).
27. Magnusson, M. K. et al. Rabaptin-5 is a novel fusion partner to platelet-derived growth factor beta receptor in chronic myelomonocytic leukemia. *Blood* **98**, 2518-25 (2001).
28. Mikkola, H. K. & Orkin, S. H. Gene targeting and transgenic strategies for the analysis of hematopoietic development in the mouse. *Methods Mol Med* **105**, 3-22 (2005).
29. Morrison, S. J. & Weissman, I. L. The long-term repopulating subset of hematopoietic stem cells is deterministic and isolatable by phenotype. *Immunity* **1**, 661-73 (1994).
30. O'Brien, S. G. et al. Imatinib compared with interferon and low-dose cytarabine for newly diagnosed chronic-phase chronic myeloid leukemia. *N Engl J Med* **348**, 994-1004 (2003).
31. Druker, B. J. et al. Five-year follow-up of patients receiving imatinib for chronic myeloid leukemia. *N Engl J Med* **355**, 2408-17 (2006).
32. Graham, S. M. et al. Primitive, quiescent, Philadelphia-positive stem cells from patients with chronic myeloid leukemia are insensitive to STI571 in vitro. *Blood* **99**, 319-25 (2002).
33. Cortes, J., O'Brien, S. & Kantarjian, H. Discontinuation of imatinib therapy after achieving a molecular response. *Blood* **104**, 2204-5 (2004).
34. Usuki, K., Iijima, K., Iki, S. & Urabe, A. CML cytogenetic relapse after cessation of imatinib therapy. *Leuk Res* **29**, 237-8 (2005).

CHAPTER 2

A Novel Use of a Cryptic Splice Site in the *Hip1* Gene Allows for the Expression of HIP1 in Select Normal and Neoplastic Tissues

Summary

Huntingtin Interacting Protein 1 (HIP1) is a 116 kDa endocytic protein that is necessary for the maintenance of several adult tissues *in vivo*. Its complete deficiency, due to homozygosity of a null *Hip1* allele, leads to degenerative adult phenotypes. HIP1 deficiency also inhibits prostate tumor progression in the prostate cancer prone TRAMP mouse model. To better understand how deficiency of HIP1 leads to such phenotypes, we carefully analyzed tumorigenic potential in mice homozygous for a *Hip1* mutant allele, designated $Hip1^{\Delta 3\text{-}5}$, which is predicted to result in a frame-shifted, nonsense mutation in the N-terminal region of the coding sequence. In contrast to our previous studies using the *Hip1* "null" allele, an inhibition of prostate tumorigenesis was not observed as a result of the homozygosity of the "nonsense" Δ3-5 allele. Also, it did not inhibit breast tumorigenesis in the MMTV-Myc breast cancer-prone background. To more closely examine the contrasting results from the two different *Hip1* mutant mice, we cultured tumor cells from homozygous Δ3-5 allele bearing TRAMP and MMTV-myc mice and discovered the presence of an approximately 110 kDa form of HIP1 in tumor cells. Upon genomic DNA and cDNA sequencing of *Hip1* from these tumors, we

determined that this 110 kDa form of HIP1 is the product of splicing of a cryptic U12-type AT-AC intron. This event results in the insertion of an AG dinucleotide between exons 2 and 6 and restoration of the original reading frame. Remarkably, this mutant protein retains its capacity to bind lipids, clathrin, AP2, and EGFR providing a possible explanation for why tumorigenesis was not altered following this "knockout" mutation. The expression and activities of this mutant form of HIP1 provide clues for future studies investigating the contribution of HIP1 to the homeostasis of specific normal and neoplastic tissues at different developmental stages.

Introduction

Huntingtin Interacting Protein 1 (HIP1) was first identified by its ability to interact with huntingtin, the protein encoded by the gene that is mutated in Huntington's disease[1,2]. HIP1 and its only known mammalian relative, HIP1-related (HIP1r), were subsequently shown to specifically interact with clathrin, AP2[3-10], and epidermal growth factor receptor (EGFR)[11]. Thus, the HIP1 family is widely thought to be involved in the regulation of growth factor receptor endocytosis and signaling. Additionally, HIP1 and HIP1r contain AP180 N-terminal homology (ANTH) inositol lipid-binding domains, which are specific to endocytic proteins[12,13]. Finally, deficiency of HIP1 leads to spinal defects, testicular degeneration, cataracts, adult weight loss, and early death[14-16]. These *in vivo* phenotypes indicate that HIP1 is necessary for fundamental cellular and organismal homeostasis. Despite their clear necessity in the maintenance of adult cells and tissues, the precise cellular and biochemical function(s) of this protein family are yet to be determined. In fact, several attempts at understanding the effects of HIP1/HIP1r

deficiency on receptor endocytosis either in cultured cells or *in vivo* have not been successful[14,16,17].

In addition to its function in normal tissue maintenance, HIP1 has been widely implicated in tumorigenesis. HIP1 was discovered to be an amino-terminal partner of PDGFβR, in the leukemogenic fusion resulting from a t(5;7) chromosomal translocation[18]. HIP1 protein also has been found to be up regulated in multiple human tumor types including prostate, colon[19], breast[20], brain[11], and lymphoid[21] cancers. Additionally, HIP1 over-expression is prognostic in prostate cancer[19]. Furthermore, heterologous human HIP1 over-expression can transform mouse fibroblasts[20], an effect that we propose to be due to altered growth factor receptor endocytosis and subsequent signal transduction cascades.

To examine the role of HIP1 in prostate cancer, we have previously used mutant mice that are deficient in HIP1 due to a spontaneous targeting event (*Hip1*^{null}). When these HIP1-deficient mice were crossed with the transgenic adenocarcinoma of mouse prostate (TRAMP) mice[22], the HIP1-deficient progeny mice contained fewer and less aggressive prostate tumors than their littermate TRAMP control mice[23]. We have expanded these studies by using a different tumor model system (MMTV-MYC model of breast cancer) and a "third generation" *Hip1* knockout mouse allele (the *Hip1*$^{\Delta 3\text{-}5}$) that does not provide the confounding issues associated with the above-described spontaneous "null" allele[16], such as possible altered expression of *HIP1*-neighboring genes caused by the neomycin cassette. In the present study, we report the surprising result that *Hip1*$^{\Delta 3\text{-}5/\Delta 3\text{-}5}$ are equally, if not more, prone to the development of prostate and breast tumors than *Hip1* wild type mice. Furthermore, we found that the tumor cells from the *Hip1*$^{\Delta 3\text{-}5/\Delta 3\text{-}5}$

genetic background express a truncated form of the Hip1 protein that is the result of a novel cryptic splicing event. These results have important implications not only for the role of HIP1 and its interacting proteins in normal and neoplastic cell biology but also for the development and analysis of mouse model systems with specific targeting events. Our data emphasize the value of how sequencing the transcript that is actually produced by an engineered knock-out allele can reveal novel types of molecular compensation at the level of splicing.

Materials and Methods

Mice.

Mx1cre (B6.Cg-Tg(Mx1-cre)1Cgn/J, The Jackson Laboratories), *Hip1*^{null}, *Hip1*^{loxp}, *Hip1*$^{\Delta 3\text{-}5}$ [16], TRAMP ([22], C57BL/6, The Jackson Laboratories) and MMTV-myc ([24], MammJ/FVB, Gift from Lewis Chodosh) allele-containing mice were maintained and bred under SPF conditions as per UCUCA guidelines at the University of Michigan. The TRAMP and MMTV-myc allele-containing mice were maintained on pure genetic backgrounds. Since the other alleles were maintained on a mixed C57BL/6;129svj background, all experiments were performed using the appropriate littermate controls.

Tumor analysis in MMTV-myc mice.

MMTV-myc transgenic mice were mated onto *Hip1*$^{null/null}$ and *Hip1*$^{\Delta 3\text{-}5/\Delta 3\text{-}5}$ backgrounds and were palpated for breast tumors weekly. Tumor size was measured with calipers. The mice were sacrificed at one year of age or if a tumor impeded movement or ulcerated.

Tumor cell culture.

Fresh tumor samples from MMTV-myc and TRAMP mice were cut into 1 mm sections, added to DMEM containing 2.2 mg/ml collagenase (Sigma), and incubated for 1 hour at 37^{o}C with agitation every 10 minutes. The digested samples were filtered through a 100 μm nylon cell strainer (Falcon) then centrifuged at 1,000 rpm for 10 minutes. The supernatant was removed, and the remaining cells were suspended in DMEM/10% FBS and plated onto 10 mm dishes. Cells were passaged every 3 days into fresh media.

Survival analysis in TRAMP mice.

The *Hip1*$^{null/null}$ and *Hip1*$^{\Delta 3\text{-}5/\Delta 3\text{-}5}$ mice were maintained on a mixed C57BL/6;129svJ background, and the TRAMP mice were maintained on a pure C57BL/6 background. Intercross matings of TRAMP and *Hip1*$^{null/null}$ and *Hip1*$^{\Delta 3\text{-}5/\Delta 3\text{-}5}$ mice were performed as previously described[23]. Fourteen TRAMP;*Hip1*$^{\Delta 3\text{-}5/\Delta 3\text{-}5}$, 13 TRAMP;*Hip1*$^{+/\Delta 3\text{-}5}$, 18 TRAMP;*Hip1*$^{+/null}$, and 15 TRAMP/*Hip1*$^{null/null}$ littermates were analyzed for tumors at 6.5 months. Prior to these necropsies, a group of mice from these cohorts either unexpectedly died or became moribund and required euthanasia. This survival data for each of these observation groups was compared.

Genomic DNA sequencing.

High-fidelity PCR amplification of the 3 kb genomic region between exons 2 and 6 of *Hip1* from a MMTV-myc;*Hip1*$^{\Delta 3\text{-}5/\Delta 3\text{-}5}$ tumor was performed. The resulting products were cloned, and single-run complete sequencing was performed on two independent clones.

Sequence analysis.

The alignment of sequences from wild type *Hip1* cDNA or MMTV-myc;*Hip1*$^{\Delta 3\text{-}5/\Delta 3\text{-}5}$ tumor genomic DNA was analyzed using a combination of Sequencer version 4.5 (GeneCodes) and the NCBI BLAST program.

RNA isolation.

Total RNA was isolated from cultured tumor cells, tissues, and early passage mouse embryonic fibroblast (MEF) extracts using the TRIzol reagent (Invitrogen).

Reverse-transcriptase PCR (RT-PCR).

RT-PCR was performed on total RNA using the SuperScriptTM One-Step RT-PCR system (Invitrogen) and primers specific to *Hip1* exon 1 (5'-ATGAAGCAGGTATCCAACCCGCTGCCC-3', forward primer) and the exon 14/15 junction (5'-ATTAGCCTGGGCCTTTCTTTCTATCTC-3', reverse primer) of murine *Hip1* cDNA. Resulting products were separated on 0.8% agarose gels. Products were extracted from the gel and amplified by nested PCR using primers specific to the exon 1/2 junction (5'-TTCGAGCGGACTCAGACGGTCAGCGTC-3'-forward primer) and the exon 13/14 junction (5'-ATGGCCCGCTGGCTCTCAATCTTCATG-3' reverse primer) of murine *Hip1* cDNA. Products were again run on 0.8% agarose gels, extracted, and directly sequenced using the PCR primers that were used for the amplification. PCR products that did not yield readable sequence were cloned using the TOPO TA Cloning Kit for Sequencing (Invitrogen). Multiple clones were selected, and plasmid DNA was isolated and sequenced.

Northern blot analysis of mouse embryonic fibroblast (MEF) mRNA.

Poly (A) RNA was isolated from total RNA using the Poly(A) Purist MAG protocol (Ambion). Then, 5μg of this poly(A) RNA was separated on a 1% agarose gel with 6%

formaldehyde, stained with ethidium bromide, transferred to Nytran membrane (Schleicher & Schuell), and cross-linked. The membrane was prehybridized in a buffer containing 5X SSC, 5X Denhardt solution, 1% sodium dodecyl sulfate (SDS) (wt/vol), and 100 μg of denatured salmon sperm DNA/ml for 3 h at 65°C. For the mouse *Hip1* Northern probe, an 850-bp *Eco*R1 and *Not*1 digested fragment encoded by m*Hip1* exons 10-14 was used. The probe was ^{32}P labeled using a random-primed labeling kit according to manufacturer's directions (Roche). The blot was hybridized overnight at 65°C, washed twice in 2X SSC for 20 min, once in 1X SSC for 10 min, and twice in 0.1X SSC for 10 min. The blot was exposed for 4 to 5 days on Kodak Biomax film. The mRNA abundance was normalized with the signal for glyceraldehydes-3-phosphate dehydrogenase (GAPDH).

Tissue preparation and western blot analysis.

Tissue harvesting, preparation, and immunoblotting of tissues was performed as previously described[17]. A polyclonal anti-HIP1 (1:5,000, UM354) antibody was used to detect HIP1 expression in MMTV-myc, TRAMP and Mx1-Cre mice, and polyclonal anti-actin (1:1000, Sigma) antibody was used as a control.

polyIpolyC (pIpC)-treatment of Mx1-cre mice.

Mice were injected intraperitoneally with 250 ug/mouse of polyinosinic-polycytidylic acid (pIpC, Sigma, St. Louis, MO) every other day for 7 or 14 days as previously described[25,26].

Bone marrow culture.

Mouse bone marrow cell monocytic culture was carried out as previously described (Bradley, 2007), except that RPMI-1640 media and M-CSF (1 ng/ml, Sigma, St. Louis,

MO) was used and femur bone marrow was plated onto 100 mm dishes. One week later, cells were directly lysed in the dishes and collected for protein analysis.

Co-immunoprecipitation of HIP1 and EGFR and endocytic factors.

Full-length and mutant EGFR and HIP1 cDNA constructs in pcDNA3 have previously been described[11]. A 15-cm dish of 70% confluent 293T cells was transfected with 20 μg of HIP1 cDNA and 20 μg of EGFR cDNA using Superfect reagent (Qiagen). Twenty-four hours post-transfection, the cells were lysed using an all-purpose lysis buffer [50 mmol/L Tris (pH7.4), 150 mmol/L NaCl, 1% Triton X-100, 1.5 mmol/L MgCl2, 5 mmol/LEGTA, 10% glycerol, Complete EDTA-free protease inhibitor tablets (Roche), 30 mmol/L sodium pyrophosphate, 50 mmol/L sodium fluoride, and 100μmol/L sodium orthovanadate]. Five milligrams of protein were incubated with pre-immune serum, polyclonal anti-HIP1 serum (UM323), or sheep polyclonal anti-EGFR (Upstate). One hundred microliters of a 3:1 slurry of protein G-sepharose beads (GE Healthcare) in lysis buffer were then incubated with the lysate-antibody mixture at 4ºC for 60 min with rotation. The protein G pellets were washed four times with 1 mL of lysis buffer. The entire pellet was dissolved in SDS sample buffer, boiled for 5 min, separated on 7% SDS-PAGE, and transferred to nitrocellulose membranes. Antibodies used for western blot analysis were the anti-HIP1/4B10 antibody (mouse monoclonal, human anti-HIP1 immunoglobulin G1, 400 ng/mL), anti-adaptin-α antibody (rabbit polyclonal, BD Biosciences), anti-clathrin heavy chain TD-1 antibody (kind gift of Linton Traub, University of Pittsburgh), and an anti-EGFR antibody (sheep polyclonal antibody, Upstate Biotechnology, Charlottesville, VA).

Generation of HIP1 expression constructs.

Generation of the pcDNA3/FL HIP1 expression construct was reported previously[19]. PCR mutagenesis using pcDNA3-FL HIP1 as a template was used to generate the insert for the pcDNA3/hHIP1Δ3-5/insAG expression construct. Two initial PCR products were generated using two separate pairs of primers. The first primer pair consisted of a forward primer specific to exon 1 (5'-AGGGAGACCCAAGCTTGGTA-3'including a *Kpn*I restriction site) and an engineered reverse primer (5'-GGGATTCTTTCTGGCGTGTTTTTCCTT-3') consisting of sequence from exon 2, an AG dinucleotide, and sequence from the 5' portion of exon 6. The second primer pair consisted of an engineered forward primer (5'-AACACGCCAGAAAGAATCCCAGGTTCC-3') consisting of sequence from the 3' portion of exon 2, an AG dinucleotide, and sequence from exon 6 and a reverse primer specific to exon 14 (5'-TTCTATCTCAGACAGGCTCC-3'; just 3' of the *Eco*RI restriction site at position 1290 of the coding sequence). The resulting PCR products were used as templates in a second PCR reaction to generate the hHIP1Δ3-5/insAG insert. The hHIP1Δ3-5/insAG insert was cloned into pcDNA3-FL HIP1 using the *Kpn*I and *Eco*RI restriction sites.

Generation and purification of GST-fusion proteins.

The 5' portions of pcDNA3/FL HIP1 and pcDNA3/hHIP1Δ3-5/insAG were cloned into pGEX4T.1 to generate GST-HIP1wt (amino acids 1-430) and GST-HIP1Δ3-5 (amino acids 1-337) expression constructs, respectively. The HIP1wt and HIP1Δ3-5 inserts cloned into the pGEX4T.1 vector were generated by PCR amplification using the forward primer, 5'-CCGGAATTCATGGATCGGATGGCCAGC-3', and the reverse primer, 5'-CCGCTCGAGACAGTCGTCGGCCGCCTGC-3' and pcDNA3/FL HIP1 and

pcDNA3/hHIP1Δ3-5/insAG as templates. Constructs were verified by sequencing. The GST-HIP1wt and GST-HIP1Δ3-5 fusion proteins were expressed in *E. coli* strain BL21 following induction with 0.1mM isopropyl-β-D-1-thiogalactopyranoside (IPTG) for 2 h at 37^{o}C. Bacteria were pelleted and resuspended in PBS containing protease inhibitors (Roche Diagnostics). Resuspended cells were lysed by sonication, and Triton X-100 was added to a final concentration of 2%. The mixture was centrifuged at 12,000 x g for 10 min. Following centrifugation, the supernatant was added to glutathione sepharose 4 beads (50% slurry) and incubated at room temperature for 30 min. The beads were washed 3 times with PBS and elution buffer (50mM Tris-HCL, 10mM reduced glutathione [pH 8.0]) to elute the fusion proteins. Eluted proteins were dialyzed in PBS at 4^{o}C for 2 h and again overnight. Dialyzed proteins were concentrated using Aquacide (Calbiochem), and protein concentrations were determined by SDS-PAGE and Coomassie blue staining. Proteins were further analyzed by western blot analysis using an anti-GST antibody (Cell Signaling Technologies) and an anti-HIP1 antibody (UM354).

Lipid-binding assay.

Lipid-binding assays using PIP strips and PIP arrays (Echelon) were performed according to manufacturer's protocol. Briefly, either PIP strips or PIP arrays were incubated overnight at 4^{o}C with 12.5 µg of purified protein in TBST with 1% milk. Binding was detected using anti-GST antibody (1:5000) or UM354 (1:2000) in TBST with 1% milk. Anti-rabbit secondary antibodies conjugated to horse radish peroxidase (HRP) were used at 1:5000 (for anti-GST) or 1:2000 (for UM354) in TBST with 1% milk.

Results

Germ line deletion of Hip1 exons 3 thru 5 leads to a phenotype similar to that of Hip1^{null} mice.

The *Hip1* gene has a complex structure consisting of 32 exons spread over 220 kilobases. To examine the role *Hip1* plays in development and disease, we have generated a series of *Hip1*[16] and *Hip1r*[17] mutant alleles. The original *Hip1^{null}* allele was serendipitously generated in an attempt to knock the human HIP1/PDGFβR fusion cDNA into the mouse *Hip1* genomic locus[16]. Using this null allele, we previously reported that HIP1 deficiency leads to a complex degenerative mouse phenotype[16] and impaired tumor progression in transgenic adenocarcinoma of the mouse prostate (TRAMP) mice[23]. Because of the complex structure of this original allele and the resultant multi-tissue phenotype, we generated a conditional *Hip1* mutant allele (*Hip1^{loxp}*). To do this, we generated a targeting vector to introduce loxP sites flanking *Hip1* exons three through five, which encode a significant portion (80%) of the ANTH domain. As predicted, cre-mediated recombination of these loxP sites resulted in the deletion of exons 3-5 as well as the neomycin selection cassette[16]. The resulting allele (*Hip1$^{\Delta 3\text{-}5}$*) contains not only a deletion of most of the ANTH domain sequences but also a frame-shifted, nonsense mutation that fuses exon 2 to exon 6. Protein expressed from this mutant allele is predicted to be a truncated amino terminal 10 kDa protein lacking the ANTH, clathrin-binding, AP2-binding, coiled-coil, and Talin homology domains (domains that span the remaining 90% of the coding sequence; **Figure 2.1**).

Previously, mice homozygous for the Δ3-5 allele were found to exhibit degenerative phenotypes similar to the *Hip1$^{null/null}$* mice (*e.g.*, kypholordosis and testicular

degeneration/infertility). However, there were two differences in the phenotypes associated with these mice. First, the *Hip1*$^{\Delta 3\text{-}5/\Delta 3\text{-}5}$ mice did not have cataracts. Second, the *Hip1*$^{\Delta 3\text{-}5/\Delta 3\text{-}5}$ mice did not display perinatal lethality[16]. These differences suggested that either the *Hip1*$^{\Delta 3\text{-}5}$ allele is not a complete null allele or that the serendipitous *Hip1*^{null} allele affects neighboring genes and that those effected genes (rather than *Hip1*) are necessary for embryogenesis and lens homeostasis.

Breast and prostate tumorigenesis is not inhibited in Hip1$^{\Delta 3\text{-}5/\Delta 3\text{-}5}$ mice.

Since HIP1 is known to transform mouse fibroblasts[20] and is over-expressed in multiple human cancers[19], it has been hypothesized to play a role in tumorigenesis. We have previously demonstrated that HIP1 deficiency inhibits prostate tumor progression in TRAMP mice[23]. To examine further the involvement of HIP1 in tumor development, we analyzed the effect of HIP1 deficiency on breast tumorigenesis using the MMTV-myc mammary tumor model[24]. Because of its less complex structure but similar phenotype to the *Hip1*^{null} allele, we have used the *Hip1*$^{\Delta 3\text{-}5}$ allele in our subsequent studies of the role of HIP1 in tumorigenesis. MMTV-myc and TRAMP transgenic mice were generated in both the *Hip1* "null" and Δ3-5 genetic backgrounds. The MMTV-myc mice were sacrificed prior to or at 12 months of age and analyzed for the appearance and progression of breast tumors (**Figure 2.2**). Consistent with our previous results using the TRAMP mice, the HIP1 "null" background inhibited tumorigenesis induced by the MMTV-myc transgene[23] such that none of the 6 *Hip*$^{null/null}$;MMTV-*myc* mice (0%) analyzed developed breast tumors. In contrast, 3 of 16 *Hip*$^{+/null}$;MMTV-*myc* mice

(18.8%) analyzed developed breast tumors. This trend supports the hypothesis that HIP1 deficiency inhibits breast tumorigenesis (**Figure 2.3A**).

The use of the Δ3-5 allele (compared to the null allele) to generate a HIP1 deficient background resulted in a different effect on tumorigenesis. For the MMTV-myc mice, 8 of 18 (44%) *Hip1*$^{\Delta 3\text{-}5/\Delta 3\text{-}5}$ mice and 19 of 37 (51%) *Hip1*$^{+/\Delta 3\text{-}5}$ mice developed palpable breast tumors (**Figure 2.3A**). This level is significantly higher than the 19% breast tumor incidence in MMTV-myc mice with the *Hip1*$^{+/null}$ backgrounds and the 0% incidence in the *Hip1*$^{null/null}$ background. Additionally, we only observed breast tumor metastasis in mice that contained the Δ3-5 allele (**Figure 2.3B**). Both multiple synchronous primary breast tumors (**Figure 2.3C**) as well as multiple metastatic foci (**Figure 2.3D**) were observed in *Hip1*$^{+/\Delta 3\text{-}5}$ and *Hip1*$^{\Delta 3\text{-}5/\Delta 3\text{-}5}$ mice.

The TRAMP;*Hip1*$^{\Delta 3\text{-}5}$ mice produced similar results with a smaller cohort of mice available for tumor analysis (**Figure 2.4**). We initially planned to compare larger groups of 6-month-old heterozygous and homozygous TRAMP;*Hip1*$^{\Delta 3\text{-}5}$ mice. This plan was based on the results of three independent prior TRAMP experiments that demonstrated that *Hip1*$^{null/+}$ and *Hip1*$^{+/+}$ mice developed prostate cancer at a similar frequency and to a similar extent in the TRAMP background and survived to at least 6 months of age. As expected, when we performed this fourth TRAMP experiment we observed that 84% (15/18) and 93% (14/15) of the TRAMP mice that were heterozygous and homozygous for the null allele, respectively, survived to 6 months of age (**Figure 2.5A**). Unexpectedly, *Hip1*$^{\Delta 3\text{-}5}$;TRAMP mice (both heterozygotes and homozygotes) began to die spontaneously by 4 months of age and only 35% (5/14) of the homozygotes and 69% (9/13) of the heterozygotes survived to the 6 month point. This reduction in survival

associated with the *Hip1*$^{\Delta 3\text{-}5}$ allele was not due to the effects of the *Hip1*$^{\Delta 3\text{-}5/\Delta 3\text{-}5}$ degenerative phenotype (*e.g.*, kypholordosis, dwarfism, etc.) as it was observed in both the heterozygotes and the homozygotes. In the TRAMP mice that were available for tumor analysis we found that 4 of the 5 surviving homozygous *Hip1*$^{\Delta 3\text{-}5}$ allele bearing TRAMP mice had gross prostate tumors (80%) and 3 of those 4 tumor bearing mice displayed gross evidence for multiple synchronous primary tumors in different lobes of the prostate (**Figure 2.5B**). In comparison, there was no evidence for multiple primary tumors in the *Hip1*$^{+/\Delta 3\text{-}5}$ (7 of these 9 (75%) mice had prostate cancer), *Hip1*$^{+/null}$ (6 of the 18 (33 %) mice had prostate cancer) or *Hip1*$^{null/null}$ (5 of the 15 (33%) had prostate cancer) TRAMP mice.

A novel cryptic splicing event allows for expression of a large mutant HIP1 protein.

The difference in tumor incidence in the *Hip1*$^{null/null}$ mice and the *Hip1*$^{\Delta 3\text{-}5/\Delta 3\text{-}5}$ mice suggests either that (1) the original null allele alters the expression of neighboring genes and that it is those genes that influence tumorigenesis or (2) the Δ3-5 allele is not a completely null allele. To investigate these two possibilities, we examined normal and tumor tissues from TRAMP and MMTV-myc mice with the Δ3-5 allele for the expression of polypeptides that react with HIP1-specific antibodies. Extracts from these tissues were analyzed by western blotting for the presence of either full-length or truncated HIP1 protein using a polyclonal rabbit antibody (UM354) specific for the amino-terminal end of the HIP1 protein (**Figure 2.6A**). Additionally, tumor tissue was dissociated and cultured so that tumor cells from these mice could be analyzed. Results of this analysis indicated that a truncated protein approximately 10 kDa smaller than the

wild type HIP1 protein was expressed in the *Hip1*$^{\Delta 3\text{-}5/\Delta 3\text{-}5}$ tumor-derived cultured cells (**Figure 2.6A**, lanes 1 and 2 versus lanes 3 and 4). Extracts derived from the bulk of the tumor as well as other select tissues from these mice showed the expected lack of expression (lanes 5-10).

In the construction of the Δ3-5 allele, exons 3 through 5 were deleted not only to disrupt the ANTH domain but also to ensure that the splicing of exon 2 with exon 6 or any of the other exons downstream of exon 6 would result in a frame shift that would lead to premature truncation at the amino terminal end of the protein. Therefore, the presence of a truncated HIP1 protein in these tumor cells that is only 10 kDa smaller than the wild type protein was quite surprising. To identify the mRNA that encodes for this truncated HIP1 protein, we performed reverse transcriptase polymerase chain reaction (RT-PCR) using total RNA derived from TRAMP and MMTV-myc tumor-derived cultured cells. Primers specific to the exon 1 and the exon 14/15 junctions of the HIP1 cDNA sequence (NCBL BLAST-Accession # NT_039314) were used in the initial RT-PCR reaction. We detected a PCR product of the expected size (1.6 kb) in tumor-derived cells generated from wild type mice and from mice heterozygous for the Δ3-5 allele (**Figure 2.6B**). An additional band approximately 300 bp smaller (*i.e.*, 1.3 kb) than expected was observed in both heterozygous and homozygous mice. These bands were excised from the gel, PCR amplified using nested primers, and the products were sequenced. The cDNA sequence for the nested 1.6 kb product was identical to that of the wild type *Hip1* cDNA. Interestingly, the sequence of the nested 1.3 kb product contained exon 2 fused to exon 6 with a dinucleotide AG insertion in the junction. This dinucleotide

insertion put the exon 2/6 fusion in frame (**Figure 2.7**) such that it encodes for an only slightly truncated HIP1 protein (**Figure 2.6C**).

To examine further the above-described HIP1 mutant protein, we sequenced the *Hip1* gene from genomic DNA derived from cultured tumor cells. Surprisingly, we did not detect a mutation. However, careful analysis of the genomic sequence revealed two unique findings to explain the aberrant protein and transcript expression. First, we found that intron 2 uses a rare "AT-AC" U12 dependent splicing mechanism. This type of intron, which represents approximately 1% of the introns in the mammalian genome[27], consists of 5'AT and 3'AC splice sites. Second, we found that the intron 5 splice acceptor (a typical AG) is immediately preceded by an AC. This ACAG sequence allows for the incorporation of an AG dinucleotide into the coding sequence of the mRNA transcript and serendipitous maintenance of the original reading frame. The predicted size of this mutant protein is 106 kDa, which is very similar to the size of the observed protein product.

Mutant HIP1Δ3-5insAG protein expression in embryonic and adult lung and brain tissues.

The presence of this AG dinucleotide insertion that placed exons 2 and 6 in frame in both Δ3-5 heterozygous and Δ3-5 homozygous cells led us to re-evaluate whether or not *Hip1* protein is expressed in normal tissues. We isolated select normal cells and tissues from wild type, Δ3-5 heterozygous, and Δ3-5 homozygous mice and analyzed them for the presence of the Hip1Δ3-5insAG protein product. Using northern blot analysis of embryonic fibroblast RNA (**Figure 2.8A**), we found that the truncated

message was evident in homozygous mice when analyzed beside wild type RNA. Using RT-PCR, we also found that tissue from the brains, lungs, and kidneys of Δ3-5 heterozygous and homozygous mice contained the HIP1Δ3-5insAG mRNA (**Figure 2.8B**). No PCR product representing the Hip1Δ3-5 mRNA was observed in wild type mice. We also found that extracts from cultured, early passage embryonic fibroblasts and embryonic brain contained easily detectable truncated HIP1Δ3-5insAG protein product (**Figure 2.9**). In contrast, nearly all adult tissues, with the exceptions of the lung and brain (**Figure 2.8**), displayed very low levels of HIP1 polypeptide expression. Either the diminished expression or the lack of function of the HIP1Δ3-5insAG product could explain why these mice display a degenerative phenotype similar to that of the original homozygous "null" mice. In addition to the altered expression levels of the HIP1 peptides in various tissues, we noted that the migration of the HIP1 protein in the embryonic brain was quite different from that in the adult brain. Analysis of the *Hip1* protein product in embryonic, newborn, pre-weaned, and adult mice indicated that this differential expression correlates with developmental stage, with the product in the adult brain migrating distinctly slower or co-migrating with the wild type form of HIP1. The molecular explanation of this striking developmental correlation remains to be determined.

Next, using the original *Hip1*$^{loxp/loxp}$ mice[16], we generated a tissue-specific Δ3-5 recombinant allele. By crossing the *Hip1*^{loxp} mice with mice carrying an interferon inducible Mx1-Cre transgene, we generated mice that expressed the Δ3-5 allele only in cells of the adult hematopoietic system, liver, and kidney following pIpC-mediated induction of Cre expression[26,28]. With these mice, we examined whether the gross

phenotype of the germ line Δ3-5 mouse could be recapitulated only in the isolated adult tissues. Interestingly, western blot analysis of extracts from the spleen, liver, kidney (**Figure 2.10A**), and bone marrow (**Figure 2.10B**) of Mx1-Cre induced mice demonstrated that the expression of the truncated HIP1 protein was most prominent in the spleen and bone marrow and loss of HIP1 expression altogether was frequently observed in the normal liver and kidney but as expected not in brain, heart, eye, uterus, ovary or the GI tract (data not shown). It is of interest that in the two tissues, liver and kidney, where we observed HIP1 protein deficiency due to a complete recombination event did not display the degenerative phenotype observed in the germ line recombined Δ3-5 mice. We therefore conclude that tissue specific HIP1 deficiency in the liver and kidney does not induce the knockout phenotype. Unfortunately, we could not make this conclusion in the hematopoietic system as despite repeated attempts to induce interferon with pIpC, the complete recombination of the $Hip1^{loxp}$ allele in the Mx1-cre mice was not achieved in hematopoietic tissues and, therefore, a significant amount of wild type Hip1 expression remained in the homozygotes.

These findings also suggest the possibility that the truncated HIP1 protein may be preferentially expressed in dividing cells, including tumorigenic cells. This prediction is supported by the finding that Δ3-5insAG protein was present in the fibroblasts and brains of Δ3-5 mouse embryos at E17.0 day. Furthermore, we discovered a gross liver tumor in an Mx1Cre;$Hip1^{loxp/+}$ mouse (**Figure 2.10C**). The tumor from this mouse expressed a truncated Δ3-5 protein product while the surrounding "normal" liver did not. Additionally, we identified a trend in which the spleen sizes of the *Hip1* floxed, Mx1cre,

pIpC-treated mice increased, although frank hematopoietic malignancies were not observed (data not shown).

The HIP1Δ3-5insAG protein retains its ability to bind lipids, clathrin, AP2, and EGFR.

We have observed some slight phenotypic differences between the *Hip1*$^{\Delta 3\text{-}5/\Delta 3\text{-}5}$ mice and the *Hip1*$^{null/null}$ mice[16]. These differences included absence of cataracts or perinatal death in the *Hip1*$^{\Delta 3\text{-}5/\Delta 3\text{-}5}$ mice, increased mortality from tumors in the TRAMP;*Hip1*$^{\Delta 3\text{-}5}$ mice relative to the TRAMP;*Hip1*$^{null/null}$ mice, no decrease in breast or prostate tumorigenesis in *Hip1*$^{\Delta 3\text{-}5}$ allele bearing backgrounds (although there was a trend toward more tumors), and a liver tumor in a young, conditional *Hip1*$^{\Delta 3\text{-}5}$ heterozygous mouse. Given these differences, we examined whether the Hip1Δ3-5insAG protein product possesses all or a subset of its cellular activities that promote normal and neoplastic cell proliferation/survival by assessing its ability to bind to lipids, endocytic factors, and EGFR.

Because this truncated protein retains its clathrin-, AP2-, and EGFR-binding regions, we predicted that the Hip1Δ3-5insAG protein product would have the ability to bind these proteins. To test this hypothesis, we expressed the *HIP1*$^{\Delta 3\text{-}5/insAG}$ cDNA in 293T cells, immunoprecipitated the mutant protein with an anti-HIP1 polyclonal antibody (UM323, bleed 8/2002), and immunoblotted the precipitates to determine the presence or absence of the endocytic proteins and EGFR. As expected, the truncated mutant protein bound EGFR, clathrin and AP2 (the alpha subunit) (**Figure 2.11A**, lanes 11 and 15). In contrast, expression of a human HIP1 mutant cDNA construct that lacks the AP2- and

clathrin-binding domains did not bind these endocytic proteins. Also, it should be noted that the interaction between HIP1 and EGFR was apparently enhanced by the deletion of either the sequences encoded for by exons 3-5 or the domains that bind to endocytic proteins, suggesting that the interaction of HIP1 with EGFR is not indirectly mediated by the its binding with clathrin and/or AP2.

Since 80% of the sequence of the lipid binding ANTH domain is deleted from the HIP1Δ3-5insAG protein, we predicted that this mutant would likely not retain its lipid binding activity. Interestingly, most of the key residues that are important for the direct binding of the ANTH domain-containing proteins to $PI(4,5)P_2$ were retained in the Δ3-5 protein product (key residues are bold in Figure 1)[12,13]. However, one key residue (homologous to K76 of epsin) that has been shown to be important in binding to the $Ins(1,4,5)P_3$ head group[13] is deleted in the truncated Δ3-5 protein. To determine whether the Δ3-5 protein product retained its lipid-binding capacity, we examined lipid binding using recombinant GST-$HIP1^{wt}$ and GST-$HIP1^{\Delta 3\text{-}5/insAG}$ fusion proteins. We generated and glutathione-sepharose purified GST-fusion proteins that contained the first 430 and 370 amino acids of the $HIP1^{wt}$ and $HIP1^{\Delta 3\text{-}5/insAG}$ proteins, respectively (**Figure 2.11B**). The purified proteins were separated by SDS-PAGE and Coomassie stained to quantitate the amount of recombinant protein. The purified recombinant proteins were also analyzed by western blot to ensure interaction with anti-GST and anti-HIP1 antibodies. Next, the purified proteins were incubated with Echelon-generated PIP strips to examine whether the fusion proteins were capable of binding lipids. Both the wild type and the $HIP1^{\Delta 3\text{-}5/insAG}$ mutant fusion proteins bound PtdIns(3)P predominantly (**Figure 2.12**). These results were confirmed using PIP arrays (Echelon), which were used to further

examine the differential abilities of these proteins to bind to lipids. Interestingly, these truncated fusion proteins displayed a higher specific binding to PtdIns(3)P than to polyphosphorylated inositol lipids. On the other hand, our previous studies using the full-length HIP1 expressed in 293T cells indicated that its lipid binding preference was polyphosphorylated 3-phosphoinositides[29]. Our contradictory results may be due to either the absence of the carboxyl-terminal end of the protein, differences in proteins expressed in bacteria versus mammalian cells or differences in the materials used in the various assays. Additional biochemical analyses are necessary to clarify this issue. Nevertheless, the specific inositol lipid binding capacity of the ANTH domain is retained in the Hip1Δ3-5insAG protein.

Discussion

We have previously demonstrated that the HIP1 family of proteins are biologically important since both single *Hip1*[15,16] and double *Hip1/Hip1r*[14] knockout mice have adult degenerative phenotypes and HIP1 protein expression is altered in multiple cancers[19]. However, the exact function of this protein family remains unclear, and more detailed cellular and biochemical analyses are needed to validate predicted functions and identify novel ones. In the current study, we describe a novel form of HIP1 that is expressed *in vivo* as the result of a novel cryptic splice event between a 5' AT-AC intron (intron 2) and a 3' GT-AG intron (intron 5). These results are important for both technical and functional reasons. First, it illustrates an unpredicted cryptic splicing event in a previously predicted "loss of function" gene targeting event, and, second, this type of

cellular natural selection may provide clues to the function of HIP1 in normal and neoplastic cells.

The technical aspects of these findings have provided us a very important lesson. The targeting event that we initially designed led to a mutation in the AT-AC intron 2. The rare splicing event that we observed reflects preferential splicing between splice sites of the same class. The identification of rare U12-dependent intron splicing sites or AT-AC introns will be important for all proteins with similar genetic structures[27]. This finding has also raised an intriguing possibility that such splicing events might occur in normal cells leading to the expression of unexpected polypeptides. Interestingly, the rare AT-AC intron 2 is conserved in both the human and mouse *Hip1* genes. This observation is consistent with previous reports that U12-type introns are usually conserved phylogenetically[30]. It has been reported previously, that genes with non-redundant, crucial cellular activities may have strong selective evolutionary pressure against the conversion of U12- to U2-type introns and, therefore, have retained them. HIP1 supports this assertion as HIP1 clearly has nonredundant, crucial activities as evidenced by the fact that its deletion in mice leads to dramatic adult phenotypes[14-16].

In terms of HIP1 function, it is evident that the expression of the truncated mutant protein in adult lung and brain tissue does not prevent the adult degenerative phenotypes, such as kypholordosis or testicular degeneration. The discovery here of concomitant expression of HIP1 sequences in the Hip1Δ3-5 homozygous mice and the degenerative phenotype suggests that this mutant protein may not be completely functional in normal cells. In contrast, the presence of the truncated mutant protein in tumor cells may explain why tumorigenesis is not inhibited by the homozygosity of this allele. This proposal is

supported by the finding that this mutant protein retains some of its functions (*i.e.*, the ability to bind to lipids, clathrin, AP2, and EGFR). These findings illustrate a prototypical example that provides insights into how mouse modeling may lead to insertion mutations and unpredicted, active protein products.

The maintenance of AP2-, CHC-, EGFR- and lipid-binding functions in the truncated mutant HIP1 protein suggests that another HIP1 cellular function must contribute to the gross phenotype of the mutant mice. This unknown function likely explains why we were unable to identify endocytic defects in either of the mutant mouse systems. Future studies are required to understand the molecular modifications and sequences of the various forms of HIP1 that are expressed in different tissues at different times during mammalian development and how these different forms affect HIP1 functions.

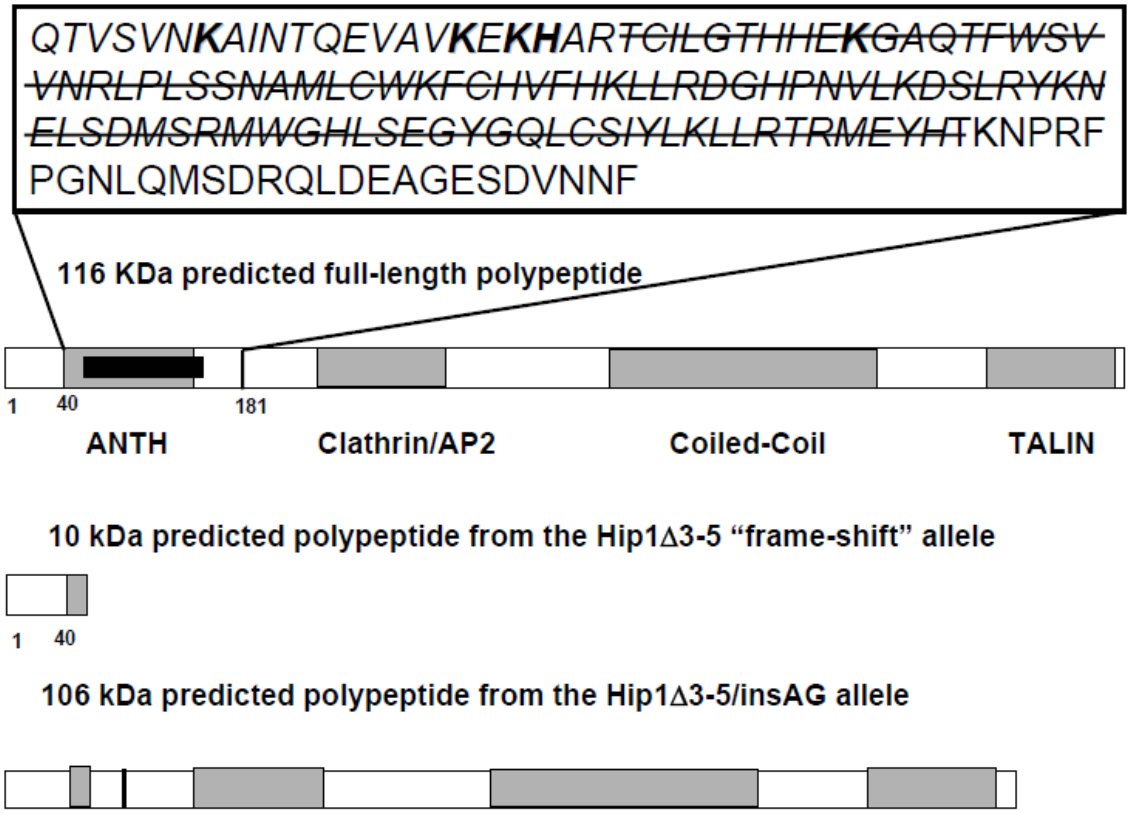

Figure 2.1: Amino acid sequence of the HIP1 ANTH domain and schematic diagram of the HIP1 domain structure.

The majority of the mouse ANTH domain is encoded by exons 3 to 5. The amino acid sequence of the mouse ANTH domain (italicized,[12,13]) and a few additional carboxyl amino acids are shown in the box above the schematic diagram of the full-length protein. A line is drawn through the amino acids that are encoded by exons 3 to 5. Residues in bold (K, K, KH, K) share homology with AP180 and epsin and are considered to be critical inositol lipid-binding residues. The predicted protein product encoded by the *Hip1*$^{\Delta 3\text{-}5}$ allele is 10 kDa and is shown schematically below the full length HIP1 diagram. The predicted protein product from the *Hip1Δ3-5insAG* cDNA is 106 kDa and is also shown schematically.

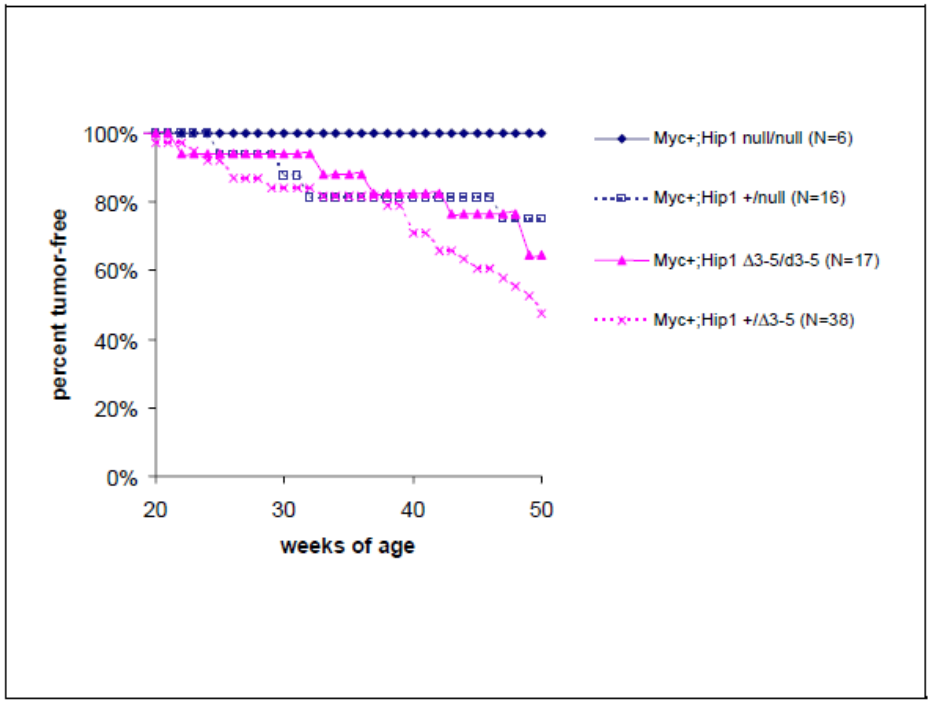

Figure 2.2: Tumorigenesis in MMTV-myc mice in the absence of HIP1. Percent tumor-free survival out to 5 weeks of age is shown for MMTV-Myc+ mice on various HIP1 knockout backgrounds. Mice were sacrificed when the tumor ulcerated or impeded movement.

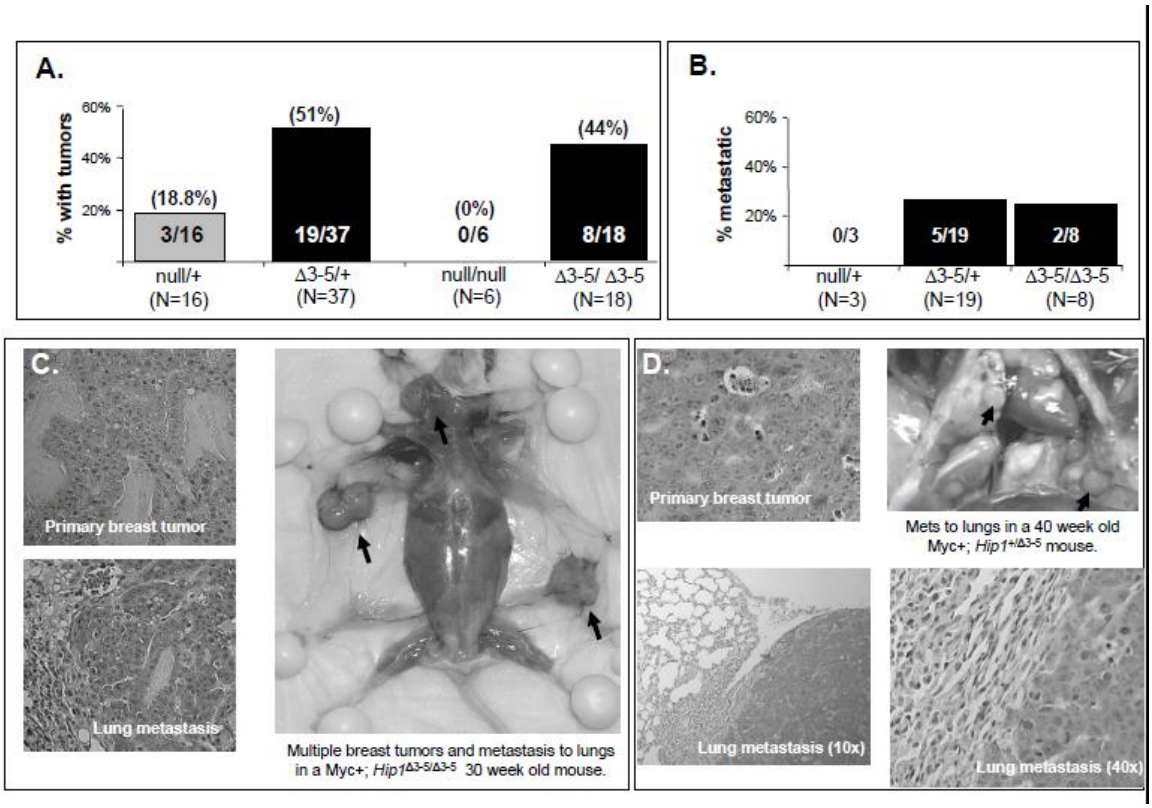

Figure 2.3: Breast tumorigenesis in the presence of the *Hip1*Δ3-5 allele.

A. MMTV-myc transgenic mice were mated on to *Hip1*$^{null/null}$ and *Hip1*$^{\Delta 3\text{-}5/\Delta 3\text{-}5}$ backgrounds. Mice were dissected at one year of age, or earlier if a tumor was found. 44% of *Myc+*;*Hip1*$^{\Delta 3\text{-}5/\Delta 3\text{-}5}$ mice developed breast tumors, compared to none of the *Myc+*; *Hip1*$^{null/null}$ mice. 51% of *Myc+*; *Hip1*$^{+/\Delta 3\text{-}5}$ mice developed breast tumors, compared to 19% of *Myc+*; *Hip1*$^{+/null}$ mice.

B. None of the *Hip1*$^{+/null}$ mice with tumors (N=3) exhibited metastasis of the breast tumors. 25% of *Myc+;Hip1*$^{\Delta 3\text{-}5/\Delta 3\text{-}5}$ mice with tumors (N=8) and 26% of *Myc+; Hip1*$^{+/\Delta 3\text{-}5}$ mice with tumors (N=19) had metastasis of the breast tumors to organs including the lungs, liver, spleen and salivary gland.

C. Multiple breast tumors and metastasis to lungs of a *Myc+; Hip1*$^{\Delta 3\text{-}5/\Delta 3\text{-}5}$ mouse at 30 weeks of age.

D. Metastasis of a breast tumor to the lungs of a *Myc+;Hip1*$^{+/\Delta 3\text{-}5}$ mouse at 40 weeks of age.

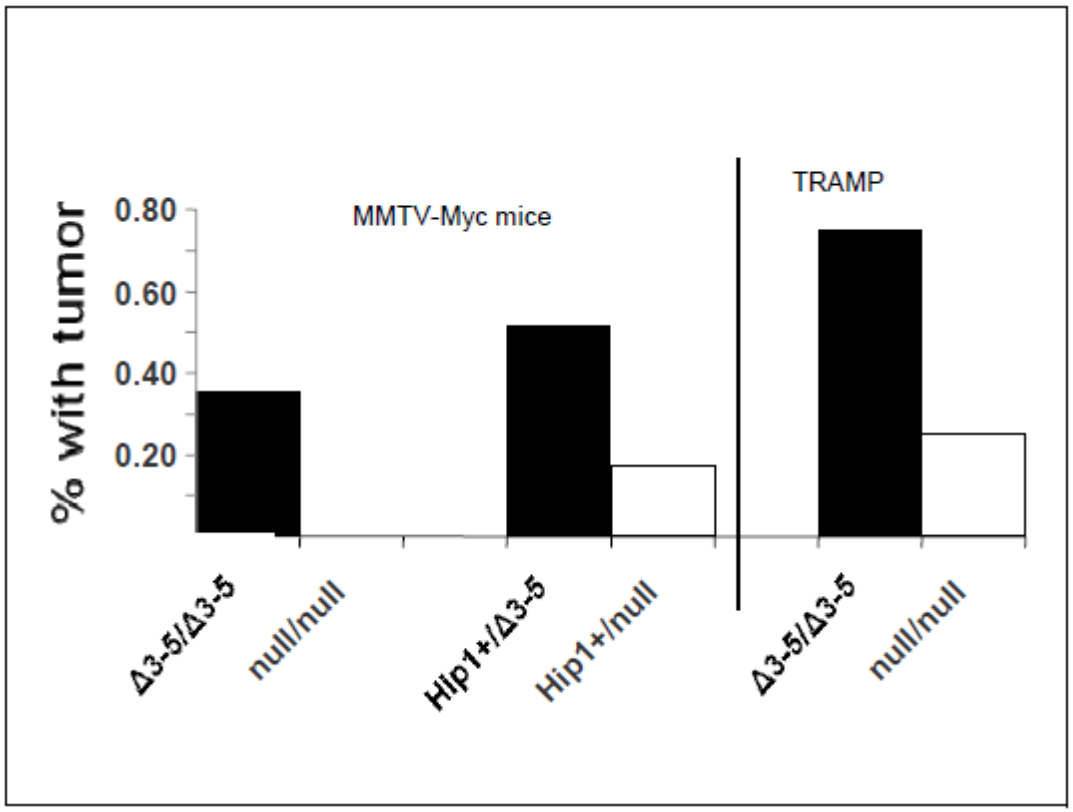

Figure 2.4: Tumor incidence in mice with *Hip1*Δ3-5 and *Hip1*null alleles. MMTV-myc transgenic and TRAMP mice were mated on the $Hip1^{null/null}$ and $Hip1^{\Delta 3\text{-}5/\Delta 3\text{-}5}$ backgrounds and analyzed for tumor incidence. TRAMP mice that survived to 6 months of age were scored for gross prostate tumors. In each case the mice with the Δ3-5 allele were afflicted with more tumors.

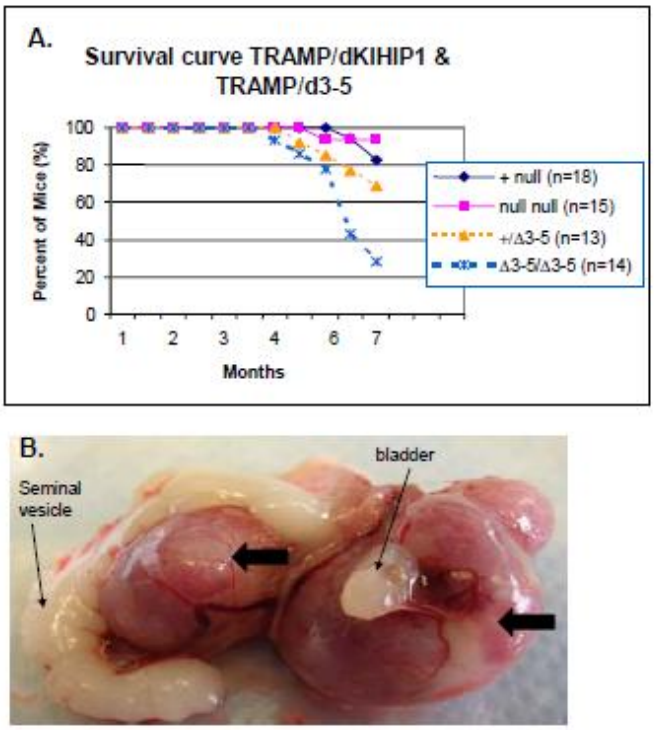

Figure 2.5: TRAMP mice on different *Hip1* mutant backgrounds.
A. Survival curve of TRAMP mice in different *Hip1* mutant backgrounds.
B. Examples of bilateral synchronous prostate tumors.

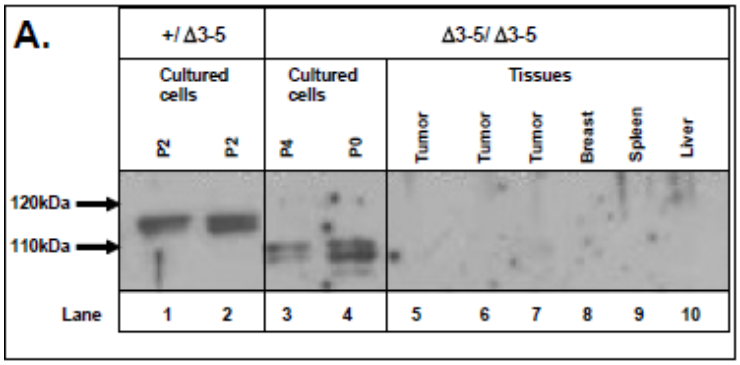
A.
+/ Δ3-5
Δ3-5/ Δ3-5
Cultured cells
Cultured cells
Tissues
P2
P2
P4
P0
Tumor
Tumor
Tumor
Breast
Spleen
Liver
120kDa
110kDa
Lane
1
2
3
4
5
6
7
8
9
10

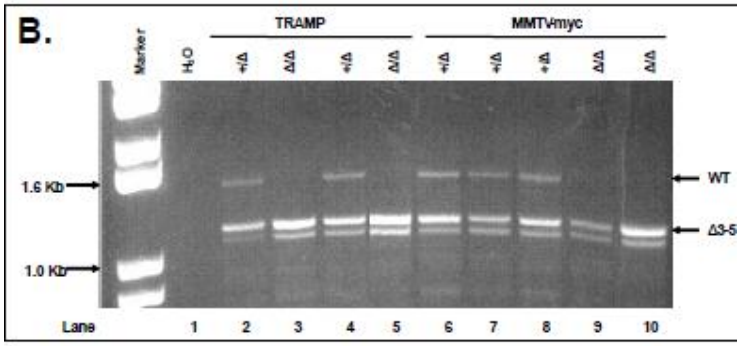
B.
TRAMP
MMTVmyc
Marker
H2O
1.6 Kb
1.0 Kb
WT
Δ3-5
Lane
1
2
3
4
5
6
7
8
9
10

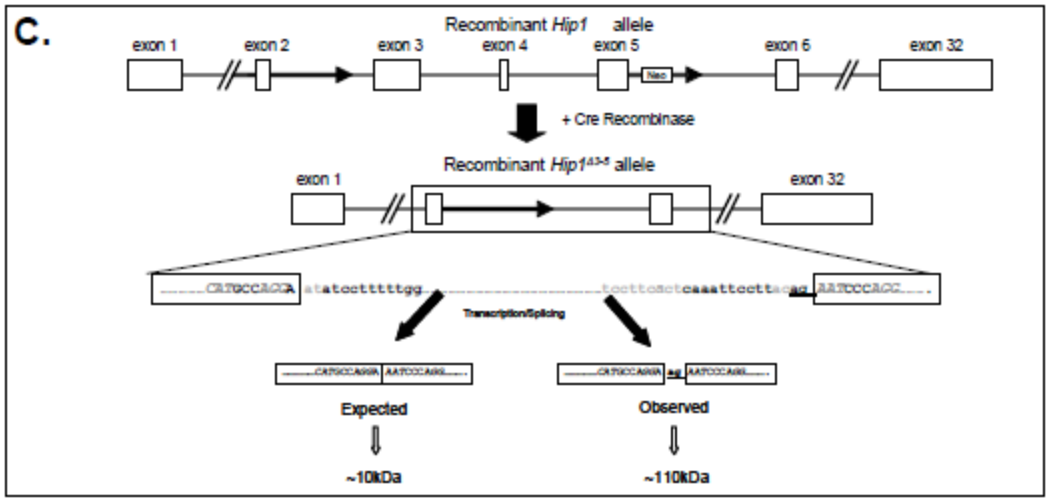
C.
Recombinant Hip1 allele
exon 1
exon 2
exon 3
exon 4
exon 5
Neo
exon 6
exon 32
+ Cre Recombinase
Recombinant Hip1Δ3-5 allele
exon 1
exon 32
Transcription/Splicing
Expected
Observed
~10kDa
~110kDa

Figure 2.6: Expression of *Hip1* sequences in *Hip1Δ3-5* mice.
A. Tumors from mice with breast (MMTV-myc) and prostate (TRAMP) cancer were grown in culture and analyzed by western blot for the presence of HIP1 polypeptides. Results from an MMTV-myc breast tumor sample are shown. P=passage number. Even at zero passages (P0), the cultured cells from Δ3-5/Δ3-5 tumors expressed a slightly truncated form of HIP1 (Lane 4). This product was not detected in the bulk tumor tissue, in the normal tissues tested of these mice, or in any cell types derived from mice heterozygous for the Δ3-5 allele (lanes 5-10).
B. RT-PCR of total RNA extracted from Δ3-5 allele-containing tumor-derived cultured cells resulted in the generation of wild type (WT) and mutant (Δ3-5) bands of expected sizes.
C. Partial *Hip1Δ3-5* cDNA sequence alignment with wild type mouse *Hip1* cDNA demonstrated an AG dinucleotide insertion between exons 2 and 6 of the *Hip1Δ3-5* cDNA sequence. This insertion maintains the open reading frame of the transcript. Tumor cell line genomic DNA contains a recombined "AT-AC" intron. Genomic DNA isolated from a Myc breast tumor-derived cell line was sequenced in the region where the recombination occurred (box). The sequence was compared to wild type *Hip1* genomic DNA and no additional mutations were observed. Note the recombinant intron flanked by exons 2 and 6 has a U12-dependent consensus branch point sequence (italicized) and a 3' AC dinucleotide (italicized) that serves as the cryptic splice site acceptor. This splicing event results in an "AG insertion" in the transcript. The region sequenced is indicated by the box that encompasses exons 2, 6 and intervening sequences including the single loxP site.

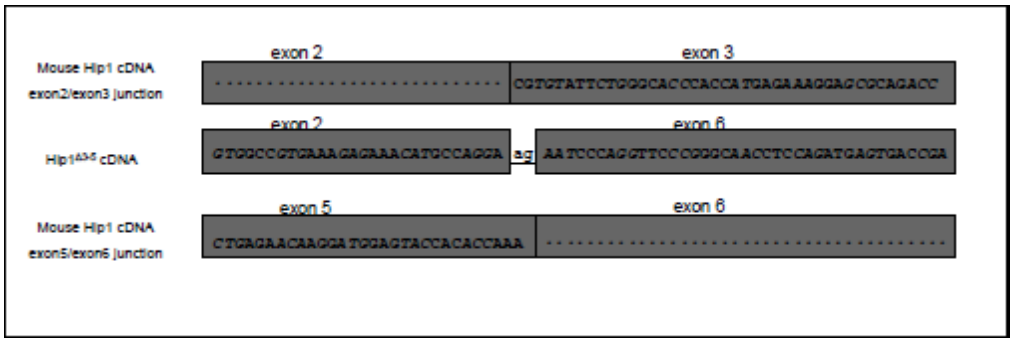

Figure 2.7: Partial *Hip1Δ3-5* cDNA sequence alignment with wild type mouse *Hip1* cDNA. Shown is an alignment of cDNA sequence from the nested PCR reaction with the exon 2/3 and exon 5/6 junctions of mouse *Hip1* mRNA reference sequence (NM_146001). Dots in the mouse *Hip1* mRNA reference sequence denote identity with the *Hip1 Δ3-5* cDNA sequence. Codons are represented by alternating bold/nonbold trinucleotide sequences. Note the AG dinucleotide insertion between exons 2 and 6 of the *Hip1 Δ3-5* cDNA sequence, which maintains the open reading frame of the transcript.

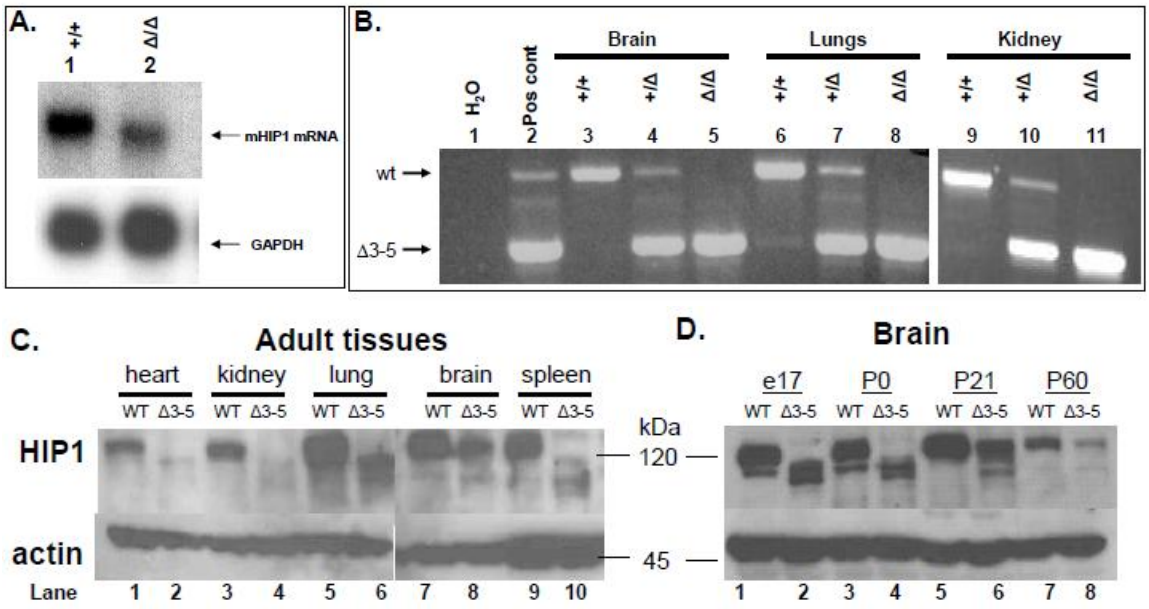

Figure 2.8: Expression patterns of the Δ3-5insAG mRNA and its putative protein product.

A. Northern blot analysis using a probe specific for the 5' end of the mouse *Hip1* mRNA (nucleotides 1-1260) demonstrated the presence of a significant amount of a slightly truncated product in the RNA of mouse embryonic fibroblast (lane 2 versus lane 1).

B. Primers specific to the exon 1/2 junction (forward) and the exon 13/14 junction (reverse primer) of murine *Hip1* cDNA were used to amplify the cDNA. The resulting products were separated on a 1.0% agarose gel. Water was used as the negative control (lane 1). RNA from a TRAMP prostate cancer cell line generated from the prostate tumor tissue of a mouse that was heterozygous for the $Hip1^{\Delta 3\text{-}5}$ allele was used as a positive control for both the wild type *Hip1* and $Hip1^{\Delta 3\text{-}5/insAG}$ mRNA transcripts (lane 2). A 1.6 kb band indicates the presence of wild type *Hip1* mRNA transcripts while a 1.3 kb band indicates the presence of the mutant $Hip1^{\Delta 3\text{-}5/insAG}$ mRNA transcripts. Brain, lung and kidney tissues from wild type *Hip1* mice (+/+) produced the 1.6 kb band but not a 1.3 kb band (lanes 3, 6 and 9). Similar tissues from heterozygous Δ3-5 mice (+/Δ) produced both a 1.6 kb band and a 1.3 kb band (lanes 4, 7 and 10). Only the 1.3 kb band was produced in brain, lung, and kidney tissues from homozygous Δ3-5 mice (Δ/Δ) (lanes 5, 8 and 11).

C. Expression of the truncated product was most prominent in lung tissue although lesser amounts are detected in all other tissues tested. Interestingly, brain tissue from Δ3-5 adult mice displayed significant amounts of a protein product that co-migrated with the wild type form. This co-migration was not observed in the extracts from embryonic brains (described in panel D). Actin blotting was performed using an anti-actin monoclonal antibody (Sigma) as a control.

D. Postnatal day zero brains (isolated immediately after birth) have HIP1 banding patterns similar to those of embryos. Pre-weaning stage brains have two distinct HIP1 bands, and the adult brains have a HIP1 band that co-migrates with the wild type band.

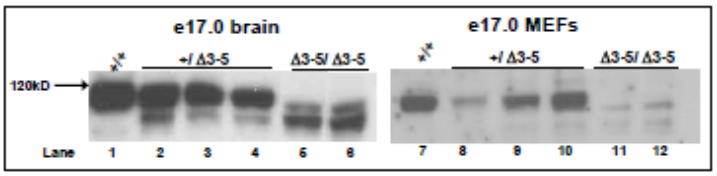

Figure 2.9: HIP1 Δ3-5/insAG 106 kDa protein is present in mouse embryonic brain and fibroblasts. Western blot analysis for HIP1 expression in the brains (left panel) and fibroblasts (right panel) of 17-day old mouse embryos of different genotypes demonstrated the presence of a slightly truncated HIP1 product. MEF cells of different genotypes were cultured from eleven individual embryos from the same mother. Only 5 samples are shown here but all demonstrated similar banding patterns as related to the distinct genotypes.

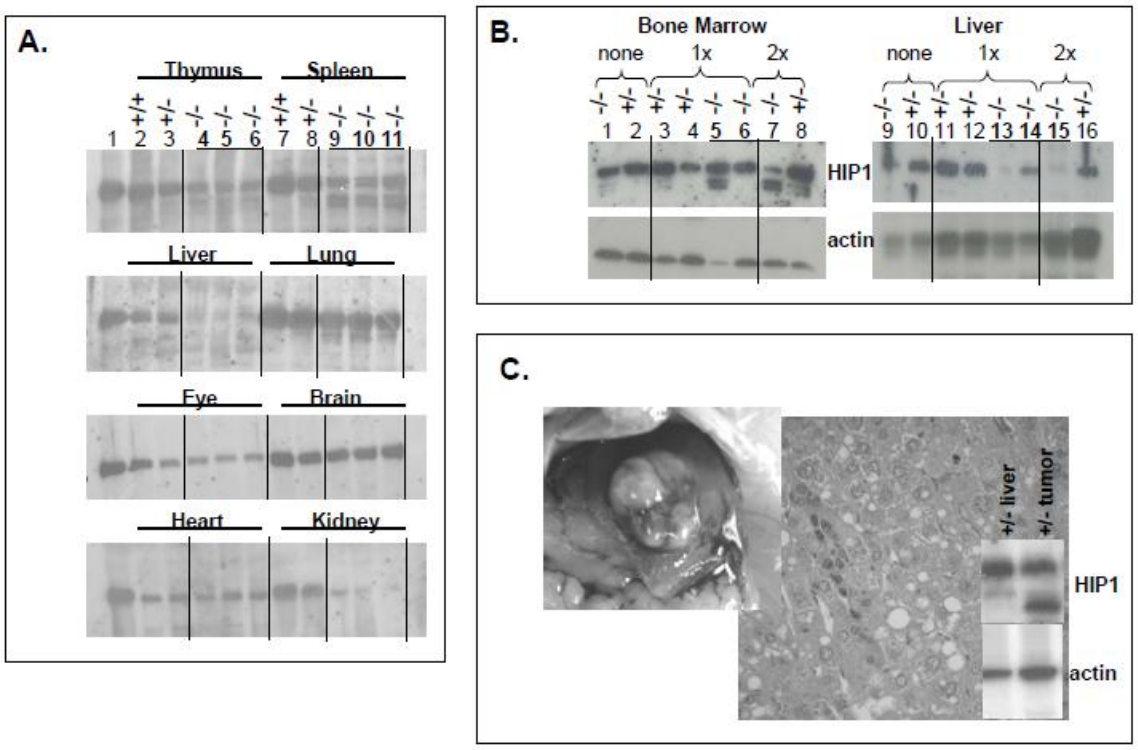

Figure 2.10: Conditional cre-mediated recombination of the floxed *Hip1* allele leads to either HIP1 deficiency or expression of the truncated product depending on tissue analyzed.

A. Mx1-Cre transgenic mice carrying none (+//+; lanes 2 and 7), one (-/+; lanes 3 and 8) or two (-/-; lanes 4-6 and 9-11) of the floxed *Hip1* alleles were treated with 3 injections of pIpC at 8-12 weeks of age then were retreated at 20 weeks of age. Their organs were harvested at 28-32 weeks of age. Organ extracts were separated on 6% SDS-PAGE and analyzed for HIP1 expression by western blotting (using the UM354 (1:5000) antibody). An extract of a wild type brain (lane 1) was included as a positive control of HIP1 expression. Near complete recombination (resulting in the deficiency of HIP1 protein) was observed in liver and kidney but not in thymus and spleen where residual wild type HIP1 and truncated HIP1 (putative □3-5insAG product) was expressed. As expected, eye, brain, and heart tissue showed no evidence for recombination since Mx1-cre is not induced in these tissues [26]. A small amount of putative □3-5insAG truncated product was observed in lung tissue and may be a result of recombination in tissue macrophages, which are abundant in the lung tissue.

B. Mice were untreated (lanes 1, 2, 9 and 10) or treated at 6 weeks of age with pIpC (6 doses IP every other day; lanes 3-6 and Lanes 11-14). A small group was treated with pIpC again at 20 weeks of age (3 additional doses every other day; lanes 7, 8 and 15, 16). The mice were sacrificed at 6 months of age, and their tissues were analyzed for HIP1 expression by western blot (UM354). Complete deficiency of HIP1 was never observed in bone marrow despite continued pIpC injections whereas complete deficiency of HIP1 was achieved was maintained in the liver without repeated recombination. Interestingly, in the mouse without complete recombination in the liver (lane 14), there was no

truncated product in its cultured bone marrow (lane 6). A small amount of the truncated product was observed in cultured bone marrow from some untreated mice (*e.g.* lane 1), a finding consistent with the possibility that the endogenous production of interferon (*i.e.* in response to viral infections) can activate Mx1-cre expression at low levels in mice in the absence of pIpC treatment. As a loading control, actin blots were performed on 10% SDS-PAGE using a monoclonal anti-actin antibody (Sigma, St. Louis, MO).

C. Mice were treated with pIpC in two stages: first at 21 weeks of age (with 6 every other day doses) and second at 55 weeks of age (with 6 every other day doses). Six treated mice (3 heterozygous and 3 homozygous) and 5 untreated mice were necropsied. At necropsy, a previously undetected liver tumor was discovered in a treated heterozygous mouse, and it was harvested for histological and protein expression analysis. Increased amounts of truncated HIP1 expression were observed in the tumor tissue compared to surrounding "normal" liver tissue. Since this was a heterozygous mouse, expression from the wild type allele was also detected.

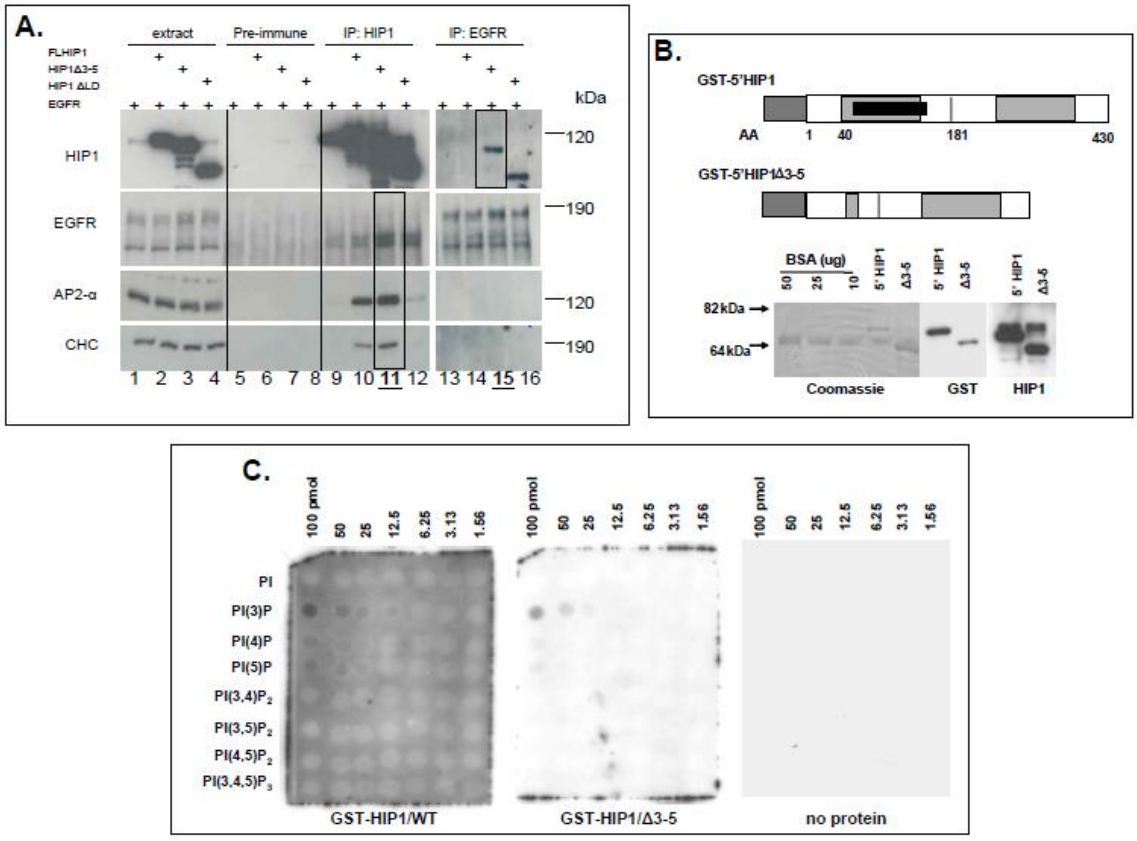

Figure 2.11: HIP1Δ3-5insAG association with clathrin, AP2, EGFR and lipids.
A. HEK 293T cells were transfected with EGFR and/or various HIP1 constructs. Cells were lysed 24 hours post-transfection and polyclonal anti-HIP1 (UM323) and anti-EGFR antibodies were used for immunoprecipitation. The immunoprecipitates were separated on 6% SDS-PAGE gels and transferred to nitrocellulose for western blot analysis using the indicated antibodies. Lanes 1-4: whole cell lysates. Lanes 5-8: Pre-immune immunoprecipitates. Lanes 9-12: anti-HIP1 immunoprecipitates. Lanes 13-16: anti-EGFR immunoprecipitates. Note the association of AP2, CHC, and EGFR with HIP1 is preserved despite deletion of sequences encoded by exons 3-5. Interestingly, the anti-EGFR antibody did not co-precipitate wild type HIP1 (top panel, lane 14) but did co-precipitate the HIP1Δ3-5 and HIP1ΔLD mutant proteins (top panel; lanes 15 and 16).
B. Schematic diagrams of GST-5'HIP1 and GST-5'HIP1/Δ3-5 fusion proteins are shown. Expression of these fusion proteins in *E. coli* BL21 was induced by treatment with 0.1 mM IPTG. The cells were pelleted and lysed, and the fusion proteins were purified from the resulting extracts using glutathione sepharose 4 beads. Ten microliters of a 1:10 dilution of the purified GST-5'HIP1 and GST-5'HIP1/Δ3-5 fusion proteins were run on a 10% polyacrylamide gel and immunoblotted with an anti-GST antibody (1:5000) or an anti-HIP1 antibody (UM354-1:2000) to ensure reaction of the proteins by the respective antibodies and to confirm their purity. Similar amounts were run on a separate 10% polyacrylamide gel along with various known concentrations of BSA, and the gel was Coomassie stained to estimate the concentrations of the purified fusion proteins.

C. Protein solutions containing 10 □g of either purified GST-5'HIP1 or GST-5'HIP1/Δ3-5 protein in TBST with 1% milk were incubated with PIP arrays (Echelon) containing various concentrations of different phosphoinositides. As with the PIP strips, both GST-5'HIP1 and GST-5'HIP1/Δ3-5 proteins bound preferentially to PtdIns(3)P. Lipid-protein interactions were detected using a polyclonal anti-GST antibody (Cell Signaling Technologies). No signal was detected using antibody alone.

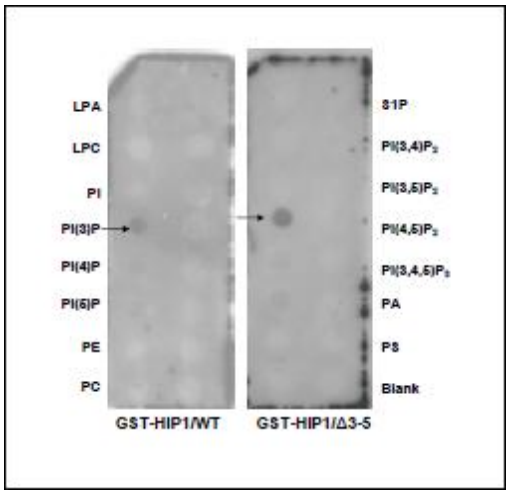

Figure 2.12: Comparison of lipid binding specificity and relative affinity GST-5'HIP1/Δ3-5 and GST-5'HIP1 using PIP strips. Protein solutions containing 10μg of either purified GST-5'HIP1 or GST-5'HIP1/Δ3-5 protein in TBST with 1% milk were incubated with PIP strips (Echelon) containing 15 different lipids at 100 pmol/spot. Lipid-protein interactions were detected using a polyclonal antibody (UM354) that recognizes both GST-5'HIP1 and GST-5'HIP1/Δ3-5 proteins. Both proteins bound preferentially to PI(3)P on the PIP strip.

References

1. Kalchman, M. A. et al. HIP1, a human homologue of S. cerevisiae Sla2p, interacts with membrane-associated huntingtin in the brain. *Nat Genet* **16**, 44-53 (1997).
2. Wanker, E. E. et al. HIP-I: a huntingtin interacting protein isolated by the yeast two-hybrid system. *Hum Mol Genet* **6**, 487-95 (1997).
3. Engqvist-Goldstein, A. E., Kessels, M. M., Chopra, V. S., Hayden, M. R. & Drubin, D. G. An actin-binding protein of the Sla2/Huntingtin interacting protein 1 family is a novel component of clathrin-coated pits and vesicles. *J Cell Biol* **147**, 1503-18 (1999).
4. Engqvist-Goldstein, A. E. et al. The actin-binding protein Hip1R associates with clathrin during early stages of endocytosis and promotes clathrin assembly in vitro. *J Cell Biol* **154**, 1209-23 (2001).
5. Hackam, A. S. et al. Huntingtin interacting protein 1 induces apoptosis via a novel caspase-dependent death effector domain. *J Biol Chem* **275**, 41299-308 (2000).
6. Legendre-Guillemin, V. et al. HIP1 and HIP12 display differential binding to F-actin, AP2, and clathrin: Identification of a novel interaction with clathrin-light chain. *J Biol Chem* (2002).
7. Metzler, M. et al. HIP1 functions in clathrin-mediated endocytosis through binding to clathrin and adaptor protein 2. *J Biol Chem* **276**, 39271-6 (2001).
8. Mishra, S. K. et al. Clathrin- and AP-2-binding sites in HIP1 uncover a general assembly role for endocytic accessory proteins. *J Biol Chem* **276**, 46230-6 (2001).
9. Rao, D. S. et al. Huntingtin interacting protein 1 Is a clathrin coat binding protein required for differentiation of late spermatogenic progenitors. *Mol Cell Biol* **21**, 7796-806 (2001).
10. Waelter, S. et al. The huntingtin interacting protein HIP1 is a clathrin and alpha-adaptin-binding protein involved in receptor-mediated endocytosis. *Hum Mol Genet* **10**, 1807-17 (2001).
11. Bradley, S. V. et al. Huntingtin interacting protein 1 is a novel brain tumor marker that associates with epidermal growth factor receptor. *Cancer Res* **67**, 3609-15 (2007).
12. Ford, M. G. et al. Simultaneous binding of PtdIns(4,5)P2 and clathrin by AP180 in the nucleation of clathrin lattices on membranes. *Science* **291**, 1051-5 (2001).
13. Itoh, T. et al. Role of the ENTH domain in phosphatidylinositol-4,5-bisphosphate binding and endocytosis. *Science* **291**, 1047-51 (2001).
14. Bradley, S. V. et al. Degenerative phenotypes caused by the combined deficiency of murine HIP1 and HIP1r are rescued by human HIP1. *Hum Mol Genet* **16**, 1279-92 (2007).
15. Metzler, M. et al. Disruption of the endocytic protein HIP1 results in neurological deficits and decreased AMPA receptor trafficking. *Embo J* **22**, 3254-3266 (2003).
16. Oravecz-Wilson, K. I. et al. Huntingtin Interacting Protein 1 mutations lead to abnormal hematopoiesis, spinal defects and cataracts. *Hum Mol Genet* **13**, 851-67 (2004).
17. Hyun, T. S. et al. Hip1-related mutant mice grow and develop normally but have accelerated spinal abnormalities and dwarfism in the absence of HIP1. *Mol Cell Biol* **24**, 4329-40 (2004).
18. Ross, T. S., Bernard, O. A., Berger, R. & Gilliland, D. G. Fusion of Huntingtin interacting protein 1 to platelet-derived growth factor beta receptor (PDGFbetaR) in chronic myelomonocytic leukemia with t(5;7)(q33;q11.2). *Blood* **91**, 4419-26 (1998).
19. Rao, D. S. et al. Huntingtin-interacting protein 1 is overexpressed in prostate and colon cancer and is critical for cellular survival. *J Clin Invest* **110**, 351-60 (2002).
20. Rao, D. S. et al. Altered receptor trafficking in Huntingtin Interacting Protein 1-transformed cells. *Cancer Cell* **3**, 471-82 (2003).
21. Bradley, S. V. et al. Aberrant HIP1 in Lymphoid Malignancies. *Cancer Res* **(In press)** (2007).
22. Greenberg, N. M. et al. Prostate cancer in a transgenic mouse. *Proc Natl Acad Sci U S A* **92**, 3439-43 (1995).
23. Bradley, S. V. et al. Serum antibodies to huntingtin interacting protein-1: a new blood test for prostate cancer. *Cancer Res* **65**, 4126-33 (2005).
24. Leder, A., Pattengale, P. K., Kuo, A., Stewart, T. A. & Leder, P. Consequences of widespread deregulation of the c-myc gene in transgenic mice: multiple neoplasms and normal development. *Cell* **45**, 485-95 (1986).

25. Higuchi, M. et al. Expression of a conditional AML1-ETO oncogene bypasses embryonic lethality and establishes a murine model of human t(8;21) acute myeloid leukemia. *Cancer Cell* **1**, 63-74 (2002).
26. Kuhn, R., Schwenk, F., Aguet, M. & Rajewsky, K. Inducible gene targeting in mice. *Science* **269**, 1427-9 (1995).
27. Patel, A. A. & Steitz, J. A. Splicing double: insights from the second spliceosome. *Nat Rev Mol Cell Biol* **4**, 960-70 (2003).
28. Gu, H., Marth, J. D., Orban, P. C., Mossmann, H. & Rajewsky, K. Deletion of a DNA polymerase beta gene segment in T cells using cell type-specific gene targeting. *Science* **265**, 103-6 (1994).
29. Hyun, T. S. et al. HIP1 and HIP1r stabilize receptor tyrosine kinases and bind 3-phosphoinositides via epsin N-terminal homology domains. *J Biol Chem* 279, 14294-306 (2004).
30. Burge, C. B., Padgett, R. A. & Sharp, P. A. Evolutionary fates and origins of U12-type introns. Mol Cell 2, 773-85 (1998).

CHAPTER 3

Persistence of Leukemia-Initiating Cells in a Novel Mouse Model of an Imatinib-Responsive Myeloproliferative Disorder

Summary

Despite remarkable responses to the tyrosine kinase inhibitor imatinib, CML patients are rarely cured by this therapy perhaps due to imatinib-refractoriness of leukemia-initiating cells (LICs). Evidence for this is limited because of poor engraftment of human CML-LICs in NOD-SCID mice and non-physiologic expression of oncogenes in retroviral transduction mouse models. To address these challenges, we generated mice bearing conditional knockin alleles of two human oncogenes: HIP1/PDGFβR (H/P) and AML1ETO (A/E). Unlike retroviral transduction, physiologic expression of H/P or A/E individually failed to induce disease, but co-expression of both H/P and A/E led to rapid onset of a fully penetrant, myeloproliferative disorder (MPD), indicating cooperativity between these two alleles. Although imatinib dramatically decreased disease burden, LICs persisted, demonstrating imatinib-refractoriness of LICs.

Introduction

A number of chromosomal translocations that contribute to leukemogenesis in humans have been identified[1]. For example, translocations that lead to the expression of a constitutively active platelet-derived growth factor beta receptor (PDGFβR) fusion

protein, such as HIP1/PDGFBR (H/P)[2], contribute to the development of chronic myelomonocytic leukemias (CMML)[3]. Although these PDGFβR-driven leukemias are clinically sensitive to imatinib therapy[4], the leukemias can still progress to acute myeloid leukemia (AML) or bone marrow failure over time. Progression to AML in chronic leukemias with tyrosine kinase mutations is associated not only with resistance to imatinib but also with additional genetic lesions such as the t(8;21)-associated AML1/ETO (A/E) fusion protein[5,6].

Molecularly-targeted cancer therapies, such as imatinib, have revolutionized patient care over the past twenty years. These drugs target molecular defects specific to cancer cells rather than simply targeting mitotically active cells. For example, the use of imatinib in CML patients has led to an enormous reduction in the five-year mortality associated with Bcr/Abl-positive CML[7]; however, only 5% of patients maintained on imatinib therapy are considered cured as defined by a molecular remission[8]. In fact, upon discontinuation of therapy, the disease aggressively relapses in the majority of patients[9]. These clinical observations suggest that while imatinib eliminates the bulk of CML cells, this drug may not eliminate the leukemia-initiating cells (LICs) that maintain the disease state.

The CML-LIC, like normal hematopoietic stem cells (HSCs), is thought to have not only the properties of self renewal and differentiation but also a relative quiescence compared to the more differentiated leukemia cells[8]. This quiescence has led to the hypothesis that the LIC is likely to be refractory to non-targeted therapies, such as chemo-or radio-therapy, which depend upon cell division for their cytotoxicity. In contrast, targeted therapies, such as imatinib, were thought to be more likely to eliminate

LICs compared to standard therapy approaches. Unfortunately, in the case of CML, the latter does not appear to be the case. Indeed, cell culture data have suggested that Bcr/Abl-expressing cells are refractory to imatinib therapy when quiescent and that awakening these cells increases their sensitivity to this drug[10]. The mechanism of this observed resistance and the *in vivo* confirmation of the relative refractoriness of CML-LICs to imatinib therapy compared to the bulk of neoplastic cells, however, has not yet been reported. These types of *in vivo* studies have been difficult to accomplish due to poor engraftment of CML LICs into NOD-SCID mice and limitations inherent in the variability associated with studying human subjects.

Modeling hematopoietic neoplasias in mice to study effects of therapies on cancer cells *in vivo* has also been challenging since the consequences of oncogene expression are different depending upon the techniques used to obtain expression. For instance, retroviral overexpression of A/E in hematopoietic cells leads to the formation of acute leukemias in some cases but not in others, and this variability may be due, in part, to expression of different isoforms[11]. This heterogeneity in outcome may also stem from variables inherent to retrovirus-mediated transduction, including copy number, expression level, integration site, the presence and identity of cooperating insertional mutations, and the identity of the infected cells. Furthermore, growth of retrovirally-infected cells may select for rare clones that have the highest levels of proliferation. In contrast to the retroviral model of A/E, Downing and colleagues developed a conditional knockin allele of A/E that was expressed from the mouse *Aml1* locus. Conditional expression of A/E under the control of native regulatory elements in the locus was never leukemogenic on its own. Treatment of disease-free conditional A/E

knockin mice with the DNA alkylating mutagen *N*-ethyl-*N*-nitrosourea (ENU) resulted in the development of acute leukemia[12]. These results suggest that the use of knockin alleles of oncogenes improves leukemia mouse modeling by achieving more realistic expression patterns; however, the A/E knockin model was still not entirely useful to leukemia investigators because these mice require unidentified cooperating mutations to develop a neoplastic phenotype.

In contrast to the existence of conditional knockin mouse models of the transcription factor oncogene A/E[12] and other transcription factor oncogenes such as the MLL translocation fusions[13,14], mouse models currently used to study tyrosine kinase oncogenes have been limited to retroviral transduction and transplantation assays[15,16], a non-targeted transgenic of BCR/ABL[17,18], and a non-conditional knockin mouse model of Flt3-Itd mutations[19,20]. Similar to the results described above for A/E, Flt3-Itd knockin animals demonstrated that knockin alleles of oncogenic tyrosine kinases likely yield different results than retrovirally-expressed alleles[19,20]. Thus, most conclusions as they relate to oncogene expression-induced leukemias to date have been based on non-physiologic expression of oncogenes. Our understanding of leukemia biology will clearly benefit from studying the consequences of oncogene expression under the control of native regulatory elements.

Since a knockin allele of an oncogenic PDGFβR kinase that is conditionally expressed under the control of native regulatory elements in adult hematopoietic progenitors is not yet available, we generated a conditional knockin allele of the H/P mutation and examined its ability to drive hematopoietic neoplasias. We postulated that this allele would not only provide us with a more realistic model of X-PDGFβR-driven

hematopoietic neoplasias for investigation of targeted therapies such as imatinib but would also serve as a mechanism to test the hypothesis that tyrosine kinase oncogenes cooperate with transcription factor oncogene knockin alleles such as A/E. Since activating mutations in the PDGFR family of receptor tyrosine kinases (c-kit, flt3, and PDGFβR) have been found concurrently with the t(8;21) mutation in AML patients[5,21], mutations in tyrosine kinase oncogenes and transcription factor oncogenes were likely to cooperate to produce the neoplastic phenotype[12]. Indeed, our studies to determine the consequences of H/P expression under the control of native regulatory elements in the adult animal provide a much improved model for characterizing tyrosine kinases in leukemogenesis and demonstrate that H/P cooperates with A/E to lead to a CML-like MPD that contains a rare population of LICs that are refractory to imatinib therapy.

Materials and Methods

Generation of Conditional H/P Knockin Mice

The conditional H/P knockin allele, *Hip1*$^{LSL\text{-}H/P}$, was generated by modifying the original H/P knockin target vector that contained a human H/P cDNA in frame with murine *Hip1* exon 2 [(22)]. Two custom vectors were constructed with desired multiple cloning sites (designated AMP1 with *Spe*I, *Eag*I, *Eco*RI, *Not*I/*Eag*I, *Bam*HI, and *Sal*I sites; and AMP2 with *Not*I, *Kpn*I, *Hin*dIII, and *Sal*I sites). The 5' *Not*I/*Bam*HI 8.2-kb fragment from the original H/P knockin vector was subcloned into the *Eag*I/*Bam*HI sites of AMP1 and named N/B7+KI. Subsequently, the *Spe*I/*Eco*RI 7.2-kb fragment from N/B7+KI was ligated into the *Eco*RI/*Eco*RI 4-kb subclone from the original HIP1/PDGFR knockin target vector and into the AMP1 vector digested with *Spe*I and *Eco*RI (named p1N/RI/RI

5’). Next, a 1.5-kb DNA fragment containing a transcription termination stop cassette flanked by *loxP* sites was inserted, as an AscI cassette, 5’ to the HIP1/PDGFR cDNA into the *Kpn*I site of HIP1’s intron 2 (*Kpn*I site modified to *Asc*I by the paired oligos: 5’–AACATTGGCGCGCCACAAGTCGTAC-3’ and 5’-GACTTGTGGCGCGCCAATGTTGTAC-3’) and designated as p1N/RI/RI 5’ stop. This stop cassette contains the SV40 polyadenylation signal, thus preventing full-length transcripts from being made until the stop cassette is removed by Cre recombinase. In addition, an ATG translation start site and 5’ splice donor are encoded to prevent correct expression of the HIP1/PDGFR fusion due to downstream transcription. The 3’ half of the target vector was constructed in the AMP2 vector by first subcloning the 4-kb HIP1 exon 6 and 7 Hind H/B subclone into the *Hin*dIII site of AMP2 (designated p2H4). A PGK-neomycin *Not*I/*Kpn*I cassette lacking *loxP* sites was generated by PCR using the original target vector as a template and the following primers: 5’-TTTGCGGCCGCTAGGTCTGAAGAGGAGTTTAC-3’ and 5’-TTTGGTACCATTAAGGGTTCCGGATCGATC-3’. This *Not*I/*Kpn*I neo PCR product was subcloned into p2H4 5’ of the HIP1 genomic DNA (named p3H4neo). The final conditional H/P knockin target vector was generated by subcloning the p3H4neo *Not*I/*Sal*I 5.5-kb fragment into the corresponding sites in p1N/RI/RI5’stop so as to fuse the neomycin resistance cassette and HIP1 3’ genomic DNA to the 3’ end of the polyadenylation signal for the H/P cDNA. The final targeting vector was ~21.5 kb. Electroporation into ES cells and screening by Southern blot for clones that were correctly targeted with the 3’ genomic probe was performed as described[22].

Southern Blot Analysis

Southern blot analysis to distinguish the targeted *Hip1*$^{LSL-H/P}$ allele and the wild-type allele was performed with the 3' probe as described for the *Hip1*^{null} allele[22]. For recombination of the targeted allele, a hHIP1 cDNA probe ("5' probe" encompassing HIP1 sequences up to the *Eco*RI site [nt 1260]; Figure 1) was used under the same conditions as those used for the 3' genomic probe.

Double and Triple Transgenic Mice

Double transgenic Mx1-Cre;*Hip1*$^{+/LSL-H/P}$ mice were generated by crossing the *Hip1*$^{+/LSL-H/P}$ mice with mice transgenic for the Mx1-Cre gene (obtained from Jackson Labs [23]). Triple transgenic Mx1-Cre;*Hip1*$^{+/LSL-H/P}$;*Aml1*$^{+/LSL-A/E}$ mice were generated by crossing the Mx1-Cre;*Hip1*$^{+/LSL-H/P}$ mice with *Aml1*$^{+/LSL-A/E}$ mice[12]. Expression of Cre recombinase was induced by injecting mice intraperitoneally with 250 □g of pIpC (Sigma, St. Louis, MO) in a 100 ul of PBS at two-day intervals for two weeks as previously described[24]. The pIpC activates interferon which activates the Mx1 promoter. For this study a total of 69 triple transgenic mice were generated and 17 (25%) had spontaneous recombination due to endogenous interferon mediated Mx1-Cre activation. We conclude this because double knockin mice that were Mx1-Cre negative never underwent recombination. Mice were mated onto a C57Bl/6 genetic background. Mice were housed in the Unit for Laboratory Animal Medicine at the University of Michigan and were monitored regularly for evidence of disease and abnormal peripheral blood cell counts.

Hematopoietic Analysis

Induced cohorts of 22 Mx1Cre; *Hip1*$^{+/LSL-H/P}$ and 23 Mx1Cre; *Hip1*$^{+/+}$ littermate animals were bled on a monthly basis for determination of CBCs. Numbers were pooled from

each time point. Induced double H/P;A/E knockin mice were bled on a weekly basis. Blood was collected into a tube containing EDTA (Sarstad, Inc) and analyzed with an 850 HEMA-VET machine (CDC Technologies, Inc.). For the time course of peripheral smears from the double knockin mice, mice were pre-bled by sub-mandibular bleed prior to treatment with pIpC. Twenty-four hours after treatment, daily tail bleeds were initiated. Smears were stained with Wright-Giemsa. Flow cytometric analysis, methylcellulose assays, and quantitation of HSCs from bone marrow and spleen were performed as described previously [24]. The total number of $CD150^{+}CD48^{-}CD41^{-}Sca\text{-}1^{+}c\text{-}kit^{+}$ cells (HSCs) per mouse was calculated based on the frequency of this population in the bone marrow and spleen, the cellularity of the spleen and long bones, and the assumption that 15% of all bone marrow is within the long bones. Blood and other tissues do not contribute significantly to the overall size of the HSC pool.

Mouse Genotyping

Mouse tail DNA was used for PCR detection of the various germline alleles. *Hip1*$^{+/LSL\text{-}H/P}$ specific primers were 5'EcoRI (5'-CTGAGAGCCAGCGGGTTGTGCTGCAGCTGA-3') and 3'EcoR1 (5'-CTCCTTTAGCTTGCTATATCGCTGTTCATTGGC–3'). Cre allele primers were IMR567 (5'-ACCAGCCAGCTATCAACTCG-3') and IMR568 (5'-TTACATTGGTCCAGCCACC-3'). Aml1 primers were Int3.up (5'-ATCAAATGATGACGACGG-3'), Ex5.low (5'-TGATGGCTCTATGGTAGGTGG–3'), and Int4.low (5'–CAGTTTAGGAAAACGGTGG–3'). The expected product sizes for *Hip1*$^{LSL\text{-}H/P}$

and Cre products were 200 base pairs. The Aml1 expected product (Int3.up and Int4.low primer pair) was 596 base pairs and, the A/E knockin product was 378 base pairs (Ex5.low and Int4.low primer pair). Pretreatment with a "gene releaser protocol" using 5 µl of gene releaser (Bioventrue, Inc.) mixed with 2 µl (100 ng/µl; 200 ng total) DNA was performed. PCR analysis for *Hip1*$^{LSL-H/P}$ recombination to *Hip1*$^{H/P}$ (Figure 3.1G) was performed as follows. Genomic DNA was isolated from lysed peripheral blood samples or organs using standard protocols. Recombination of the floxed stop cassette was detected with the following primers: 5'-CTATCCAAGGGACCTGATGG-3' and 5'GCCAGTCCAAGGTGGATTTA -3'. The PCR conditions were as follows: 7 min at 94 ºC, 35 cycles of (30 sec at 94 ºC, 1 min at 55 ºC, 1 min at 72 ºC), and 7 min at 72ºC. The predicted recombined product was 336 base pairs, whereas the wild-type product was predicted at 200 base pairs. The non-recombined product, which contained the entire stop cassette, was 2 kilobases and not amplified under these conditions. PCR analysis for A/E recombination was performed as described previously[12].

Histology Analysis

Tissue obtained at necropsy was[25] fixed in 10% formalin/PBS. Paraffin embedding and standard hematoxylin and eosin staining were performed by the University of Michigan Comprehensive Cancer Center Research and Histology and Immunoperoxidase Laboratory Core or Histoserv, Inc. MPO staining was carried out on deparaffinized and hydrated sections (xylene followed by 100-50% EtOH). Antigen was retrieved with citrate buffer followed by incubation of the slide with 10% goat serum block and primary antibody (polyclonal anti-M PO, Abcam). Slides were blocked

for endogenous peroxidase with 0.3% peroxide. The secondary antibody was biotinylated goat anti-rabbit (1:200, Jackson Immuno Research). The signal was amplified using the ABC kit (Pierce) and visualized with the DAB kit (Vector labs). A hematoxylin counterstained. TUNEL assay was performed using the In Situ Cell Death Detection Kit (Roche), and non-specific esterase staining was achieved with the non-specific esterase staining kit (Sigma) following the manufacturers instructions.

Imatinib experiments

For the mouse treatment experiments, Imatinib mesylate capsules (Novartis, 100 mg) were crushed and dissolved in sterile PBS with 10% DMSO at a final concentration of 20 mg/mL. The solution was filtered through a 0.1 uM syringe tip filter (Millipore). Mice were injected intraperitoneally once daily with 100 mg/kg. Mice were treated in pairs (vehicle or imatinib) until a complete hematologic response (normalized WBC) was observed in the imatinib-treated mouse (7-10 days), and then both the vehicle and imatinib-treated mice bone marrow was transplanted into irradiated syngeneic lethally irradiated Ly5.2 recipient mice as described previously[24]. **ENU mutagenesis**

Seven-to eleven-week-old Mx1-Cre positive H/P or wild type mice were intraperitoneally injected 6 times with 250 μg pIpC at two day intervals. Mice were then subcutaneously injected with 4 doses of 1 μg G-CSF followed by a single IP dose of 50mg/kg ENU as described previously[12]. Mice were then observed for disease for 11 months.

Results

Generation of H/P Conditional "Knockin" Mice

To model the human t(5;7) translocation, we engineered the human H/P cDNA into the mouse *Hip1* locus downstream of a *loxP*-bracketed transcriptional stop cassette (*Hip1*$^{LSL\text{-}H/P}$, **Figure 3.1A**). This conditional knockin allele allows use of specific Cre transgenic mice to guide tissue-specific expression together with the endogenous mouse *Hip1* promoter to regulate the expression of the oncogenic fusion protein both spatially and temporally. We targeted ES cells to generate mice carrying the *Hip1*$^{LSL\text{-}H/P}$ allele (**Figure 3.1B**). *Hip1*$^{+/LSL\text{-}H/P}$ mice were born at predicted Mendelian frequency and exhibited normal growth curves; however, these mice were distinguishable from wild-type littermates by the presence of gross microopthalmia and cataracts as seen previously in the heterozygous *Hip1*$^{+/null}$ mice[22]. The *Hip1*$^{+/LSL\text{-}H/P}$ mice were crossed with transgenic Mx1-Cre mice. The Mx1 promoter is activated by interferon, which is induced by treatment with the synthetic double-stranded RNA, polyinosinic-polycytidylic acid (pIpC)[12,23,24]. The pIpC treatment leads to Cre expression in an array of hematopoietic and non-hematopoietic cells, but because the expression of the knockin allele depends on many of the natural regulatory elements of the HIP1 locus, we predicted that its expression would closely mimic that found in the original CMML patient. Southern blot analyses demonstrated that pIpC-induced recombination occurred in liver, kidney, and spleen but not in brain or testes (**Figure 3.1C**).

Absence of Neoplasia in pIpC-Induced Mx1-Cre;*Hip1*$^{+/LSL\text{-}H/P}$ Mice

Mx1-Cre;Hip1$^{+/LSL\text{-}H/P}$ and *Mx1-Cre;Hip1*$^{+/+}$ littermate controls were treated with pIpC at 6 weeks of age (n=20 for each genotype) and monitored by peripheral blood analysis for eighteen months (**Figure 3.1D**). Almost all of the animals survived to 1.5 years of age without gross evidence of disease, although two moribund pIpC-induced

Mx1Cre;Hip1$^{+/LSL\text{-}H/P}$ mice (three and nine months of age) were discovered. The three month-old had splenomegaly with a moderately effaced splenic structure (**Figure 3.1E**). The H/P fusion protein was detectable by western blot of lysates from cultured bone marrow cells from this mouse (**Figure 3.1E**, lane 2). The nine-month-old had a well-differentiated hepatocellular carcinoma (**Figure 3.1F**). Interestingly, the neoplastic liver tissue exhibited complete recombination of the *Hip1*$^{LSL\text{-}H/P}$ allele, but the kidney from this mouse maintained a 50% rate of recombination in the *Hip1*$^{LSL\text{-}H/P}$ allele (**Figure 3.1F**). The remaining mice appeared healthy up to 1.5 years of age without abnormalities in peripheral blood cell counts (data not shown).

At the experimental endpoint of 1.5 years, the mice were sacrificed and necropsied for gross abnormalities. Eight pIpC-induced Mx1-Cre;*Hip1*$^{+/LSL\text{-}H/P}$ mice (47%) and three Mx1-Cre;*Hip1*$^{+/+}$ mice (20%) were discovered to have enlarged spleens (>150 mg) upon necropsy. The histology of the enlarged spleens showed signs of myeloproliferation with enlarged red pulp. MPD was histologically diagnosed from five of the H/P (29%) and one of the wild type (7%) enlarged spleens. An additional Mx1-Cre;*Hip1*$^{+/LSL\text{-}H/P}$ mouse had a liver tumor (**Table 3.1**). Flow cytometry and methylcellulose analyses of bone marrow from the 1.5-year-old pIpC-treated *Mx1-Cre*$^{;}$*Hip1*$^{+/LSL\text{-}H/P}$ mice did not display significant abnormalities (data not shown). Excision of the floxed stop cassette was detected by PCR in hematopoietic tissue from the 1.5-year-old mice, indicating that the lack of significant disease was not due to selective loss of cells with the recombined *Hip1*$^{H/P}$ allele (**Figure 3.1G**). Since the pIpC-treated *Mx1-Cre*$^{;}$*Hip1*$^{+/LSL\text{-}H/P}$ mice did not frequently develop hematopoietic malignancies even after 1.5 years, we conclude that physiologic H/P expression is not

sufficient to cause hematopoietic transformation. These results are in contrast with evidence from models that rely on retroviral bone marrow expression of tyrosine kinase oncogenes such as Bcr/Abl[16], TEL/PDGFBR[15], and H/P (**Figure 3.2**). In these animals, these oncogenes alone efficiently induce a lethal myeloproliferative disease similar to CML.

The infrequent occurrence of neoplasms after a long latency in the mice bearing the H/P knockin allele suggests that additional genetic events are required to transform hematopoietic cells. To begin to test this hypothesis, 7-11-week-old H/P mice were mutagenized with ENU to induce secondary mutations following pIpC induction of H/P recombination. A week after pIpC induction, the mice were treated with G-CSF for four days to induce myeloid proliferation, and the following day the mice were administered a single mutagenic dose of ENU (50 mg/kg). Since this dose of ENU efficiently induces only single base mutations[26], we did not observe any neoplasias in mutagenized wild-type control animals as expected (0/12; **Table 3.1**). By contrast, 67% of the H/P-expressing mice died or developed disease by 10 months after treatment (17/24). Disease was scored as "present" when gross thymic tumors, splenomegaly, and/or spontaneous death were observed. Interestingly, histological and FACS analysis of the spleens demonstrated both myeloid and lymphoid neoplasias, suggesting that the H/P mutation does not specifically transform cells of the myeloid lineage. Finally, it remains unknown if disease penetrance in mice bearing the H/P knockin allele is modified by different genetic backgrounds since all of the studies presented here are on a pure C57/BL6 background.

CML-Like MPD in pIpC-Induced H/P;A/E Mice

The A/E mutation has been identified in many human tyrosine kinase-driven

leukemias[5,6,21]. We, therefore, tested whether conditional co-expression of the H/P and A/E fusion oncogenes from their endogenous loci in adult mice led to hematopoietic transformation. A previous report showed that Mx1-Cre-activated A/E expression from the mouse *Aml1* locus is insufficient for leukemogenesis[12,27]. Dual conditional knockin mice were generated by intercrossing Mx1-Cre;*Hip1*$^{+/LSL\text{-}H/P}$ mice with *Aml1*$^{+/LSL\text{-}A/E}$ knockin mice (**Figure 3.3A**). The double knockin Mx1-Cre transgenic uninduced H/P;A/E mice, which were genotyped at weaning, were born and survived at a significantly lower than predicted Mendelian frequency (7.5% observed vs. 12.5% expected; $p<0.001$ **Figure 3.4**), indicating some embryonic or perinatal lethality. All surviving mice, however, were developmentally normal.

To study the consequences of simultaneous H/P and A/E expression in adult bone marrow, we treated H/P;A/E mice with six doses of pIpC every other day beginning at six weeks of age. In contrast to wild-type and single knockin mice, 100% of the induced double knockin (H/P;A/E) mice developed a fully penetrant, aggressive MPD, some within days of initiation of pIpC treatment (**Figure 3.3, 3.4**). The CML-like disease was easily identifiable by severe myeloid leukocytosis (**Figure 3.3D and 3.3E**) and palpable hepatosplenomegaly as early as 72 hours following the start of pIpC induction (range 3-42 days; **Figure 3.3F**). White blood cell (WBCs) counts at the time of euthanasia were increased an average of 25-fold above wild-type levels with a range of 50-700 K/μL (**Figure 3.3E**). While the white cell differential demonstrated a reversal of the normal 1:3 neutrophil-to-lymphocyte ratio (**Figure 3.3E**, right), an increase in absolute numbers of all lineages was also observed. Compared to wild-type or single knockin animals, spleen and liver weights of diseased H/P;A/E animals were

increased ten-fold and two-fold, respectively (Figure 3.3F, left). Myeloid blasts were never observed at a frequency greater than 20% in bone marrow cytospins, precluding a diagnosis of acute leukemia (**Figure 3.4D**)[27].

In addition, histological analysis demonstrated a gross effacement of normal splenic architecture with expansion of the red pulp (comprised of sheets of mature and maturing granulocytic cells) and disappearance of organized follicles (**Figure 3.3F**, right hand panel). Mutant livers displayed similar mature myeloid cells surrounding portal cavities and infiltrating the parenchyma (**Figure 3.3F**, right hand panel). Lung sections showed infiltration of alveolar wall spaces with these same mature myeloid cells (**Figure 3.4E**). Immunohistochemical analysis demonstrated that the majority of the myeloid cells in the spleen and liver were granulocytic rather than monocytic since the cells were myeloperoxidase-positive but non-specific esterase negative (Supplemental Figure 3 and data not shown). TUNEL analysis did not demonstrate changes in the frequency of apoptotic cells. In contrast, the neoplastic cells were often positive for the proliferation marker Ki67, whereas normal spleen and liver contained only rare Ki67-positive cells (**Figure 3.5**).

While kidney, liver, and spleen displayed 50% recombination of H/P alleles in healthy single H/P knockin mice (**Figure 3.1C**), neoplastic double H/P;A/E knockin spleen samples consistently demonstrated complete recombination of the H/P allele, suggesting expansion of cells harboring the recombined allele (**Figure 3.2C**). Recombination of the H/P and A/E stop cassettes was also detected in peripheral blood by PCR (data not shown). Bone marrow cells from diseased H/P;A/E mice readily grew under monocytic (or myeloid) culture conditions, and the H/P protein was detected in

these cells by western blot (data not shown). These data indicate that simultaneous activation of the H/P and A/E oncogenes confers a selective growth advantage to hematopoietic cells.

We next examined the cellular characteristics of the spleen and bone marrow from a cohort of wild type, single knockin or double knockin mice 4-weeks post pIpC induction to more thoroughly analyze the hematopoietic neoplasias. Spleen cellularity was sharply elevated in induced H/P;A/E mice (**Figure 3.6A**), whereas bone marrow cellularity was diminished (**Figure 3.6B**). In both tissues, the frequency of Mac-1^+Gr-1^+ myeloid cells was significantly increased (**Figure 3.6A** and **B**, right hand panels). This expansion of differentiated myeloid cells was associated with a relative decrease in frequency of B, T, and erythroid cells in bone marrow and spleen (**Figure 3.7**). Although hematopoietic stem cell (HSC) frequency was significantly reduced in the bone marrow of both the single H/P knockin mice and the H/P;A/E mice (**Figure 3.6C**, left hand panel), the absolute number of HSCs in the H/P;A/E spleen was significantly increased (**Figure 3.6C**, right hand panel), consistent with the onset of extramedullary hematopoiesis, which often occurs in the context of hematopoietic malignancies. The diminished frequency of HSCs in the single H/P knockin mice was not observed in the 1.5-year old single H/P knockin mice (data not shown) and was therefore not pursued further for this study. In addition, the frequency of bone marrow cells that formed primitive GEMM colonies or GM colonies in methylcellulose was also significantly reduced by H/P;A/E induction (**Figure 3.6D**). Together, these cellular characteristics are consistent with the development of an MPD in induced H/P;A/E mice.

It is possible that the diminished bone marrow HSC frequency was due to an

intrinsic effect of oncogene expression on HSC maintenance or due to an extrinsic effect of the leukemic cells on normal HSC survival (or both). To test these possibilities in the H/P;A/E-expressing mice, we conducted a competitive bone marrow repopulation experiment. In this experiment, 1,000,000 bone marrow cells from uninduced Mx1Cre;H/P;A/E or Cre negative control mice (CD45.2) together with 500,000 wild-type cells from recipient-type bone marrow (CD45.1) were used as donor cells (**Figure 3.8A** shows schematic). Recipients (CD45.1) were analyzed for stable peripheral blood chimerism at 6 weeks post-transplant and then induced with pIpC. As expected, all of the Mx1Cre;H/P;A/E recipients developed a CML-like MPD that was grossly and histologically identical to that of the primary mice (**Figure 3.9**). Two weeks after induction (during early stages of disease), groups of mice from Mx1Cre;H/P;A/E and control transplants were euthanized, and their bone marrows were analyzed for HSC distribution (n=3 each group). For both groups, HSCs were distributed in the expected 2:1 ratio of CD45.2 donor-type to CD45.1 recipient-type (**Figure 3.8B**). However, the total numbers of recipient *and* donor-type HSCs were significantly decreased in the Mx1Cre+;H/P;A/E recipients compared to Cre-negative controls (**Figure 3.8C**). Together, these data indicate the presence of an extrinsic inhibitory effect of the H/P;A/E-expressing CML-like MPD on the HSC compartment.

We next attempted to transplant the CML-like MPD from H/P;A/E mice into secondary recipients. The direct transfer of unfractionated primary neoplastic cells from diseased H/P;A/E mice to immunocompromised or syngeneic recipient mice was highly inefficient, consistent with prior studies that have found MPDs relatively difficult to transplant[27,19,28]. For example, when sublethally irradiated (1 x 240 rad)

NOD/SCID-IL2Rγ mice were retro-orbitally injected with unfractionated bone marrow cells (2×10^6) from H/P knockin, A/E knockin, or diseased double H/P;A/E knockin animals. None of the recipients displayed evidence of disease for up to 20 weeks (data not shown). In lethally irradiated syngeneic CD45.1 recipients, up to $6x10^6$ whole bone marrow cells from multiple diseased donors (n=4) were also highly inefficient at transplanting the disease (**Table 3.2**, "vehicle"). Similar results were obtained with unfractionated splenocytes. The relative inability of cells from animals with H/P;A/E-induced disease to transfer the neoplasias upon transplantation is consistent with the idea that the vast majority of CML cells have a limited capacity to proliferate[8,9,29]. Furthermore, these data also support the categorization of this hematopoietic neoplasias as a CML-like MPD rather than a transplantable leukemia[27].

To begin to identify the LIC from the diseased mice, we performed transplant experiments with FACS-purified HSCs. Although transplantation of HSCs from these mice did not transfer a florid CML-like MPD into syngeneic recipients, these cell transfers resulted in rapid death post-transplant in a high frequency of recipients (data not shown). This was despite the fact that sufficient "radioprotective" bone marrow cells were mixed with the purified HSCs for transplant success. Histological analysis of the spleens from the deceased mice that received the purified HSC transplantation demonstrated myeloid infiltrates that were consistent with an MPD. These data provide evidence that tumorigenic cells (or LICs) from the diseased H/P;A/E mice are highly enriched in the HSC fraction compared to unfractionated bone marrow or spleen.

Imatinib Treatment Reduces Leukemic Burden but Enriches LICs

To determine whether PDGFβR signaling from H/P was critical to the maintenance of the H/P;A/E-induced neoplasias, a group of diseased mice were treated with imatinib or vehicle for 10-12 days by intraperitoneal injection (n=4 imatinib, n=3 vehicle). All vehicle-treated H/P;A/E-induced mice exhibited progressive hepatosplenomegaly, effacement of splenic architecture, and myeloid infiltration of their livers and lungs. Imatinib therapy did not appear to exert any discernible effects on wild-type animals (data not shown). In contrast, imatinib treatment of H/P;A/E-induced mice led to a rapid response as evidenced by reduction of WBCs to wild-type levels (p=0.01, **Figure 3.10A**). Upon necropsy, significant decreases in spleen (p=0.0005) and liver (p=0.004) size were also observed (**Figure 3.10B** and data not shown). Histologically, splenic architecture was normalizing, and the liver appeared free of myeloid infiltrates (**Figure 3.10C**). This rapid hematological response to imatinib is consistent with that observed following imatinib treatment in humans with CML[9] and in mice with retroviral expression of tyrosine kinases such as BCR/ABL[30] and TEL/PDGFβR[15].

We next analyzed the effect of imatinib on HSC frequency in H/P;A/E mice. Compared to vehicle-treated mice, bone marrow from imatinib-treated mice displayed a restoration of nearly normal HSC frequency in bone marrow (0.0026 +/-0.0018, p=0.05; **Figure 3.10D** and data not shown). Interestingly, in contrast to the reduction observed in spleen cellularity, bone marrow cellularity was not immediately restored, presumably due to the depletion of CML-like MPD cells from the bone marrow (**Figure 3.10B**). The increase in bone marrow HSC numbers concomitant with the depletion of neoplastic cells suggests the presence of a differential effect of imatinib on bulk tumor cells as compared to HSCs.

In order to begin to determine whether imatinib affected the frequency of LICs, we transplanted unfractionated bone marrow from vehicle-or imatinib-treated H/P;A/E mice into lethally irradiated syngeneic recipients along with a radioprotective dose of 200,000 wild-type bone marrow cells. We predicted that imatinib therapy would eliminate the limited transplantability of unfractionated bone marrow. Transplants were performed after 10-12 days of imatinib therapy, when imatinib-treated mice displayed normalized WBC counts. Regardless of the transferred cell number, bone marrow cells and splenocytes from imatinib-treated mice were consistently *more* likely to transfer disease than cells from vehicle-treated mice (**Figure 3.11A, Table 3.2**). The recipient disease was grossly and histologically similar to that in the donors, and no recipients showed evidence of progression to accelerated or blast crisis phases of the disease (**Figure 3.11B**). The disease in recipient mice remained hematologically sensitive to imatinib therapy (**Figure 3.11B**), indicating that the transferred cells did not represent imatinib-resistant clones from the donor animals. The increased transplantability of bone marrow LICs in H/P;A/E mice after imatinib treatment contrasted dramatically with the reduced neoplastic burden in these mice and suggested that LICs are less sensitive to imatinib than other neoplastic cells of the MPD. Further evidence for this refractoriness of the LICs was accumulated when a rapid return of the MPD disease state was observed following withdrawal of imatinib from H/P;A/E-expressing mice that were put into remission with imatinib therapy (data not shown). For example, we have continuously treated H/P;A/E mice for up to 26 days with imatinib and found that upon withdrawal of imatinib there was a rapid return of disease.

Clear differences in long-term multilineage reconstitution activity were also

evident between recipients of vehicle-and imatinib-treated bone marrow samples (**Figure 3.11C**). Only 60% of recipients of vehicle-treated bone marrow cells showed long-term multilineage reconstitution by donor cells, confirming the decrease in HSC frequency in untreated, induced H/P;A/E mice. In contrast, almost all recipients of bone marrow cells from imatinib-treated mice showed long-term multilineage reconstitution (**Figure 3.11C**). This correlation of increased functional HSC activity (reconstitution) with the increased transplantability of the MPD in imatinib treated mice is additional evidence (to the HSC transplant data) that the LIC is contained in the HSC fraction.

Although we have not yet definitively purified the LIC in these mice, the evidence thus far indicates that LICs are found in the HSC compartment and are relatively refractory to imatinib. Interestingly, FACS-isolated HSCs from imatinib-treated mice upon transplantation into irradiated mice more frequently led to early lethality with an MPD compared to HSCs from vehicle-treated mice (data not shown), suggesting that the increased bone marrow transplantability observed in the imatinib-treated mice (**Figure 3.11**) may not just induce a change in LIC frequency but may also modulate their tumorigenicity.

A few possible mechanisms for how the LICs may be insensitive to imatinib while the bulk tumor cells readily respond to imatinib include the following: lack of expression of the H/P protein in the LICs despite recombination, extremely high levels of H/P expression that overwhelm "therapeutic" levels of the drug, or lack of addiction of these cells to H/P due to quiescence or other unknown "context" factors. We have gathered some evidence that indicates that H/P expressing cancer cells may or may not be addicted to H/P signaling depending on the milieu they are in. For example, H/P -

expressing Ba/F3 cells are sensitive to imatinib ("addicted") in the absence of IL-3; however, when IL-3 is present, the survival of these cells in the presence of imatinib is no different than wild type Ba/F3 cells (**Figure 3.12**). In this case we know that the H/P protein is expressed in the cells in the presence or absence of IL-3 so the relative resistance is not due to lack of H/P expression and instead is due to IL-3 induced environmental changes that cure the cells of their H/P addiction. Until we are able to purify enough LICs from H/P;A/E-expressing mice to characterize them, the precise mechanism of their imatinib refractoriness in vivo remains to be determined and the above list of possibilities comprise only a subset of avenues for future investigation of this complex issue.

DISCUSSION

The role of activating mutations of receptor tyrosine kinases (RTKs) in hematopoietic malignancies is well-established. PDGFβR is one such RTK that is a frequent target in myeloid leukemias. More than fifteen different translocations have been identified in human CMML patients that lead to constitutively active fusion variants of PDGFβR[31]. Accumulating evidence suggests that all PDGFR-containing translocations share many properties and are functionally interchangeable. For example, one such translocation, t(5;7)(q33;q11.2), fuses the majority of the *HIP1* gene to the transmembrane and catalytic domains of the *PDGFβR* gene[2]. Like all of the other PDGFBR fusions, the H/P fusion protein is a constitutively active tyrosine kinase that is able to transform hematopoietic cells to factor-independent growth in culture[2] and activate the PI3K, MAPK, PLC-gamma and STAT5 pathways[32]. The role of these

oncogenes *in vivo* has only been studied using the retroviral bone marrow transduction and transplantation assays. In the current study, we employed a previously described knockin strategy[12] that couples a *loxP* bracketed transcriptional stop cassette with an inducible Cre transgene to generate a mouse in which lineage-specific expression of H/P can be temporally and spatially controlled. This strategy allows us to bypass any embryonic lethality that results from the expression of H/P [22] and to directly determine the development of disease in the adult mouse in the presence or absence of other genetic lesions such as a conditional A/E knockin allele[12].

Following the generation of the *Mx1-Cre;Hip1*$^{+/LSL\text{-}H/P}$ mice, we found that these mice did not frequently develop hematopoietic malignancies following pIpC induction even after 1.5 years. H/P expression is, therefore, not sufficient to cause cancer, though a minority of mice did exhibit enlarged spleens and liver tumors suggesting that H/P expression may increase the risk of carcinogenesis. This finding contrasts starkly with bone marrow retroviral transduction and transplantation assays where retroviral expression of tyrosine kinase oncogenes such as H/P, TEL/PDGFβR[15] and BCR/ABL[16] induced a lethal myeloproliferative disease similar to CML. Importantly, since healthy, non-neoplastic tissues (kidney, liver, spleen) from pIpC-treated *Mx1-Cre*$^{;}$*Hip1*$^{+/LSL\text{-}H/P}$ mice maintained *Hip1*$^{H/P}$ alleles, the possibility that *Hip1*$^{H/P}$-containing cells were selected against over time is an unlikely explanation for the lack of disease after 1.5 years. Since use of endogenous regulatory elements to express the H/P oncogene did not lead to the myeloproliferative disease observed following retroviral expression of tyrosine kinase oncogenes, the cell type and/or oncogene levels are seemingly key variables to control when developing accurate

mouse models of human cancers.

In contrast to the finding that expression of H/P alone did not result in transformation of hematopoietic cells *in vivo*, co-induction of H/P with A/E led to a florid MPD within days of induction. The disease rapidly disseminated throughout the animals. Thus, contrary to bone marrow transduction/transplantation models of tyrosine kinase oncogene and A/E oncogene cooperation that yield prolonged disease latency and predominantly acute leukemia[15,21], this murine model provides direct evidence that expression of A/E in adult myeloid progenitors *in vivo* does not completely block differentiation but instead cooperates with H/P (and likely other PDGFβR fusion proteins) to induce an explosive myeloproliferative neoplasm. Moreover, these data confirm that A/E-induced leukemia is a multi-step process, in which secondary genetic alterations, such as H/P fusion protein generation, cooperate with A/E to induce full transformation. This report is the first to demonstrate that a human oncogene cooperates with the A/E knockin allele to produce transformation[12].

While a clear hematologic response to imatinib was observed in these double knockin mice, transplant and drug withdrawal experiments demonstrated that LICs were not eliminated by this therapy. In fact, imatinib treatment appeared to increase the disease transplantability and bone marrow reconstitution frequency (functional HSC activity) of unfractionated bone marrow. This H/P;A/E disease model highlights the need for therapies that not only target oncoproteins but also preferentially kill leukemogenic cells. The mechanism(s) of resistance of LICs to imatinib therapy is not yet understood, but possibilities such as limited expression of the oncogene, relative quiescence, or lack of addiction to the oncogene due to presence of other growth factors that support LIC

survival and proliferation are all currently under investigation.

Not only do these mice model the neoplastic role of the growing family of PDGFBR human translocations, but these animals represent the first conditional knockin model of a PDGFβR tyrosine kinase oncogene. Furthermore, these experiments provided intriguing new insights into how the different ways used to model leukemia in mice influence outcomes and conclusions. We expected that activation of a single copy of H/P cDNA knocked into the endogenous *Hip1* locus in the adult mouse would be sufficient to induce a chronic MPD. In addition, based on the report by Grisolano et al.[15,33], we expected that co-induction of A/E with this H/P allele would result in an increased frequency or severity of the H/P-induced disease and would inhibit myeloid differentiation leading to acute leukemia. To our surprise, however, a very low frequency of neoplasias was observed in the single H/P knockin mice, and a shockingly high frequency (100% penetrance) and an essentially absent disease latency of an explosive MPD (rather than acute leukemia) was observed in the double knockin mice. This observation directly counters the prevailing idea that A/E functions via prevention of hematopoietic differentiation[33]. If this notion were true, the H/P;A/E knockin mice would be immediately blastic and have impaired differentiation. These findings raise the possibility that modeling leukemogenic events under the most genetically realistic conditions may help us identify novel environmental or genetic triggers that lead to the development of CML accelerated phase or frank blast crisis.

In sum, the conditional activation of H/P in the hematopoietic system of adult mice leads to an explosive, mature, imatinib-sensitive MPD when co-expressed with A/E. Importantly, LIC activity was surprisingly enriched in induced H/P;A/E mice following

imatinib treatment as their bone marrow was able to transplant this imatinib sensitive MPD more readily than vehicle treated mice. This model will therefore serve as an invaluable tool for in depth studies of the therapeutic effect of PDGFβR (imatinib, MAPK inhibitors, rapamycin) and A/E (trichostatin A, SAHA) inhibitors as well as allow for further rigorous *in vivo* characterization of the cellular and molecular mechanisms of hematopoietic transformation and drug resistance.

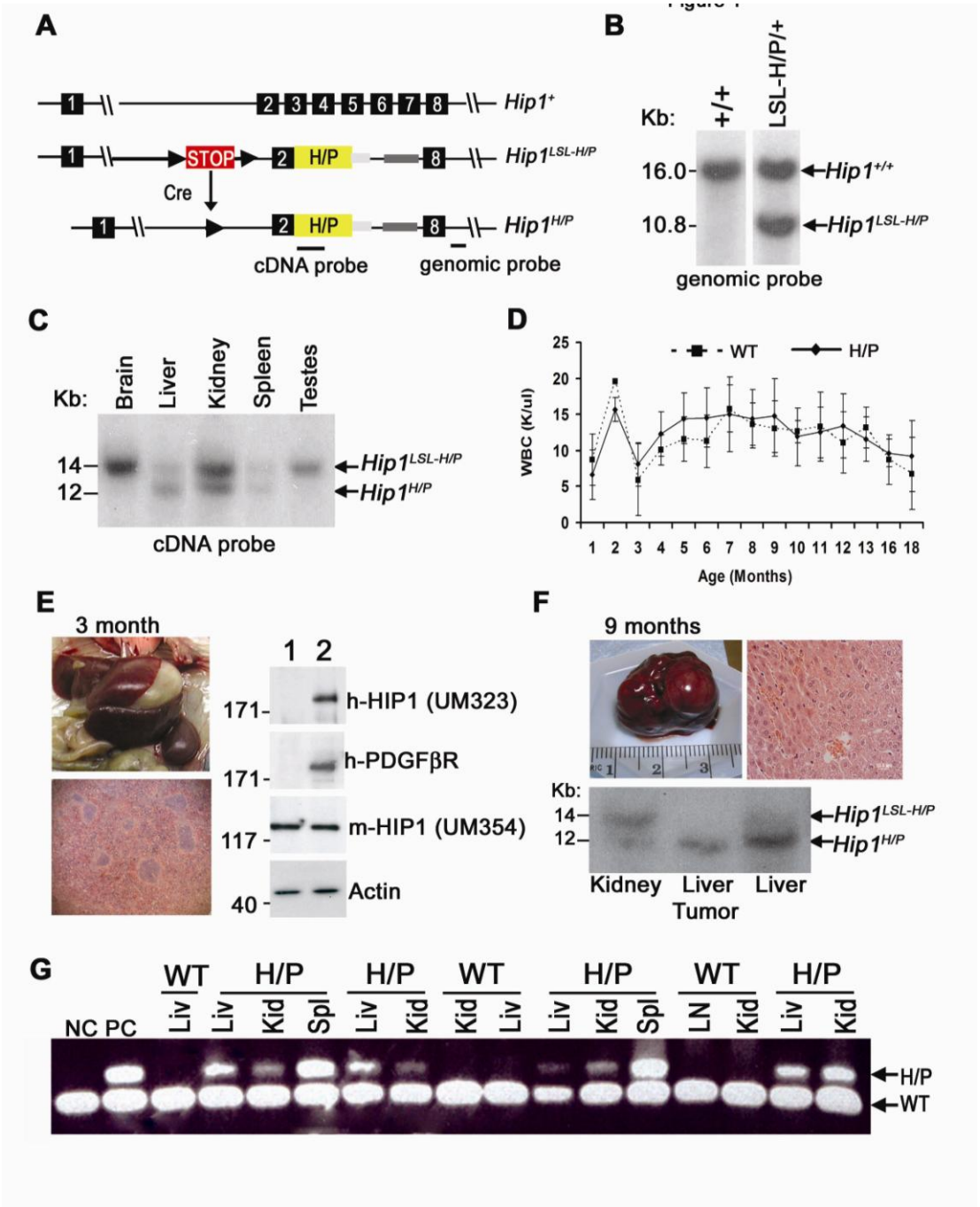
A
Hip1+
Hip1LSL-H/P
Cre
Hip1H/P
cDNA probe
genomic probe
B
Kb:
+/+
LSL-H/P/+
16.0
10.8
Hip1+/+
Hip1LSL-H/P
genomic probe
C
Kb:
Brain
Liver
Kidney
Spleen
Testes
14
12
Hip1LSL-H/P
Hip1H/P
cDNA probe
D
WT
H/P
WBC (K/ul)
Age (Months)
E
3 month
1 2
171
h-HIP1 (UM323)
171
h-PDGFβR
117
m-HIP1 (UM354)
40
Actin
F
9 months
Kb:
14
12
Hip1LSL-H/P
Hip1H/P
Kidney
Liver
Tumor
Liver
G
NC PC
WT
H/P
H/P
WT
H/P
WT
H/P
Liv
Liv
Kid
Spl
Liv
Kid
Kid
Liv
Liv
Kid
Spl
LN
Kid
Liv
Kid
H/P
WT

Figure 3.1: Phenotype of pIpC induced Mx1.Cre;*Hip1*$^{+/LSL\text{-}HP}$ mice.
(A) Schematic of the first 8 of 32 exons of the murine *Hip1* genomic locus (*Hip1*$^{+}$), the targeted *Hip1*$^{LSL\text{-}H/P}$ knockin allele generated by homologous recombination, and the activated allele with a deleted stop cassette (*Hip1*$^{H/P}$) following Cre-mediated recombination. The following features are indicated: stop cassette bracketed by *loxP* recombination sequences (LSL), partial human H/P cDNA, and cDNA or genomic hybridization probes. Just 3' of the H/P cDNA is a poly A tail (light grey box) and 3' of this was a neomycin selection cassette (dark grey box). **(B)** Southern blot analysis (genomic probe) of EcoRI-digested DNA from wild-type and Mx1Cre-*Hip1*$^{+/LSL\text{-}H/P}$ **(C)** Southern blot analysis (cDNA probe) of EcoRV-digested DNA from multiple tissues shows partial recombination in the kidney, liver and spleen and no recombination in brain or testis tissue. **(D)** Complete blood counts (CBC) from wild-type and single knockin H/P mice were normal. A cohort of pIpC treated Mx1Cre;Hip1$^{+/LSL\text{-}H/P}$ mice (n=18) and Mx1Cre;Hip1$^{+/+}$ mice (n=18) were observed until 18 months of age. Bleeds were taken pre-induction and then monthly post-induction. No significant differences were observed between the two groups in WBC counts or any shifts in differentials over the entire time coarse up to the final bleed. At eighteen months of age the mice were euthanized and necropsied to observe any disease either by gross observation or histologically. **(E)** Enlarged spleen (0.27gm) from the youngest morbid Mx1Cre;Hip1$^{H/P}$ (tag #1156, 3 months-old) shows myeloproliferation. Western blot analysis for H/P expression in this mouse was performed on bone marrow culture from the same mouse (lane 2) and from its control littermate (lane 1). The bone marrow cells were cultured for seven days in monocytic culture conditions prior to analysis (41). Anti-human HIP1 (UM323), anti-PDGFβR (BD Bioscience), anti-mouse HIP1 (UM354), and anti-actin (Sigma) polyclonal antibodies were used to detect the human fusion protein, endogenous mouse HIP1, and actin as indicated. **(F)** A liver tumor from a 9-month-old Mx1Cre;Hip1$^{H/P}$ mouse (tag #1151) shows a well differentiated hepatocellular carcinoma histopathology. Southern blot analysis (cDNA probe) of EcoRV-digested DNA from kidney, "normal" gross liver, and liver tumor DNA from the second pIpC induced Mx1Cre;Hip1+/LSL-H/P (H/P) mouse that was moribund and sacrificed at nine months of age. Note that the DNA from the kidney was partially recombined (50%), allowing for demonstration of both alleles, while the liver tumor is fully (100%) recombined. **(G)** Analysis for recombination in tissues from 18 month old mice demonstrates that the *Hip1*$^{H/P}$ allele was not lost over time. NC = negative control wild type DNA; PC = positive control for presence of the recombined allele. The 336 bp band is the recombined allele and the 200 bp band is the wild type allele.

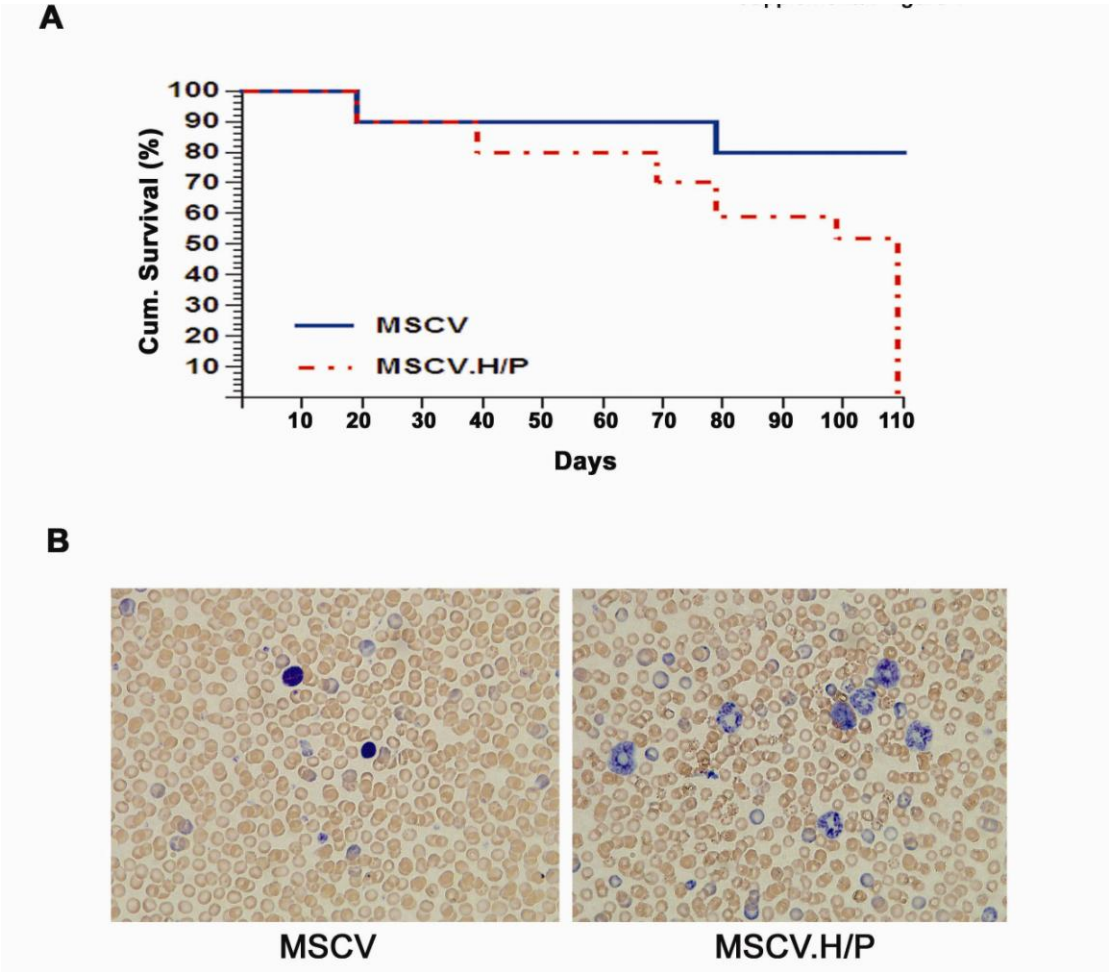

Figure 3.2: MPD results in mice transplanted with MSCV.H/P infected bone marrow.

(A) Kaplan-Meier plot demonstrating survival of mice after transplantation with bone marrow cells that express H/P. MSCV.neo represents empty vector (n=10) and MSCV.H/P is MSCV.neo with the H/P cDNA inserted after the LTR (n=10). In this experiment bone marrow cells were isolated from femurs of donor mice pretreated with 5-FU. Cells were cultured in transplant medium for 48 h. The cells were infected with two rounds of spinoculation using MSCV.neo or MSCV.H/P retroviral supernatants. Recipients were conditioned with 1,000 cGy and then transplanted with 10 million transduced bone marrow cells. **(B)** Peripheral blood smears from empty MSCV vector and MSCV.H/P retrovirally transduced and transplanted mice four weeks post transplantation. Note the increased number of mature neutrophils (ring forms) in the MSCV.H/P containing mice.

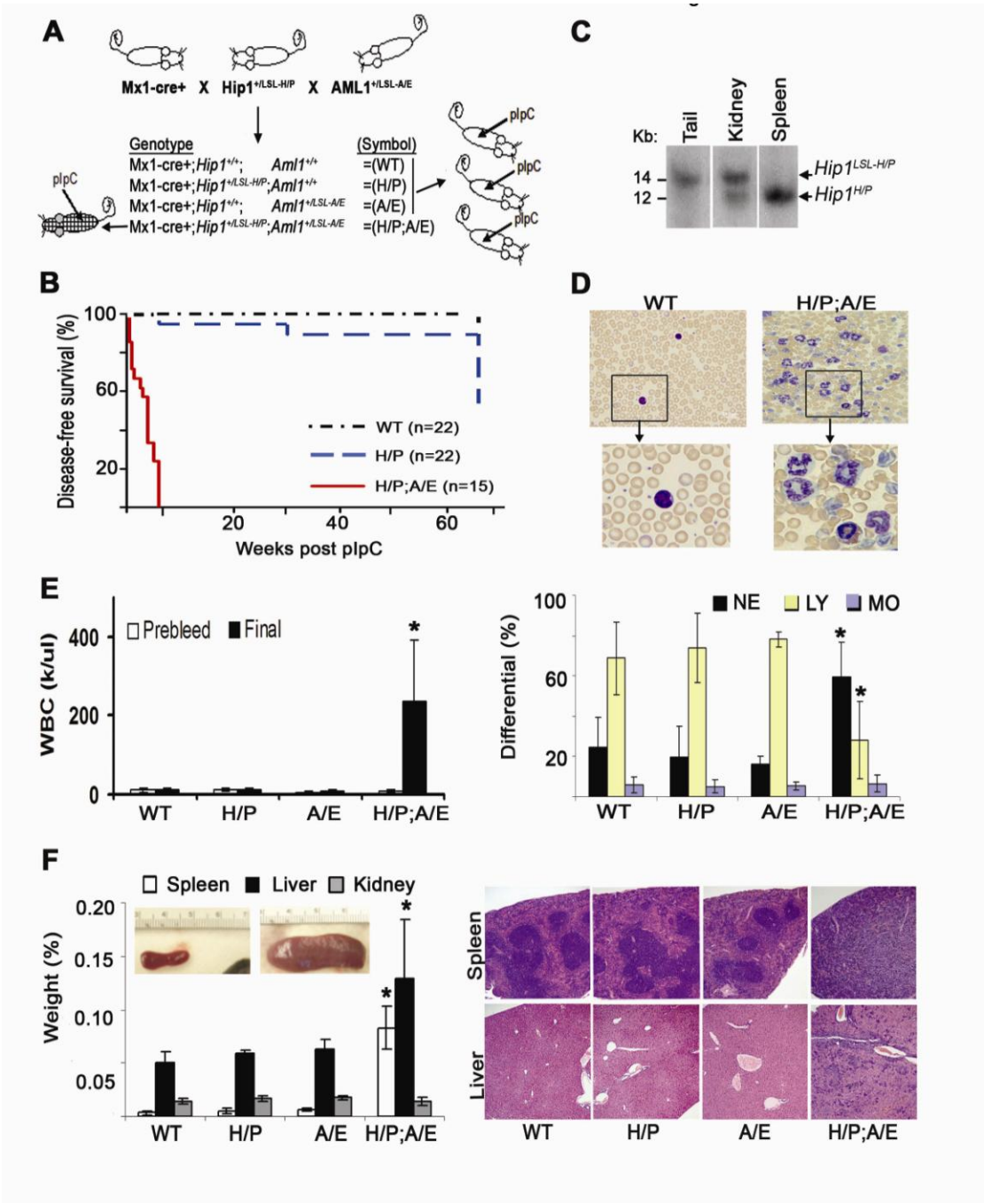
A
Mx1-cre+ X Hip1+/LSL-H/P X AML1+/LSL-A/E
Genotype
(Symbol)
Mx1-cre+;Hip1+/+; Aml1+/+ =(WT)
Mx1-cre+;Hip1+/LSL-H/P;Aml1+/+ =(H/P)
Mx1-cre+;Hip1+/+; Aml1+/LSL-A/E =(A/E)
Mx1-cre+;Hip1+/LSL-H/P;Aml1+/LSL-A/E =(H/P;A/E)
pIpC
C
Kb:
Tail
Kidney
Spleen
14
12
Hip1LSL-H/P
Hip1H/P
B
Disease-free survival (%)
100
60
20
20
40
60
Weeks post pIpC
WT (n=22)
H/P (n=22)
H/P;A/E (n=15)
D
WT
H/P;A/E
E
WBC (k/ul)
Prebleed
Final
400
200
0
WT
H/P
A/E
H/P;A/E
Differential (%)
NE
LY
MO
F
Spleen
Liver
Kidney
Weight (%)
0.20
0.15
0.10
0.05

Figure 3.3: Expression of H/P;A/E Leads to a CML-Like MPD
(A) Schematic of the mating scheme that was used to produce the double knockin mice used in this study. Also shown are the symbols used to designate the different genotypes. **(B)** The Kaplan-Meier curve depicts disease-free survival as a function of time in weeks since pIpC induction. The rapid decline in disease-free survival of H/P mice at 67 weeks reflects occult abnormalities discovered at necropsy (Table I). **(C)** Southern blot analysis (cDNA probe) of EcoRV-digested DNA from multiple tissues from a pIpC-induced H/P;A/E mouse shows no recombination in the tail, partial recombination in the kidney and complete recombination in a neoplastic spleen. **(D)** Peripheral blood smears from control (WT) and diseased mice (H/P;A/E) are represented. **(E)** Complete blood counts (CBC) from wild-type (WT; n=9), H/P (n=11), A/E (n=3), and H/P;A/E (n=8) mice were determined prior to pIpC induction (pre-bleed) and then after pIpC induction once weekly to determine onset of disease. Final WBCs at necropsy are displayed (left panel). H/P;A/E mice developed a severe myeloid leukocytosis (right panel; NE=neutrophil, LY=lymphs, MO=monocytes). Values are mean ± s.d. *denotes a significant difference ($p<0.01$) compared to WT mice. **(F)** Massive hepatosplenomegaly in H/P;A/E mice. All livers and spleens (left inset is a WT spleen, and right inset is a H/P;A/E spleen) from H/P;A/E mice were greatly enlarged at necropsy while kidneys were normal (WT n=9, H/P n=11, A/E n=3, H/P;A/E n=8; *$p<0.01$). Histological analysis of H&E-stained spleen and liver tissue from WT, H/P, A/E or H/P;A/E mice were examined (right hand panels). Magnification was 100x. Effacement of the normal follicular architecture of the spleen and infiltration of the liver was observed only in the H/P;A/E mice.

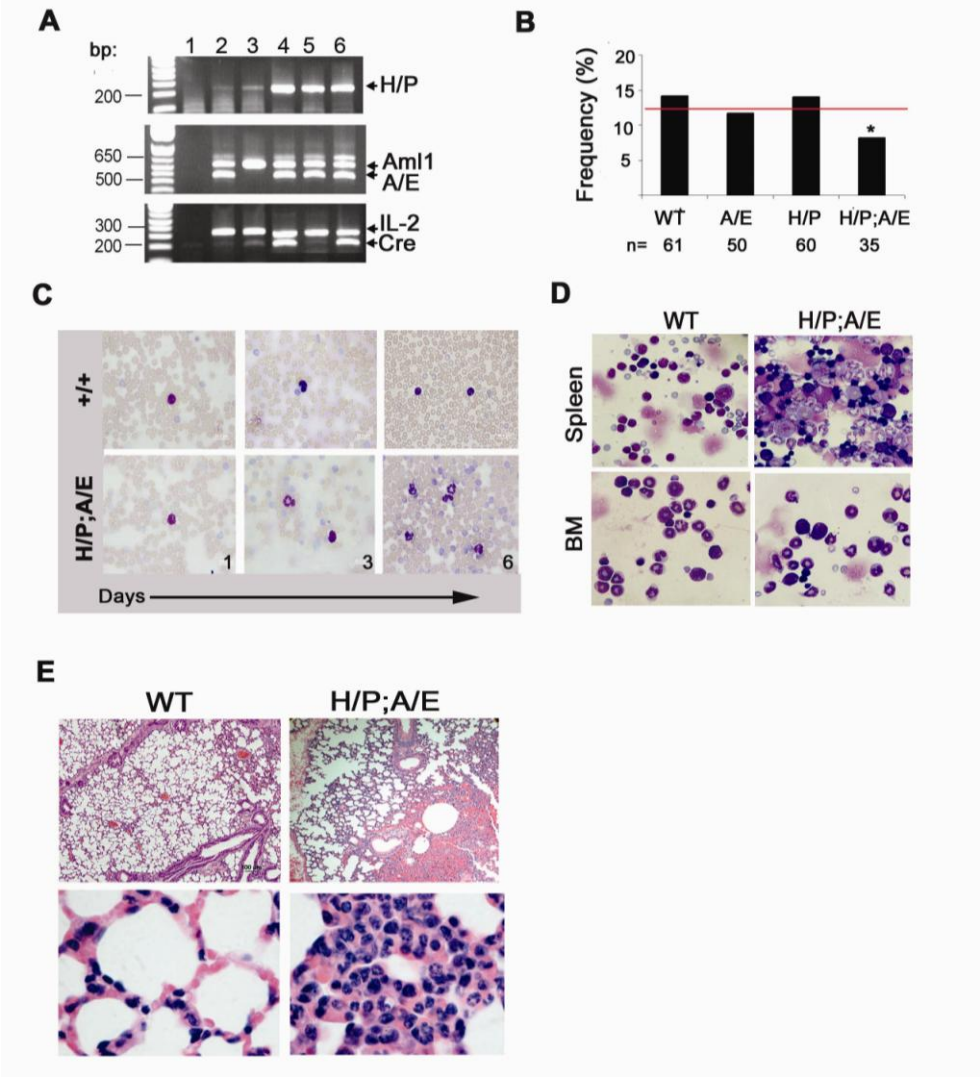

Figure 3.4: Generation and analysis of H/P;A/E-expressing mice.
(A) PCR analysis for the presence of Mx1-cre, *Aml1*$^{LSL\text{-}A/E}$ and *Hip1*$^{LSL\text{-}H/P}$ alleles in mouse tail DNA. H/P;A/E mice were successfully generated as indicated by the presence of a Cre, H/P and A/E specific PCR products in lanes 4 and 6. Lane 1 = no template control. Lanes 2, 3, and 5 lack at least one of the three mutant alleles. The IL-2 primer pair was used as an internal control for DNA quality. **(B)** Embryonic/pre-weaning lethality occurs in the Mx1-cre transgenic double knockin mice. The frequency of mice with various genotypes is displayed. The expected frequency is 12.5% in all cases. *Indicates significantly different than expected. We have observed cases (16%, 7/43) of spontaneous recombination and CML-like disease in the adult H/P;A/E animals and this phenomenon may be responsible for this pre-weaning lethality. **(C)** Daily blood smears (right hand panels show representative series from an H/P;A/E mouse) were prepared from tail bleeds and demonstrated a myeloid leukocytosis with severe neutrophilia within 6 days of initiating a 2 week course of pIpC induction. **(D)** Control (WT) and diseased H/P;A/E-expressing mice were sacrificed and 100 ul of single cell suspensions (each in a total of 3 ml of HBSS/2%FBS) of spleen and total bone marrow (two tibias and two femurs) were visualized for morphology and density after spinning the cells onto a coverslip (cytospin). **(E)** Lung tissue from the induced H/P;A/E mice was infiltrated with leukemia cells.

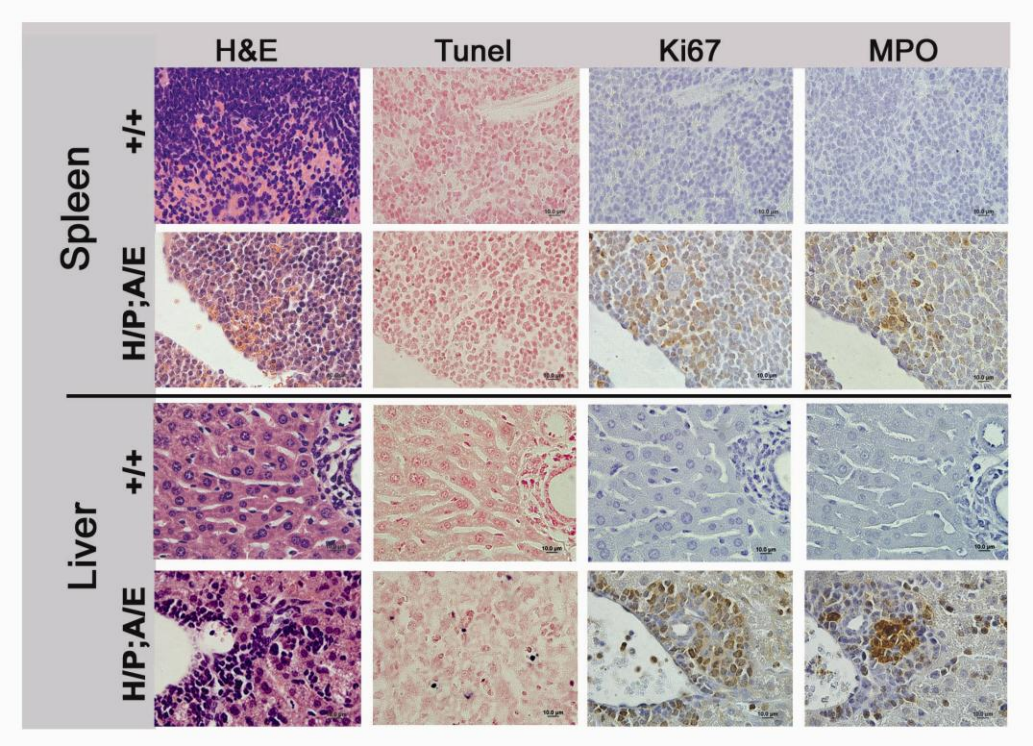

Figure 3.5: Histology of H/P;A/E induced MPD
Spleen and liver tissues from wild-type and double knockin mice were embedded in paraffin. H/E, MPO, Ki67, and TUNEL staining was then performed. 400x magnified images are displayed.

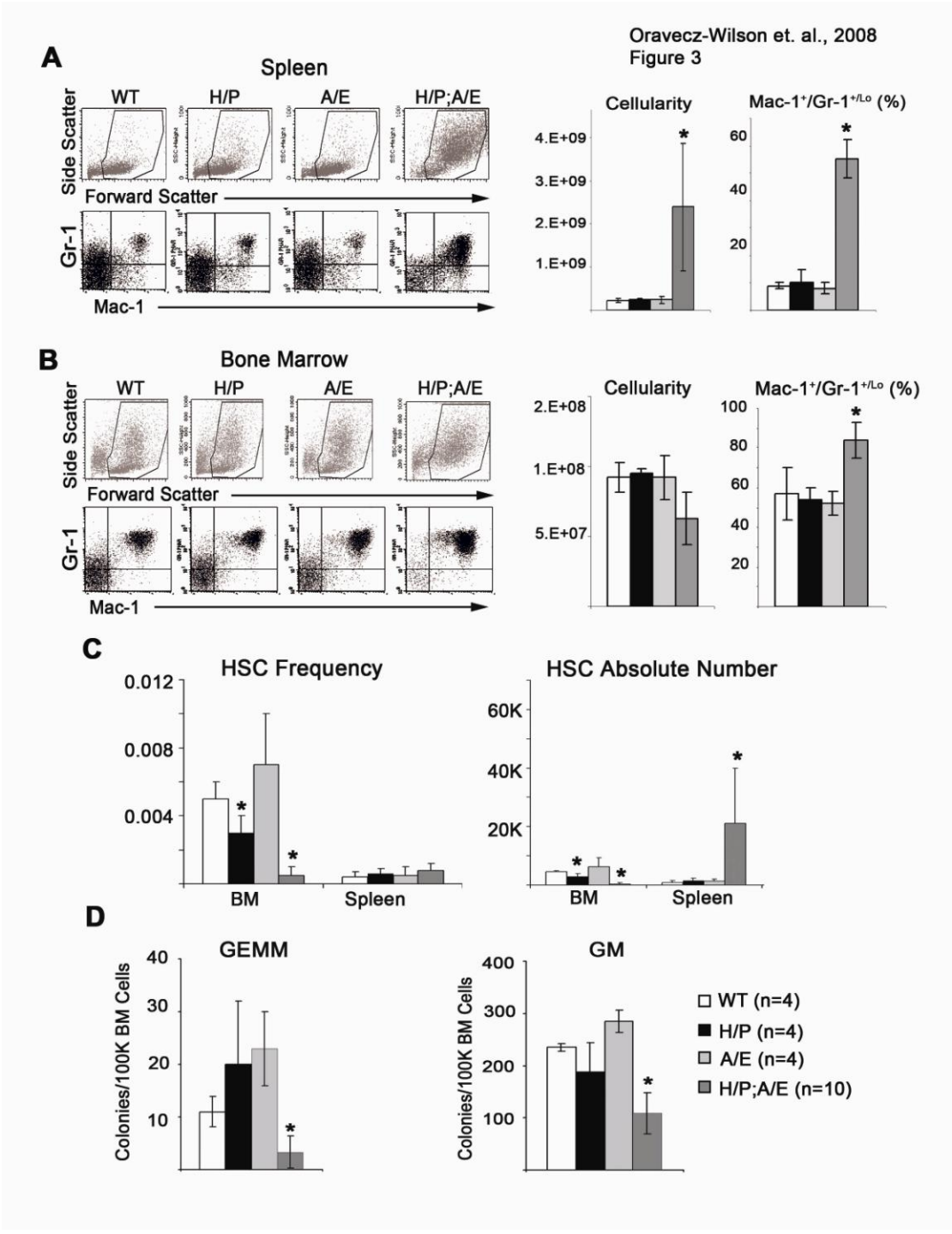
Oravecz-Wilson et. al., 2008
Figure 3
A
Spleen
WT
H/P
A/E
H/P;A/E
Side Scatter
Forward Scatter
Gr-1
Mac-1
Cellularity
Mac-1+/Gr-1+/Lo (%)
4.E+09
3.E+09
2.E+09
1.E+09
60
40
20
B
Bone Marrow
2.E+08
1.E+08
5.E+07
100
80
60
40
20
C
HSC Frequency
HSC Absolute Number
0.012
0.008
0.004
60K
40K
20K
BM
Spleen
D
GEMM
GM
Colonies/100K BM Cells
40
30
20
10
400
300
200
100
WT (n=4)
H/P (n=4)
A/E (n=4)
H/P;A/E (n=10)

Figure 3.6: Abnormal immunophenotype of hematopoietic cells from the bone marrow and spleen of H/P;A/E mice

Single cell suspensions of bone marrow and spleen cells from pIpC-induced Mx1-Cre transgenic mice (average 3 weeks after induction) that were either WT, H/P, A/E, or H/P;A/E were analyzed by flow cytometry. Representative flow cytometry profile of forward and side scatter of spleen cells **(A)** and bone marrow cells **(B)**. These profiles illustrate the presence of a distinct, uniform population of enlarged cells (box) in the spleen and bone marrow of H/P;A/E mice. Representative profile of the myeloid immunophenotype illustrates a significant increase in both mature granulocytic ($Gr1^+/Mac1^+$) and monocytic ($Gr1^{lo}/Mac1^+$) populations (**A, B**, left lower panels) in H/P;A/E mouse spleen and bone marrow. Values in the bar graphs are mean ± s.d. For WT (white bar), H/P (black bar), and A/E (light grey bar) mice, n=4. For H/P;A/E (dark grey bar) mice, n=10. ***** denotes a significant difference ($p<0.01$) between H/P;A/E mice and WT, H/P, or A/E mice. **(C)** The frequency of CD150+CD48-CD41-Sca-1+c-kit+ HSCs in the bone marrow of H/P;A/E (dark grey bars) mice was significantly reduced. *denotes a significant difference between H/P;A/E and WT mice ($p< 0.01$). **(D)** The frequencies of CFU-GEMM and CFU-GM colonies were significantly diminished in the bone marrow from H/P;A/E mice (dark grey bar) compared to WT (white), H/P (black) or A/E (light grey) mice.

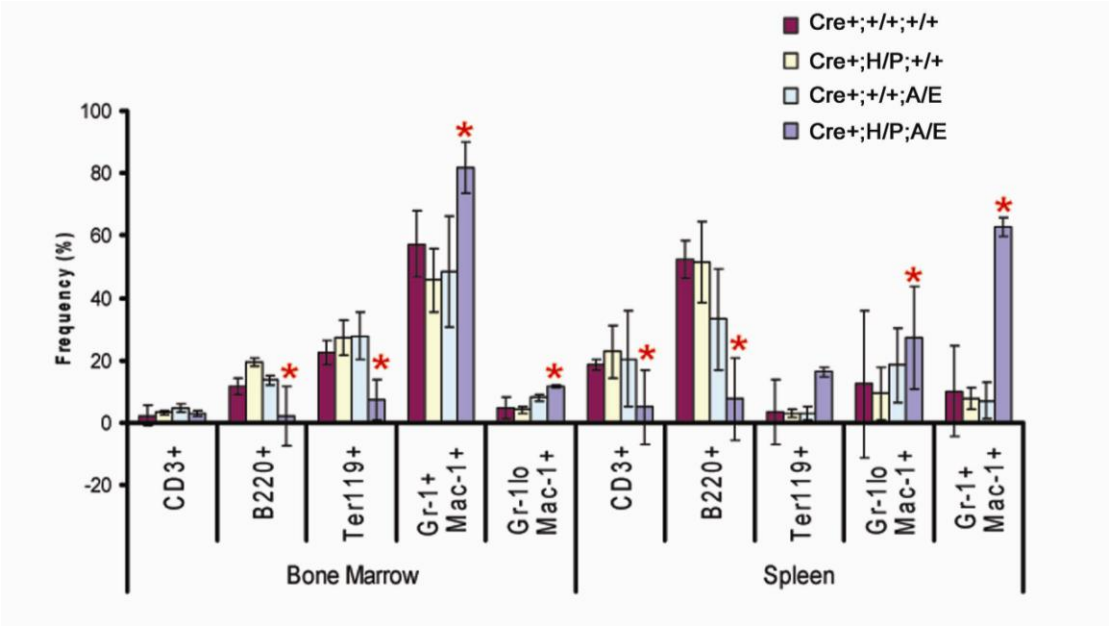

Figure 3.7: Flow cytometry analysis of bone marrow and spleen from induced Mx1-Cre;Hip1$^{LSL-H/P}$;Aml1$^{LSL-A/E}$ mice.

Mice at 6 weeks of age were induced with pIpC and two weeks later bone marrow and spleens were harvested and analyzed with FACS for various lineages as shown. Lymphoid (B220 and CD3) and erythroid (Ter119) lineages were diminished in frequency while the myeloid (Gr-1 and Mac1) lineage were increased.

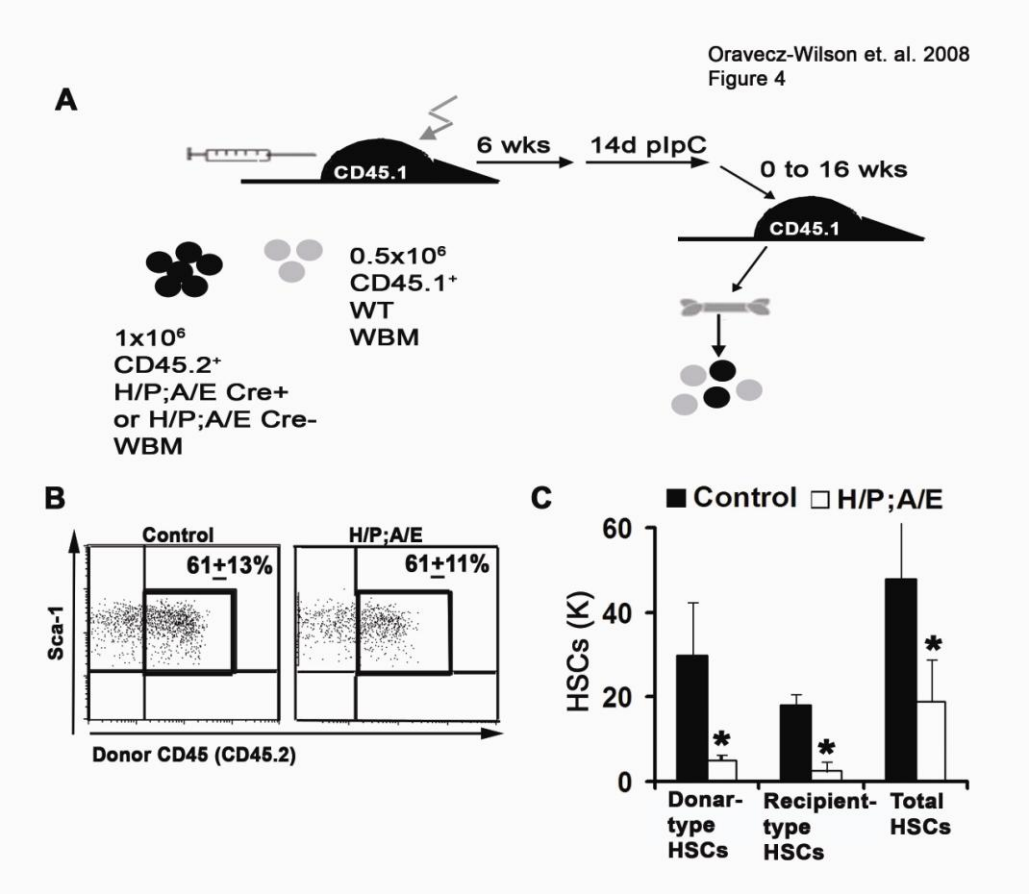

Figure 3.8. Although an H/P;A/E-expressing MPD results from an intrinsic transforming effect, there is an extrinsic inhibitory effect on normal BM HSC frequency.

(A) Irradiated (CD45.1) recipients were transplanted with twice as many donor (CD45.2) Mx1-Cre;H/P;A/E or control bone marrow cells to recipient (CD45.1) bone marrow cells. Six weeks after transplantation, recipient mice were treated with pIpC for two weeks to induce recombination. Mice were bled 4 weeks after induction to monitor disease progression. All of the mice transplanted with the Mx1-Cre;H/P;A/E bone marrow were with splenomegaly and leukocytosis similar to the primary disease whereas the H/P;A/E Cre negative donors were disease free (Supplemental Figure 5). **(B)** Cells from bone marrow 4 weeks post pIpc induction were analyzed for frequency of CD150+CD48-CD41-Sca-1+c-kit+ (SLAM HSCs) donor versus recipient cells. The donor cells accounted for 61% of HSCs in recipient mice as expected, whether the mice had been transplanted with control donor cells or H/P;A/E donor cells. Values represent mean ± s.d. of 3 mice per treatment. **(C)** The absolute number of both donor-type (H/P;A/E) and recipient-type (WT) HSCs decreased significantly in HP/AE recipients when compared to control recipients. The total number of HSCs (donor-type + recipient-type) was also drastically reduced. *denotes significantly different ($p<0.05$) compared to control recipients.

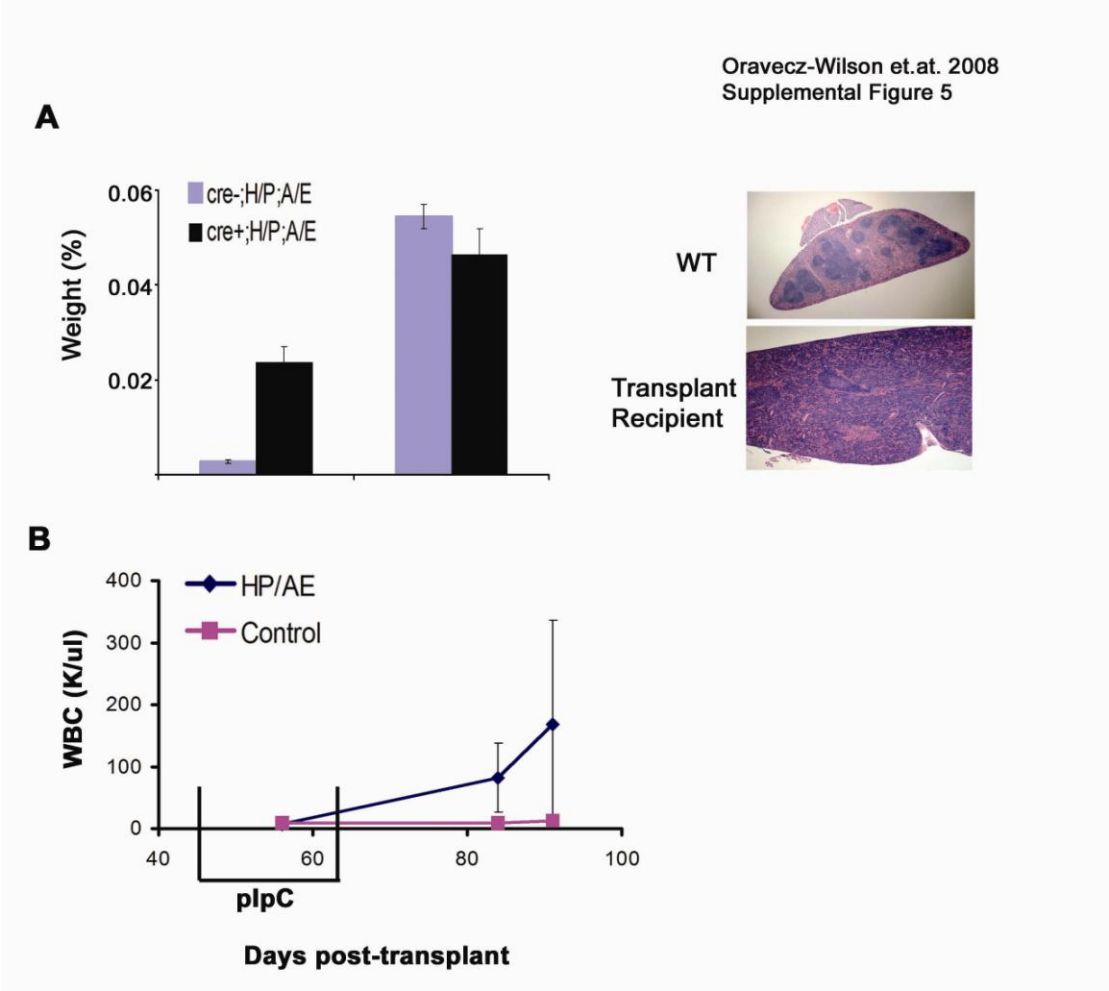

Figure 3.9. MPD results in mice transplanted with uninduced bone marrow and then treated with pIpC.

(A) Upon pIpC induction, recipients of uninduced Mx1Cre;Hip1$^{+/LSL-H/P}$;AML1$^{+/LSL-A/E}$ bone marrow develop an CML-like MPD that mimics the disease of induced primary mice. The spleens of these "pre-induction" transplant recipients are enlarged and histologically effaced (right). **(B)** WBC counts rise dramatically within 4 weeks of pI-pC induction in these mice.

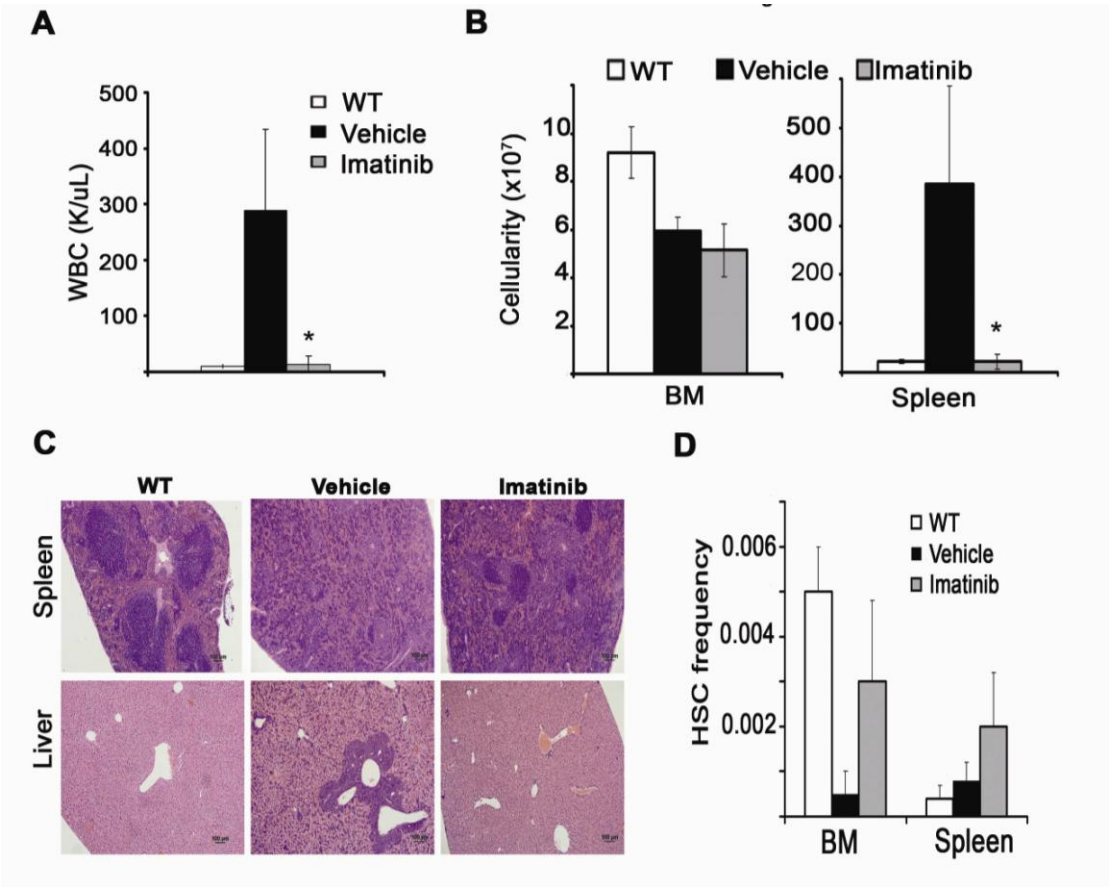

Figure 3.10: Imatinib Treatment Eliminates the Bulk of the Neoplasia
(A) Imatinib normalized WBCs after 10 days of treatment (**p*=0.01, vehicle vs. imatinib). **(B)** Imatinib-treated mice exhibited markedly reduced spleen cellularity (**p*=0.01, vehicle vs. imatinib), but bone marrow cellularity was not immediately normalized. **(C)** Imatinib treatment began to restore splenic architecture and cleared myeloid infiltrates from the liver. **(D)** The frequency of HSCs was partially rescued in the bone marrow (*p*=0.05, imatinib vs. vehicle) but not in the spleen. Splenic HSC frequency was increased in imatinib –treated mice (presumably because leukemic burden was dramatically reduced, increasing the frequency of normal HSCs in the spleen), but the difference was not statistically significant. +/+ = untreated wild-type mice (n=7); vehicle = vehicle-treated pIpC-induced H/P;A/E mice (n=3); imatinib = imatinib-treated pIpC-induced H/P;A/E mice (n=4).

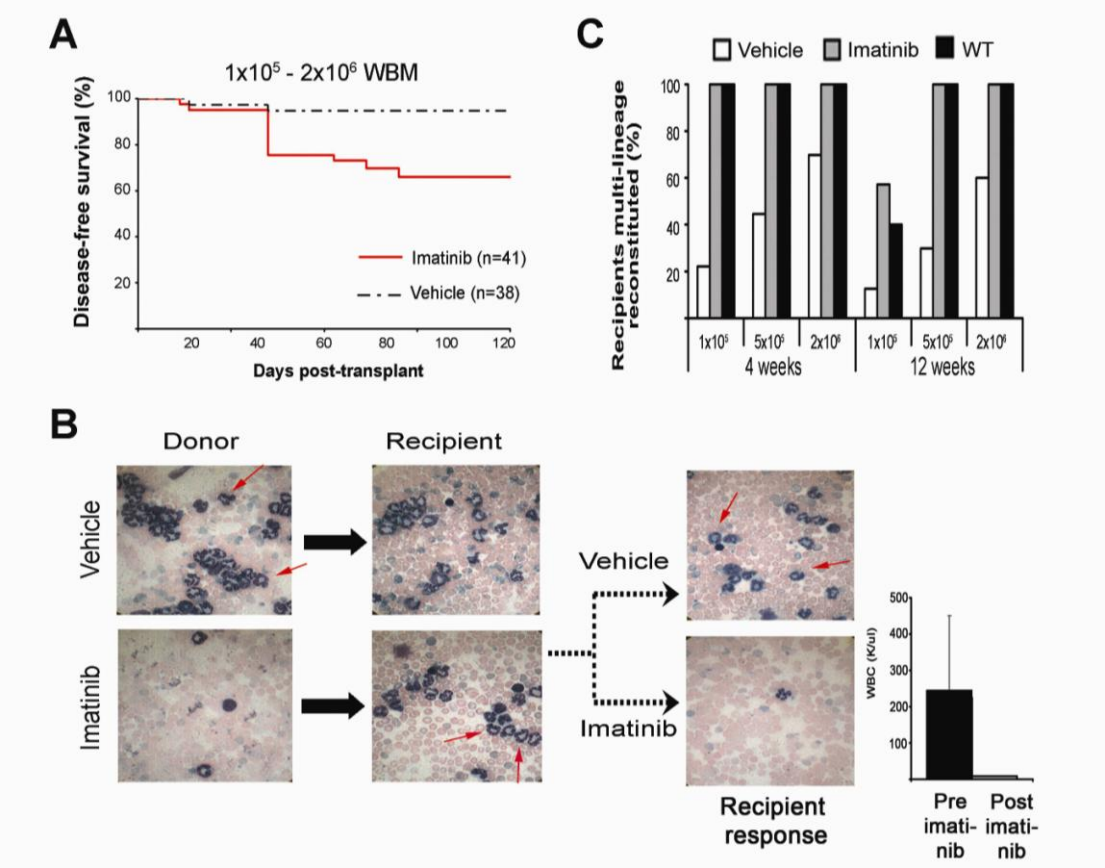

Figure 3.11: Imatinib Treatment Rescues HSC Activity but Also Increases the Frequency of LICs

(A) Graded doses of $1x10^5$ to $2x10^6$ whole bone marrow cells (WBM) from pIpC-induced H/P;A/E CD45.2 mice that were treated with vehicle (n=4 donors, 38 recipients) or imatinib (n=3 donors, 40 recipients) for 7-10 days were transplanted into lethally irradiated CD45.1 recipients along with $2x10^5$ wild-type CD45.1 bone marrow cells. Recipients of bone marrow cells from imatinib-treated mice developed CML at a greater frequency than recipients of vehicle-treated bone marrow cells. **(B)** Representative peripheral blood smears of pIpC-induced H/P;A/E donor mice treated with vehicle displayed an abundance of mature granulocytes (upper left, arrows), which were greatly reduced in imatinib-treated mice (lower left). This CML-like MPD was transplantable, with some recipients of vehicle-(middle, top) and imatinibtreated (middle, bottom) WBM developing a similar disease. Note the predominantly mature granulocytic cells in the bottom panels and the absence of blasts. The primary mice that were treated with imatinib displayed the most transplantable disease and the disease remained sensitive to imatinib treatment (right hand panels). **(C)** WBM from imatinib-treated mice more frequently gave rise to multilineage reconstitution (donor myeloid, B, and T cells) at 12 weeks post-transplantation compared to vehicle-treated mice (at 4 weeks: total n=29 for vehicle, n=27 for imatinib; at 12 weeks: total n=27 for vehicle, n=18 for imatinib). Reconstitution was defined as the presence of greater than 0.3% donor type CD45.1 marker in B (B220), T (CD3), and myeloid (Mac1, Gr1) lineages. Black bars indicate multilineage reconstitution of Cre^{neg} H/P;A/E (control) bone marrow recipients (n=15).

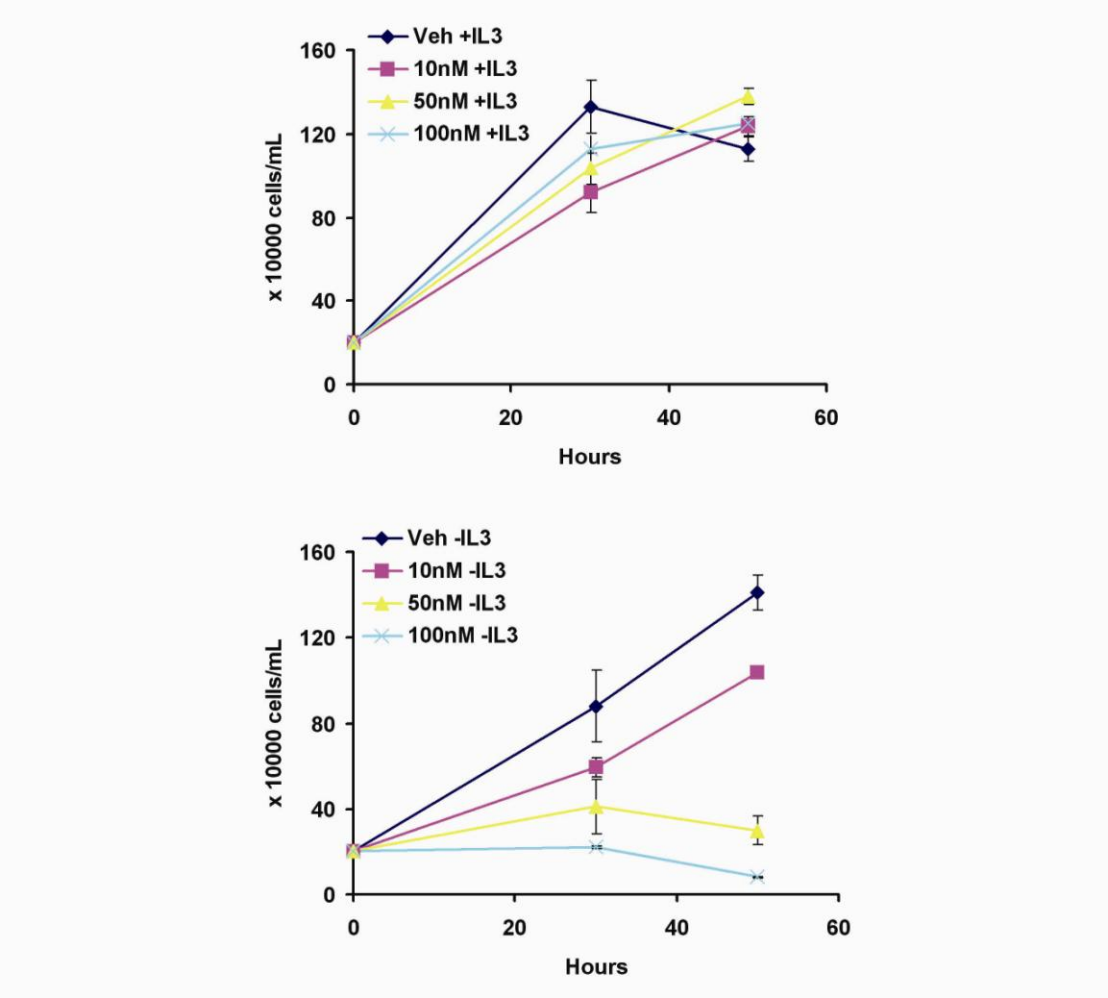

Figure 3.12. Imatinib resistance of H/P-expressing BaF3 cells in the presence of IL-3.

BaF3 cells that had been infected with MSCVneoH/P (BaF3-H/P) to transform them to IL-3 independent growth were used (Ross et al., 1997). 200,000 of the BaF3-H/P cells were plated in each well of a 12-well plate in RPMI +/-recombinant IL-3. Vehicle (DMSO) or imatinib at various concentrations in DMSO (DMSO at 0.1% final volume) was added to the different wells. Cells were counted at 30 and 50 hours by manual counting of viable cells (trypan blue exclusion microscopy). The upper panel represents cells growing in the presence of IL-3. The lower panel presents the result of cells growing in the absence of IL-3. Veh = vehicle (0.1% DMSO). 10, 50 and 100 nM = imatinib at various combinations in 0.1% DMSO.

Genotype	n[a]	Age[b]	Liver Tumor	Lethal dis.	Large Spleen (>150 mg)	Large Thymus (>100 mg)	Mesenteric Lymphoma	Total with dis.
+/+	7	<1 yr	0	0	0	0	0	0 (0%)
H/P	6	<1 yr	1	2	1	0	0	2 (33%)
+/+	15	1.5 yr	0	0	3	0	0	3 (20%)
H/P	17	1.5 yr	1	0	8	0	0	9 (53%)
ENU-Treated Mice								
+/+	12	~1 yr	0	0	0	0	0	0 (0%)
H/P	24	~1 yr	0	7	14	4	1	17 (71%)

[a] All mice were Mx-1Cre+ and pIpC treated between 6 and 11 weeks of age.
[b] At 18 months of age, although all non-ENU treated surviving mice were apparently healthy, we did discover at necropsy that 8 of 17 remaining H/P mice had enlarged spleens compared with 3 of 15 of the wild-type mice (>150 mg).

Table 3.1: Neoplasms in H/P mice

Donor Cell No.	Treatment[a]	Donor N	Recipients with Disease[b] Diseased/Total (%)
Whole Bone Marrow (WBM) Transplants			
100,000	Vehicle	2	1/8 (12%)
500,000	Vehicle	2	0/10 (0%)
2,000,000	Vehicle	3	1/14 (7%)
6,000,000	Vehicle	2	0/8 (0%)
100,000	Imatinib	3	3/14 (21%)
500,000	Imatinib	3	5/14 (36%)
2,000,000	Imatinib	3	7/13 (54%)
Hematopoietic Stem Cell (HSC) Transplants			
50	Vehicle	1	1/5 (20%)
10	Vehicle	1	3/5 (60%)
5	No Rx	1	1/7 (14%)
50	Imatinib	1	5/5 (100%)
10	Imatinib	1	5/5 (100%)

[a] H/P;A/E CML-like diseased mice were treated for 10–14 days with imatinib or vehicle prior to transplant of their bone marrow cells into lethally irradiated syngeneic recipient mice. WBM or FACS isolated HSCs were cotransplanted with 200–400,000 wild-type bone marrow cells.

[b] Fraction of recipients with overt CML-like MPD or rapid death after transplant. All of the HSC transplanted mice died rapidly after transplant and were found to have evidence of an MPD.

Table 3.2: Imatinib does not eliminate LICs from H/P;A/E induced MPD

References

1. Gilliland, D. G. Molecular genetics of human leukemias: new insights into therapy. *Semin Hematol* **39**, 6-11 (2002).
2. Ross, T. S., Bernard, O. A., Berger, R. & Gilliland, D. G. Fusion of Huntingtin interacting protein 1 to platelet-derived growth factor beta receptor (PDGFbetaR) in chronic myelomonocytic leukemia with t(5;7)(q33;q11.2). *Blood* **91**, 4419-26 (1998).
3. Grand, F. H. et al. p53-Binding protein 1 is fused to the platelet-derived growth factor receptor beta in a patient with a t(5;15)(q33;q22) and an imatinib-responsive eosinophilic myeloproliferative disorder. *Cancer Res* **64**, 7216-9 (2004).
4. Tefferi, A. & Gilliland, D. G. Oncogenes in myeloproliferative disorders. *Cell Cycle* **6**, 550-66 (2007).
5. Golub, T. R., Barker, G. F., Lovett, M. & Gilliland, D. G. Fusion of PDGF receptor beta to a novel ets-like gene, tel, in chronic myelomonocytic leukemia with t(5;12) chromosomal translocation. *Cell* **77**, 307-16 (1994).
6. Miyoshi, H. et al. t(8;21) breakpoints on chromosome 21 in acute myeloid leukemia are clustered within a limited region of a single gene, AML1. *Proc Natl Acad Sci U S A* **88**, 10431-4 (1991).
7. Druker, B. J. et al. Five-year follow-up of patients receiving imatinib for chronic myeloid leukemia. *N Engl J Med* **355**, 2408-17 (2006).
8. Kavalerchik, E., Goff, D. & Jamieson, C. H. Chronic myeloid leukemia stem cells. *J Clin Oncol* **26**, 2911-5 (2008).
9. Savona, M. & Talpaz, M. Getting to the stem of chronic myeloid leukaemia. *Nat Rev Cancer* **8**, 341-50 (2008).
10. Jorgensen, H. G. et al. Intermittent exposure of primitive quiescent chronic myeloid leukemia cells to granulocyte-colony stimulating factor in vitro promotes their elimination by imatinib mesylate. *Clin Cancer Res* **12**, 626-33 (2006).
11. Yan, M. et al. A previously unidentified alternatively spliced isoform of t(8;21) transcript promotes leukemogenesis. *Nat Med* **12**, 945-9 (2006).
12. Higuchi, M. et al. Expression of a conditional AML1-ETO oncogene bypasses embryonic lethality and establishes a murine model of human t(8;21) acute myeloid leukemia. *Cancer Cell* **1**, 63-74 (2002).
13. Cano, F., Drynan, L. F., Pannell, R. & Rabbitts, T. H. Leukaemia lineage specification caused by cell-specific Mll-Enl translocations. *Oncogene* **27**, 1945-50 (2008).
14. Chen, W. et al. Malignant transformation initiated by Mll-AF9: gene dosage and critical target cells. *Cancer Cell* **13**, 432-40 (2008).
15. Grisolano, J. L., O'Neal, J., Cain, J. & Tomasson, M. H. An activated receptor tyrosine kinase, TEL/PDGFbetaR, cooperates with AML1/ETO to induce acute myeloid leukemia in mice. *Proc Natl Acad Sci U S A* **100**, 9506-11 (2003).
16. Neering, S. J. et al. Leukemia stem cells in a genetically defined murine model of blast-crisis CML. *Blood* **110**, 2578-85 (2007).
17. Huettner, C. S., Zhang, P., Van Etten, R. A. & Tenen, D. G. Reversibility of acute B-cell leukaemia induced by BCR-ABL1. *Nat Genet* **24**, 57-60 (2000).
18. Jaiswal, S. et al. Expression of BCR/ABL and BCL-2 in myeloid progenitors leads to myeloid leukemias. *Proc Natl Acad Sci U S A* **100**, 10002-7 (2003).
19. Lee, B. H. et al. FLT3 mutations confer enhanced proliferation and survival properties to multipotent progenitors in a murine model of chronic myelomonocytic leukemia. *Cancer Cell* **12**, 367-80 (2007).
20. Li, L. et al. Knock-in of an internal tandem duplication mutation into murine FLT3 confers myeloproliferative disease in a mouse model. *Blood* **111**, 3849-58 (2008).
21. Schessl, C. et al. The AML1-ETO fusion gene and the FLT3 length mutation collaborate in inducing acute leukemia in mice. *J Clin Invest* **115**, 2159-68 (2005).
22. Oravecz-Wilson, K. I. et al. Huntingtin Interacting Protein 1 mutations lead to abnormal hematopoiesis, spinal defects and cataracts. *Hum Mol Genet* **13**, 851-67 (2004).
23. Kuhn, R., Schwenk, F., Aguet, M. & Rajewsky, K. Inducible gene targeting in mice. *Science* **269**,

1427-9 (1995).
24. Yilmaz, O. H. et al. Pten dependence distinguishes haematopoietic stem cells from leukaemia-initiating cells. *Nature* **441**, 475-82 (2006).
25. Oravecz-Wilson, K. I. et al. Persistence of leukemia-initiating cells in a conditional knockin model of an imatinib-responsive myeloproliferative disorder. *Cancer Cell* **16**, 137-48 (2009).
26. Breuer, M., Wientjens, E., Verbeek, S., Slebos, R. & Berns, A. Carcinogen-induced lymphomagenesis in pim-1 transgenic mice: dose dependence and involvement of myc and ras. *Cancer Res* **51**, 958-63 (1991).
27. Kogan, S. C. et al. Bethesda proposals for classification of nonlymphoid hematopoietic neoplasms in mice. *Blood* **100**, 238-45 (2002).
28. Sirard, C. et al. Normal and leukemic SCID-repopulating cells (SRC) coexist in the bone marrow and peripheral blood from CML patients in chronic phase, whereas leukemic SRC are detected in blast crisis. *Blood* **87**, 1539-48 (1996).
29. Sawyers, C. L., Gishizky, M. L., Quan, S., Golde, D. W. & Witte, O. N. Propagation of human blastic myeloid leukemias in the SCID mouse. *Blood* **79**, 2089-98 (1992).
30. Wolff, N. C. & Ilaria, R. L., Jr. Establishment of a murine model for therapy-treated chronic myelogenous leukemia using the tyrosine kinase inhibitor STI571. *Blood* **98**, 2808-16 (2001).
31. Curtis, C. E. et al. A novel ETV6-PDGFRB fusion transcript missed by standard screening in a patient with an imatinib responsive chronic myeloproliferative disease. *Leukemia* **21**, 1839-41 (2007).
32. Ross, T. S. & Gilliland, D. G. Transforming properties of the Huntingtin interacting protein 1/ platelet-derived growth factor beta receptor fusion protein. *J Biol Chem* **274**, 22328-36 (1999).
33. Reilly, J. T. Receptor tyrosine kinases in normal and malignant haematopoiesis. *Blood Rev* **17**, 241-8 (2003).

CHAPTER 4

Leukemia Initiating Cells revert to HSC Functionality in the Presence of Imatinib

Summary

Physiologic co-expression of the human oncogenes HIP1/PDGFβR (H/P) and AML1/ETO (A/E) from the endogenous mouse *Hip1* and *Aml1* loci results in an aggressive myeloproliferative disease (MPD)[1]. Despite a robust response to the tyrosine kinase inhibitor (TKI) imatinib mesylate, leukemia-initiating cells (LICs) persist *in vivo*. We used the H/P;A/E mouse model of MPD to investigate potential mechanisms of LIC persistence focusing on the putative necessity of oncogenic tyrosine kinase signaling for cell survival. In the presence of tyrosine kinase inhibition, LICs, which share surface marker expression with HSCs, are inhibited from generating an MPD but not from normal hematopoietic self-renewal and differentiation. Similar to *in vitro* studies with human CD34+ CML cells, imatinib induced an anti-proliferative but not an apoptotic response of H/P;A/E-LICs *in vivo*. Unlike *in vitro* data from CD34+ CML cells, mobilization of the H/P;A/E-LIC population into cell cycle did not enhance sensitivity to imatinib. These results suggest that LIC survival is independent of tyrosine kinase signaling and cannot be manipulated into kinase-addiction by mobilizing agents.

Introduction

Despite suppression of disease with targeted TKI therapy, persistence of LICs is a significant clinical problem in the treatment of CML[2]. While most CML patients achieve hematologic and cytogenetic response within 5 years of therapy, only 4% of patients achieve a major molecular response as measured by absence of BCR/ABL transcripts using quantitative RT-PCR[3]. LICs are a source of potential disease relapse as evidenced by the fact that most patients who have discontinued imatinib therapy relapse[4-6]. Persistent cells harboring leukemogenic mutations may be susceptible to further genetic instability leading to development of resistant clones and/or disease progression. Understanding the mechanism of LIC persistence is of paramount importance in developing new therapeutic strategies for elimination of LICs.

Many mechanisms of LIC persistence have been proposed, but they can be described as either kinase-dependent or kinase-independent. Kinase-dependent mechanisms assume that the LIC relies on oncogenic kinase signaling for survival and leukemogenic potential. Examples of kinase-dependent mechanisms include kinase-domain mutations, amplification of kinase transcript and reduction of intracellular TKI concentration. Kinase-independent mechanisms assume that the LIC may rely on oncogenic kinase signaling for leukemogenic potential, but not for survival. Examples of kinase-independent mechanisms include activation of other survival pathways and hijacking the normal stem cell property of quiescence.

While there is some debate regarding the identity of the LIC in CML and whether it is phenotypically distinct from the hematopoietic stem cell (HSC), it is clear that these

two cells share many properties including self-renewal, pluripotency and quiescence[7]. This last property has been proposed as a potential mechanism by which LICs evade TKI therapy. *In vitro* data using the stem cell containing $CD34^+$ fraction of human CML samples has shown that the quiescent population is insensitive to imatinib[8]. Further *in vitro* studies have shown that exposure of primitive quiescent CML cells to high growth factor conditions enhances their sensitivity to imatinib[9,10]. However, *in vivo* validation of these findings is lacking due to inadequate mouse models of CML.

We have used the H/P;A/E knockin mouse model of MPD to investigate potential mechanisms of LIC persistence. We began by further characterizing the cellular and molecular alterations induced by H/P and A/E. We then used the chimeric transplant system to functionally and phenotypically demonstrate persistence of LICs. Finally, we have used this animal model to test the hypothesis that enhanced cycling of LICs will increase their sensitivity to imatinib.

Materials and Methods

Mice and competitive transplant model

The Mx1-Cre;$Hip1^{+/LSL\text{-}H/P}$;$Aml1^{+/LSL\text{-}A/E}$ mouse has been described in the previous chapter[1]. Expression of Cre recombinase was induced by injecting mice intraperitoneally with 250 micrograms of pIpC (Sigma, St. Louis, MO) in 100 microliters of PBS at two-day intervals (6 injections total)[11]. Vav1-iCre mice were crossed with $Hip1^{+/LSL\text{-}H/P}$;$Aml1^{+/LSL\text{-}A/E}$ mutant mice. MRP8-Cre-GFP mice were generously supplied to us by Dr. Irv Weissman (Stanford University). Mice were routinely genotyped by RT-PCR (Transnetyx, Inc, Memphis, TN). All experimental mice were on a C57Bl/6 (CD45.2)

genetic background for transplant experiments. Mice were housed in the Unit for Laboratory Animal Medicine at the University of Michigan and were monitored regularly for evidence of moribundity and/or abnormal peripheral blood cell counts. For bone marrow transplant experiments, B6.SJL-Ptprc<a>Pepc<b>/BoyJ (SJL) recipient mice (CD45.1, Jackson Labs #002014) were administered 2 doses of 520 rads, separated by 3 hours. Donor cells were transplanted retro-orbitally within 24 hours of the second dose of irradiation. For HSC transplants, cells were double-sorted using a FACS-AriaII, directly into individual wells of a 96-well V-bottom plate containing $5x10^5$ SJL whole bone marrow cells per well. For analysis of engraftment, peripheral blood was collected from the submandibular plexus and analyzed for CD45.1 and CD45.2 as previously described[11].

Flow cytometry

Flow cytometric analysis (FACS), methylcellulose assays, and quantitation of HSCs from bone marrow and spleen were performed as described previously[11]. Cell analysis was carried out on a BD FACS-Canto and sorting was performed using a BD FACS-AriaII. Antibodies used for lineage exclusion were CD2, CD3, CD8, B220, ter119 and Gr1 (eBiosciences, BD Biosciences).

Cell cycle and apoptosis analysis

Testing of BrdU incorporation was performed essentially per manufacturer's instructions (BD Biosciences). Cells were stained for surface marker expression prior to fixation and DNAse treatment. Flow cytometric analysis of AnnexinV surface staining was also performed as described by the manufacturer (BD Biosciences).

Drug administration

Imatinib was administered by oral gavage twice daily separated by 8-12 hours. Each dose was 100mg/kg of IM (obtained from the clinic) dissolved in water and filtered through a 0.45 micron syringe filter. Nilotinib (Tasigna, Novartis) was dissolved in 10%NMP/90%PEG-300 and administered once daily at a dose of 100mg/kg by oral gavage. The cyclophosphamide/G-CSF protocol for HSC mobilization has been previously described[12]. Recombinant human G-CSF (Neupagen, obtained from the clinic) was administered for four consecutive days by subcutaneous injection.

Results

Sequential activation of H/P followed by A/E leads to MPD.

We have previously shown that 100% of Mx1-Cre;*Hip1*$^{\text{LSL-HP}}$;*Aml1*$^{\text{LSL-AE}}$ mice rapidly develop an aggressive MPD following simultaneous activation of the "knocked-in" human oncogenes[1]. We wondered whether the order of oncogene activation impacted the disease profile. Because heterozygous expression of A/E in the germline leads to an embryonic lethal phenotype characterized by complete absence of definitive hematopoiesis[13], we did not attempt to generate mice with an A/E germline knockin allele. As an alternative, we chose to first activate H/P in the germline and then cross this global H/P knockin with the Mx1Cre conditional knockin allele of A/E. To achieve this, we first crossed mice carrying the *Hip1*$^{\text{LSL-HP}}$ allele with the EIIA-Cre transgenic mouse (Jackson Labs). The adenovirus EIIA promoter induces Cre expression in a mosaic pattern in the early embryo, including germ cells[14]. Offspring of the EIIA-Cre;*Hip1*$^{\text{LSL-HP}}$ founders that transmitted the recombined H/P allele (but not the Cre transgene) were designated H/P knockin mice (H/P-KI). Complete excision of the transcriptional stop

cassette was confirmed by PCR in various hematopoietic and non-hematopoietic tissues (data not shown). Similar to pIpC-induced Mx1Cre-Hip1$^{LSL-H/P}$ mice, germline H/P-KI mice did not develop hematopoietic or non-hematopoietic neoplasms during a one year observation period (n=16 H/P-KI mice, **Table 4.1**). ENU mutagenesis of these H/P-KI mice led to a low frequency of tumorigenesis that was not significantly different from that observed in ENU-treated control mice (n=18). These data suggest that H/P is insufficient for tumorigenesis in hematopoietic as well as non-hematopoietic tissues. The germline H/P-KI mouse was then crossed with the Mx1-Cre;*Aml1*$^{LSL-AE}$ mouse. This triple transgenic mouse has the potential to express the H/P oncogene constitutively in all tissues and the A/E oncogene only in Mx1-restricted tissues following pIpC treatment. Following pIpC, 100% of H/P-KI;Mx1-Cre;*Aml1*$^{LSL-AE}$ mice developed an MPD characterized by hepatosplenomegaly and neutrophilic leukocytosis (n=2, **Table 4.1**). The MPD in pIpC-induced H/P-KI;Mx1-Cre;*Aml1*$^{LSL-AE}$ mice was grossly and histologically indistinguishable from the MPD in Mx1-Cre;*Hip1*$^{LSL-HP}$;*Aml1*$^{LSL-AE}$ mice. These data suggest that H/P activation preceding A/E activation in hematopoietic tissues does not influence the latency or type of myeloid leukemia that develops.

Co-activation of H/P and A/E in hematopoietic stem cells is required for development of MPD.

Upon pIpC induction, the Mx1 promoter drives expression of Cre recombinase in many hematopoietic cell types including the HSC[15]. Our previous data suggest that the LIC in the Mx1-Cre;H/P;A/E mouse MPD shares phenotypic characteristics with normal hematopoietic stem cells (HSC). To determine if activation of H/P and A/E in HSCs

rather than more differentiated cells is required for induction of MPD, we crossed the *Hip1*$^{LSL-HP}$ and *Aml1*$^{LSL-AE}$ alleles onto different Cre-transgenic backgrounds. First, we used the Vav1-iCre transgenic allele which limits Cre recombinase activity to endothelial and hematopoietic cells[16]. Vav1 regulatory elements have been shown to induce transgene expression throughout the hematopoietic system, presumably due to expression at the level of the HSC[17]. All Vav1-Cre;*Hip1*$^{LSL-HP}$;*Aml1*$^{LSL-AE}$ mice developed an MPD within 7 weeks of birth (n=3, **Table 4.1**). This MPD was characterized by hepatosplenomegaly and neutrophilic leukocytosis, similar to the Mx1-Cre induced disease. We next used the MRP8-Cre-IRES-GFP transgenic mouse which restricts Cre and GFP expression to granulocytes and a fraction of granulocyte/macrophage progenitors (GMPs) [18]. By 12 weeks of age, none of the MRP8-Cre-IRES-GFP;*Hip1*$^{LSL-HP}$;*Aml1*$^{LSL-AE}$ showed signs of disease (n=2). MRP8Cre expression was confirmed indirectly by detection of GFP fluorescence in peripheral blood leukocytes. The absence of myeloproliferation in these mice suggests that activation of the H/P and A/E oncogenes in HSCs is required for induction of the MPD.

To test the functional capacity of the stem cell compartment in diseased Mx1-Cre;*Hip1*$^{LSL-HP}$;*Aml1*$^{LSL-AE}$ mice (H/P;A/E), we conducted transplant experiments with sorted cells. Cells were sorted from the bone marrow compartment of Cre^{neg} or diseased H/P;A/E mice (C57Bl/6 strain, CD45.2, see Methods). Cells were then co-transplanted into lethally irradiated syngenic SJL recipients (SJL/J strain, CD45.1) along with a protective dose of wildtype SJL bone marrow cells. The hematopoietic stem cell population is found within Lin$^-$Sca1$^+$c-Kit$^+$ (LSK) cells, a population that includes long-term and short-term HSCs (LT-HSC, ST-HSC) as well as non self-renewing multipotent

progenitors (MPP) (**Figure 1.2**). None of the recipients of 3000 LSK cells developed disease or exhibited long-term multilineage engraftment from donor cells (**Figure 4.1A**). This suggests that LSK from the H/P;A/E induced MPD are depleted of HSC activity and are unable to transfer the MPD. As we have reported previously[1], some recipients of LT-HSCs ($CD150^{+}CD48^{-}CD41^{-}$LSK) from diseased H/P;A/E mice die with evidence of MPD early after transplant. We have confirmed this result with further transplants and also find that LT-HSCs from diseased mice form smaller colonies in methylcellulose than control LT-HSCs (**Figure 4.1B**).

Competitive transplant system to study H/P;A/E induced MPD.

We previously employed a competitive transplant system, which permits analysis of large cohorts of mice that have only a fraction of their hematopoietic cell compartment expressing the H/P and A/E oncogenes (**Figure 4.2**). This system utilizes expression of two different isotypes of the pan-hematopoietic marker CD45 (CD45.1 and CD45.2) to differentiate between recipient and donor populations. Briefly, bone marrow from uninduced Mx1-Cre;H/P;A/E (H/P;A/E) or control Cre^{neg};H/P;A/E (Cre^{neg}) mice was used as the donor population (C57Bl/6J strain, CD45.2) in a specific ratio with wildtype bone marrow (SJL strain, CD45.1) and transplanted into lethally irradiated SJL/J recipients (see figures for ratios, minimum of $5x10^5$ total cells in each independent transplant). Cre^{neg};H/P;A/E donors were chosen to control for the heterozygous state of the *Hip1* and *Aml1* loci. After a 4-6 week engraftment period, recipient mice were examined for stable multi-lineage chimerism in the peripheral blood and absence of disease. Only a small proportion of Cre^{+};H/P;A/E chimeric mice (~1%) develop

spontaneous disease (data not shown). Disease-free recipients were treated with pIpC to activate H/P and A/E expression in the donor cell population. Chimeric mice uniformly developed an MPD (range 28-56 days post pIpC), that appeared grossly and histologically similar to that of primary Mx1Cre;H/P;A/E mice. We did observe that primary mice developed more severe hepatosplenomegaly and consequently were more prone to becoming moribund. As with primary Mx1Cre;H/P;A/E mice, chimeric recipients (hereafter referred to as H/P;A/E) with MPD displayed a rapid hematologic response to imatinib therapy as depicted by the frequency of mature myeloid cells in the bone marrow (**Figure 4.3A**). White blood cells counts, spleen and liver size also returned to normal (data not shown). This chimeric system is a more accurate model of human CML than primary H/P;A/E mice because the somatic mutations are limited to a subset of hematopoietic cells. Furthermore, this system allows for the analysis of larger cohorts of mice with MPD.

As mentioned above, the H/P;A/E MPD is characterized by expansion of the mature myeloid compartment in bone marrow. When diseased H/P;A/E mice are treated with imatinib, the frequency of $Gr1^{+}Mac1^{+}$ myeloid cells in the bone marrow space returns to Cre^{neg} control levels within days (**Figure 4.3A**). The mature myeloid compartment of Cre^{neg} control mice was unaffected by short or long-term imatinib treatment (data not shown). This complete hematologic response is consistent with the therapeutic effects of imatinib therapy in human CML[2]. We have previously shown that despite this sustained hematologic response to imatinib therapy, cells capable of transplanting the MPD to syngenic recipients persist in the H/P;A/E mouse[1]. We referred

to these cells as LICs and showed that at least some of this leukemia-initiating functionality is contained within the phenotypic LT-HSC population.

Hematopoietic stem and progenitor cell abnormalities are rescued by imatinib.

To begin to determine the mechanism of this LIC persistence, we first analyzed the frequency of stem and progenitor populations in vehicle and imatinib treated H/P;A/E mice. In mouse bone marrow, myeloerythroid colony-forming potential is found among c-kit$^+$ cells that do not stain for IL7Rα or lineage markers. Self-renewing hematopoietic stem cells (HSCs) can be removed from this analysis by exclusion of Sca1$^+$ cells. This IL7Rα$^-$Lin$^-$Sca1$^-$c-Kit$^+$ (LK) population can be further separated into three distinct populations: a common myeloid progenitor (CMP) which is thought to differentiate into a granulocyte/monocyte progenitor (GMP) and a megakaryocyte/erythrocyte progenitor (MEP) (**Figure 1.2**). The separation of these myeloid progenitor subpopulations is based on CD34 and FcγRII/III expression as shown in Figure 4.1B[19]. In the H/P;A/E disease, the frequency of LK cells in WBM was slightly decreased but this was not statistically significant (**Figure 4.3C**). There were however, statistically significant changes in the frequency of myeloid progenitor subpopulations. Although the overall frequency of GMPs did not change, the CMP and MEP frequencies were reduced by 17-fold and 4-fold, respectively. Within the myeloid progenitor compartment, the proportion of CMP:MEP:GMP cells shifted dramatically and nearly 100% of LK cells expressed GMP markers (**Figure 4.3C**). Because GMPs express relatively less c-Kit than CMPs or MEPs, a decrease in overall c-Kit expression within the LK population was observed. Imatinib restored most myeloid progenitors to wild type frequencies with the exception of overall

CMP frequency which remained suppressed. However, imatinib did increase the frequency of CMPs significantly above vehicle-treated mice and it is possible that further therapy would normalize this progenitor compartment. These dramatic alterations in the myeloid progenitor compartment, particularly the increase in relative GMP frequency, suggest a key role for these cells in the maintenance of the MPD. However, the absence of a persistent defect during imatinib therapy, in addition to the absence of disease in MRP8-Cre;H/P;A/E mice, suggests that the LIC does not share phenotypic characteristics with non self-renewing myeloid progenitors.

Because of the lack of a persistent abnormal cell population in the myeloid progenitor compartment, we analyzed the hematopoietic stem cell compartment in imatinib treated mice. This population is most broadly defined as $Lin^{-}Sca1^{+}c\text{-}Kit^{+}$ (LSK) cells and includes long-term and short-term HSCs (LT-HSC, ST-HSC) as well as non self-renewing multipotent progenitors (MPP) (**Figure 1.1** and **Figure 4.4A**). Mice with the H/P;A/E induced MPD did not have a change in overall LSK frequency in the bone marrow. However, LSK cells in diseased mice had diminished c-Kit staining intensity and increased Sca1 staining relative to wildtype LSKs. While it is unclear what the functional consequences of these changes may be, it is intriguing to hypothesize that because c-Kit is a member of the same family of tyrosine kinase receptors as the PDGFβR (Type III), H/P signaling may provide negative feedback to c-Kit expression to circumvent redundant tyrosine kinase signaling. We have previously demonstrated that the H/P;A/E MPD leads to a dramatic decrease in LT-HSC frequency ($CD150^{+}CD48^{-}CD41^{-}$LSK) and that this defect is rescued by imatinib therapy[1]. Here we have confirmed this finding and have extended this analysis to include other LSK subpopulations such as

the $Flt3^{+}$LSK which represents a non-self renewing multipotent progenitor (MPP). We observed a 5-fold reduction in MPP frequency (0.155% vs. 0.03% of live bone marrow cells, $p<0.001$, **Figure 4.4B**). There was a corresponding non-significant increase in $Flt3^{-}$ LSK, a population that includes LT-HSCs and ST-HSCs (0.154% vs. 0.221%). It is possible that this shift in Flt3 expression represents a decrease in the frequency of functional MPPs (via altered stem cell differentiation). However, because Flt3 is a Type III receptor tyrosine kinase as well, it is possible that the decreased expression is due to a similar negative feedback mechanism as proposed for c-Kit. Importantly, treatment of diseased mice with imatinib for 10-36 days led to normalization of $Flt3^{+}$LSK frequencies to wild type levels (**Figure 4.4B**). We did not observe any significant alterations in the stem and myeloid progenitor cell frequencies of Cre^{neg} control mice treated with imatinib or primary Mx1-Cre;H/P or Mx1-Cre;A/E single knockin mice (data not shown).

Functional evidence for the persistence of MPD-initiating cells.

We previously utilized a transplant strategy to demonstrate persistence of LICs in the imatinib responding H/P;A/E mice. While this assay is useful for prospective isolation of putative LICs by flow cytometry, it may underestimate LIC persistence particularly if these cells are incapable of appropriate homing and engraftment. We reasoned that LIC persistence could be qualitatively ascertained by MPD relapse upon therapy withdrawal, thus avoiding a transplantation step. We withdrew imatinib therapy from a group of hematologically responding chimeric recipient mice. Within three weeks of imatinib withdrawal, there was relapse of the MPD in all mice (**Figure 4.5A**, n=8). These mice displayed progressive expansion of $Gr1^{+}Mac1^{+}$ peripheral blood leukocytes

within days after therapy withdrawal (data not shown). Mice sacrificed at 7-21 days after imatinib withdrawal had enlarged spleens relative to mice maintained on therapy. These relapsed mice also had significant decreases in LT-HSC frequency and similar myeloid progenitor alterations as observed in untreated mice (**Figure 4.5A** and data not shown). The relapsed MPD maintained sensitivity to imatinib as depicted in the sample WBC timeline for an individual mouse cycled on and off therapy (**Figure 4.5B**, left). This uniform disease relapse (and our previous data showing increased disease transplantability from imatinib treated mice) suggests that imatinib suppresses, but does not eliminate, the cell or cells that initiate and maintain the MPD. In a similar experiment, we treated chimeric recipient mice with imatinib 11 days after completion of pIpC (prior to evidence of MPD) (**Figure 4.5B**, right). All 5 mice in this suppression study maintained normal absolute white blood cell counts at 30 days after pIpC completion while 16 of 25 untreated mice developed MPD during that same period. Importantly, within 30 days of withdrawing imatinib, these mice all developed MPD. The ability of imatinib to suppress the emergence of florid MPD suggests that H/P signaling is critical for initiation of the disease.

Phenotypic evidence for the persistence of MPD-initiating cells.

Because imatinib returned stem, progenitor and mature cells populations to wildtype frequencies, we turned to the competitive transplant system to more precisely determine which donor cell types persist during imatinib therapy. Wild type C57Bl/6 (CD45.2) and wild type SJL (CD45.1) mice were analyzed in parallel to set the appropriate gates for CD45 expression. Donor chimerism was calculated by dividing the

number of CD45.2 positive cells by the total number of cells expressing either CD45 marker ([CD45.2]/[CD45.1+CD45.2]), thus excluding non-hematopoietic cells from the analysis. The sample plots shown in **Figure 4.6A** are from a 1:4 competitive transplant in which $2x10^5$ experimental WBM cells were co-transplanted with $8x10^5$ SJL WBM cells. Non-diseased Cre^{neg} control mice from that experiment demonstrated ~40% donor chimerism in WBM as well as in specific cell types analyzed. Regardless of the transplanted ratio, we consistently observed higher than expected donor chimerism (i.e. 40% vs. 20%), perhaps due to slight errors in cell counting or in slight age differences between experimental mice (age-matched) and SJL controls. Importantly, we did not observe differences in donor chimerism between Cre^{neg} and H/P;A/E prior to pIpC treatment. Following development of the MPD, H/P;A/E recipients displayed significant donor expansion of WBM (**Figure 4.6B**, black bars). This expansion was observed in mature myeloid cells ($Gr1^+Mac1^+$), myeloid-restricted progenitors (LK) and stem cells (LSK). Importantly, these mice did not have donor expansion of non-myeloid cells ($B220^+$ cells). This myeloid specific donor expansion suggests that co-expression of H/P and A/E in the HSC population shifts the balance between lymphoid and myeloid differentiation. We hypothesized that long-term treatment with imatinib would result in progressive reduction of the mutant donor cells to below Cre^{neg} control levels. Moreover, we theorized that only a rare donor-type cell would persist and that it would have the phenotypic characteristics of an HSC. To our surprise, after 14-35 days of imatinib therapy, chimeric mice maintained ~60% donor chimerism in WBM which was not significantly different from Cre^{neg} control bone marrow (**Figure 4.6B**, grey bars). While the donor chimerism of all cell types in imatinib-treated bone marrow remained slightly

higher than Cre^{neg} control donor cells, the only population that remained significantly higher than Cre^{neg} controls were the cells in the LSK compartment. Interestingly, spleen chimerism dropped significantly below Cre^{neg} levels suggesting that the spleen may be a reservoir for overproduced myeloid cells rather than the primary source of the disease. These data suggests that under the pressure of tyrosine kinase inhibition, H/P;A/E LICs are inhibited from generating the MPD but are not eliminated and in fact revert to normal HSC function. Thus, while H/P is the driver of the myeloproliferation, the LIC in the H/P;A/E MPD is not addicted to H/P signaling. In this mouse model of CML, tyrosine kinase inhibition by imatinib results in suppression of leukemogenesis but not suppression of normal hematopoiesis.

LICs do not upregulate H/P transcription to overcome imatinib.

In vivo persistence of LICs despite TKI treatment in humans is a serious problem that prevents complete remission of CML. It has not been proven definitively whether LIC persistence is due to insufficient inhibition of tyrosine kinase oncogene signaling or non-addiction of the LIC to the TK signals. The former possibility includes multiple mechanisms by which LICs can suppress or evade tyrosine kinase inhibition. One clinically relevant possibility is the emergence of point mutations that confer inhibitor resistance. In human Ph^{+} CML, the Bcr/Abl T315I mutation is a common mechanism of imatinib resistance[20]. We have demonstrated that the H/P;A/E MPD retains hematologic sensitivity to imatinib upon disease relapse. Thus, it seems more plausible that the LIC persistence in this model is a result of relative imatinib refractoriness, not resistance. One potential mechanism of refractoriness is increased production of the oncogenic kinase to

overcome small molecule inhibition. To determine if the LIC in our mouse model of CML persists secondary to increased oncogene production, we tested for H/P and A/E mRNA levels with qRT-PCR analysis of unfractionated WBM and splenocytes from imatinib treated mice. As compared to vehicle treated WBM, imatinib treated WBM expressed equal amounts of H/P transcript. However, H/P transcript levels dropped 4-fold in spleen ($p<0.05$) (**Figure 4.7**). Two conclusions can be drawn from this finding. First, oncogenic tyrosine kinase transcript is still being produced *in vivo* despite a clear hematologic response and normalization of hematopoietic stem/progenitor cell frequencies. This is further "molecular" evidence for LIC persistence consistent with the functional (Figure 3A,B) and phenotypic (Figure 3C,D) data presented earlier. Second, at the level of unfractionated hematopoietic cells, there is no obvious amplification of H/P transcript to explain imatinib refractoriness. In subsequent experiments, we have sorted LSK cells from imatinib responding mice and detected levels of H/P not significantly greater than untreated mice (data not shown).

Interestingly, we observed significant increases in A/E transcript in unfractionated WBM and spleen of mice responding to imatinib (10-fold, 8-fold respectively, $p<0.005$, **Figure 7**). In bone marrow, this corresponded with a 4-fold increase in *Aml1* transcript indicating that the Aml1 promoter itself may be activated. It is unclear whether these changes represent a numerical expansion of A/E expressing cells or an LIC-specific increase in A/E transcription. Analysis of A/E expression in different cells did not show any such changes. Regardless, these data suggest that co-existing non-tyrosine kinase abnormalities may play a role in TKI resistance/refractoriness.

LICs are not eliminated by enhanced H/P kinase inhibition.

Nilotinib is a Bcr/Abl inhibitor with 20-fold more potency against Bcr/Abl than imatinib. It is used clinically because it possesses TKI activity against common kinase domain point mutants with IM resistance[21]. It is also a potent inhibitor of PDGFβR and *in vitro* work has shown that nilotinib has a lower IC50 than imatinib in TEL/PDGFβR transformed Ba/F3 cells[22,23]. To determine if more potent inhibition of oncogenic H/P signaling would lead to enhanced LIC elimination, we treated a cohort of diseased chimeric H/P;A/E mice with nilotinib. After 21 days of therapy, nilotinib-treated mice displayed a complete hematologic response with normalization of spleen size and reduction of leukocytosis (**Figure 4.8**). Interestingly, WBC count dropped below Cre^{neg} levels suggesting more potent inhibition of myelopoiesis than imatinib. Cytometric analysis of bone marrow and spleen demonstrated reduction of $Gr1^{+}Mac1^{+}$ frequency to Cre^{neg} levels, similar to the effects observed with imatinib. Unlike the response to imatinib, we did not observe a rescue of the HSC depletion associated with the MPD. To functionally assess for elimination of the LIC(s), nilotinib therapy was withdrawn from a group of mice after 14 days of treatment. All mice in this group relapsed with MPD within 7 days of therapy withdrawal (n=3). The relapsed MPD appeared grossly and histologically similar to the un-treated disease (data not shown). We conclude from this data that more potent inhibition of H/P signaling by nilotinib is not able to effectively eliminate the LIC in this mouse model.

LICs do not maintain CD47 upregulation during imatinib treatment.

Another potential mechanism of imatinib refractoriness is LIC evasion of normal immunosurveillance. It has recently been shown that normal HSCs upregulate surface expression of the phagocytosis resistance marker CD47 in response to hematopoietic mobilizing stimuli (LPS, G-CSF etc), and that this protects HSCs from macrophage-mediated phagocytosis during peripheral migration[24]. The authors of that study hypothesized that leukemic stem cells might co-opt this normal physiologic process to evade therapy. They found CD47 up-regulated on stem, progenitor and $Mac1^{+}$ cells in an MRP8-BcrAbl/Bcl2 transgenic mouse model CML. However those mice do progress to AML and it is unclear at what stage CD47 expression was observed. To test this hypothesis in the H/P;A/E model of CML, we measured CD47-FITC fluorescence intensity on various cell populations of Cre^{neg} control mice, as well as vehicle and imatinib treated H/P;A/E mice. When normalized to Cre^{neg} control levels, we found ubiquitous up-regulation of CD47 staining intensity with the largest increase found in the LSK compartment (**Figure 4.9**, black bars, $p<0.005$ for all cell populations). However, imatinib treatment reduced CD47 expression to Cre^{neg} control levels even in the LSK population (grey bars). In fact, no unique cell population maintained significantly increased CD47 expression during imatinib treatment suggesting that protection from peripheral phagocytosis is not the principal mechanism of LIC persistence in this mouse model of CML. Because we also observed upregulation of CD47 on CD45.1 recipient cells in diseased mice, an extrinsic mobilization effect of the disease was likely (data not shown). We conclude that global upregulation of CD47 in the H/P;A/E MPD is secondary to a mobilization effect of the disease itself on the bone marrow. What cytokines are produced as a result of the disease to produce mobilization is unknown.

Clearly, immune evasion by increasing expression of CD47 is not the cause of LIC persistence in this mouse.

Imatinib inhibits hyperproliferation but does not induce apoptosis of LSK cells in H/P;A/E MPD.

Like tissue stem cells, HSCs have a robust capacity to increase their proliferative rate upon insult or injury. This capacity for increased proliferation is balanced by a relative state of quiescence during homeostasis to minimize the genetic risks associated with cell division. LICs may or may not share these properties with HSCs[25]. We hypothesized that a population of leukemogenic cells in the H/P;A/E MPD might display abnormally increased proliferative rates despite disease control with imatinib. To test this hypothesis, as well as determine the cell types that drive abnormal myeloproliferation, we tested for short-term bromodeoxyuridine (BrdU) incorporation. BrdU is incorporated into the DNA of cells in S-phase of the cell cycle and a 24 hour window of BrdU exposure has been shown to label 6% of long-term HSCs[26]. Diseased chimeric transplant recipients (Cre^{neg} or H/P;A/E) were treated for 14-35 days with vehicle or imatinib. Twenty-four hours prior to sacrifice, mice were injected intraperitoneally with 1mg of BrdU. Whole bone marrow was isolated and stained for surface markers, followed by cell fixation, DNAse treatment, BrdU labeling and flow cytometric analysis. **Figure 4.10** shows representative FACS plots of cells from Cre^{neg} control, vehicle and imatinib treated mice. We did not observe any statistically significant change in BrdU incorporation into whole bone marrow or LK cells of vehicle treated diseased mice. However, LSK cells from these mice displayed an almost 2-fold increase in BrDU incorporation ($p=0.042$)

compared to Creneg controls. This increased proliferation was observed in all of the LSK subpopulations analyzed including $Flt3^+$ and $Flt3^-$ cells as well as $CD48^+$ and $CD150^+48^-$ cells (data not shown). This indicates that a stem-like hematopoietic cell, not a myeloid progenitor, is driving the aberrant myeloproliferation. After 14 days of imatinib treatment, BrdU incorporation into LSK cells had dropped to levels not significantly different from Cre^{neg} mice. This effect was also observed after just 3 days of treatment (data not shown). There was no concurrent drop in the proliferation of non-stem progenitor cells suggesting that H/P inhibition by imatinib is specific to the stem cell compartment. Imatinib treatment did not affect the 24-hour BrdU incorporation of any Cre^{neg} cell populations. However, we did observe increased BrdU incorporation into both CD45.1 and CD45.2 cells in diseased mice, suggesting an extrinsic hyperproliferative effect (data not shown). After 7 days of imatinib withdrawal and subsequent MPD relapse, BrdU incorporation into LSK cells increased again. These short term BrdU incorporation results indicate that a cell or cells within the LSK compartment are hyperproliferative and the increased cell cycle activity is dependent on H/P signaling.

Given the striking effect of imatinib on the proliferative rate of mutant LSK cells, we wanted to know if an apoptotic response was also being evoked. *In vitro* data from human CML samples indicates that physiologic concentrations of imatinib induce cell cycle arrest without inducing apoptosis of $CD34^+$ cells[27]. We conducted AnnexinV surface staining of bone marrow cells from chimeric mice treated with imatinib for 3 days. We chose this length of therapy because proliferation of LSK was inhibited but no significant changes in gross hematologic response were detected (spleen size, WBC count). We did not observe statistically significant changes in $AnnexinV^+$ frequency in

any cell population (**Figure 4.11**). This lack of an apoptotic response is consistent with *in vitro* evidence that physiologic concentrations of imatinib are cytostatic, rather than cytotoxic.

Induction of HSC cell cycle entry by cyclophosphamide/G-CSF does not increase the ability of imatinib to eliminate LICs.

Another potential mechanism by which LICs evade TKI-mediated cell death is by "hiding" in a quiescent state similar to the mechanism by which normal HSCs avoid chemotherapeutic toxicity. It is hypothesized that in this resting state, LICs do not rely on oncogenic signaling for survival and thus are able to withstand potent kinase inhibition. We wanted to test this hypothesis by inducing LIC cell cycle entry (mobilization) and concomitantly inhibiting H/P with imatinib. Based on our previous findings that LICs share phenotypic characteristics with HSCs, we used the well-established cyclophosphamide/G-CSF regimen (Cy/G) to induce mobilization[12]. To quantify the efficacy of this therapeutic combination, we measured donor chimerism at the study endpoint. If mobilization exhibited additive effects to TKI therapy, we would expect to see a decrease in the proportion of hematopoietic cells that are derived from the mutant donor population. We were specifically interested in the effect of this combination therapy on the LSK population given our data that donor LSKs are hyperproliferative and remain significantly expanded after imatinib therapy.

Chimeric mice were induced with pIpC and, following development of MPD, were treated as depicted in **Figure 4.12A**. Mice were first treated with imatinib for 14 days and hematologic response was confirmed. Mice were then split into two arms, one

receiving mock injections, the other receiving a 5-day Cy/G regimen ("mock" and "mobilized", see Methods[12]). Imatinib was continued throughout this mock/mobilization treatment to avoid interruption of H/P inhibition. Peripheral blood analysis on the day after mobilization demonstrated significant myeloid shifts in all mice (data not shown) consistent with the ability of G-CSF to induce myeloid differentiation *in vitro/vivo*. All mice were continued on imatinib for 10 days following mobilization to allow for H/P inhibition in mobilized LICs. At the end point mice were sacrificed for analysis of bone marrow cells.

Gross pathologic analysis of the two treatment groups did not show any significant additional therapeutic effect of the Cy/G treatment (**Figure 4.12B**). Spleen size remained unchanged and WBC counts trended down, but were not significantly different. There was a modest increase in the frequency of $Gr1^{+}Mac1^{+}$ cells in mobilized bone marrow. The only significant finding on cytometric analysis was depletion of bone marrow HSCs. While it is tempting to interpret this finding as indicative of elimination of LICs, the Cy/G regimen had an HSC depleting effect on Cre^{neg} mice as well (data not shown). Bone marrow cells were then quantitated for the fraction of cells that were donor derived. We did not detect significant differences in donor chimerism between mock and mobilized for any of the cell populations analyzed (**Figure 4.12C**). The donor chimerism of both groups (independent of cell type) trended higher than Cre^{neg} control donor chimerism. As seen in **Figure 4.6B**, LSK chimerism was significantly higher in mock mice compared to controls (Cre^{neg} vs. Mock, p=0.01). Mobilized mice maintained this difference indicating that HSC/LIC mobilization did not eliminate the persistent donor LSKs in chimeric mice (Cre^{neg} vs. Mobilized p=0.04). The absence of any clear

difference in chimerism between non-mobilized and mobilized groups suggests that Cy/G-CSF does not improve the ability of imatinib to eliminate donor LICs. In a separate group of mice, AnnexinV+ staining was measured on cells immediately following G-CSF treatment (**Figure 4.12D**). In this experiment, mice were treated with G-CSF alone (which has been shown to have HSC mobilizing effects[28]) and stained for apoptotic cells 24 hours after the final G-CSF injection. Imatinib was administered for 14 days prior to, and during the mobilization regimen. We did not detect any differences in the frequency of apoptotic cells between mock and mobilized mice in this experiment. These experiments suggest that manipulating LICs out of quiescence does not alter the ability of imatinib to effectively induce apoptosis and eliminate the tumorigenic cells.

DISCUSSION

We have previously shown that concomitant expression of H/P and A/E from the endogenous mouse *Hip1* and *Aml1* loci leads to a fully penetrant, rapid onset imatinib-sensitive MPD[1]. In that study, we found that LICs share phenotypic characteristics with HSCs and are not eliminated by imatinib therapy despite a robust hematologic response to the drug. We have built on those findings by further characterizing the hematopoietic system of H/P;A/E mice and investigating the mechanism of LIC persistence. In the present study, we primarily use a chimeric competitive transplantation model of the H/P;A/E induced MPD. This system provides unique advantages over the germline primary Mx1-Cre H/P;A/E mice. First, it more accurately reflects human leukemias because induction of somatic translocations is limited to a fraction of hematopoietic cells. Second, it allows for analysis of large cohorts of mice derived from the same primary

donor, thus minimizing the variability of pre-existing mutations as well as the variability of disease progression. Third, it allows differentiation between the effects of therapies on wildtype (i.e. toxic) and mutant (i.e. therapeutic) populations.

Using the chimeric transplant system, we have further characterized hematopoietic stem and progenitor cells within the MPD. While phenotypic "definitions" of various hematopoietic cells are continuously evolving, we used well established surface marker combinations[19,29]. As expected, significant alterations within the myeloid progenitor compartment were found. The frequency of CMPs and MEPs was drastically reduced while the frequency of GMPs remained unchanged. As a fraction of all myeloid progenitors, GMPs were significantly increased, indicating a shift in differentiation favoring granulocyte production. Following 14 days of imatinib treatment, all myeloid progenitor frequencies and ratios returned to wildtype levels. We did not observe an increased rate of proliferation of any myeloid progenitor subtypes. Importantly, limiting activation of H/P and A/E to GMPs (but not HSCs) with an MRP8-Cre transgene did not lead to development of MPD. Taken together these data indicate that the LIC is unlikely to reside in the GMP population. It should be noted that in human blast crisis CML, GMPs gain the stem cell property of self-renewal via activation of β-catenin[30]. We are currently conducting GMP transplants from diseased and imatinib-responding mice to determine if this progenitor population is capable of initiating and maintaining the MPD in recipient mice.

In addition to the dramatic progenitor cell alterations described above, we have continued to find significant changes within the stem cell compartment. Most interestingly, we found a decrease in phenotypic MPPs ($Flt3^{+}LSK$) and LT-HSCs

($CD150^{+}CD48^{-}CD41^{-}LSK$). While it is difficult to functionally validate the phenotypic MPP depletion, we have shown that the LT-HSC depletion is functional as well as phenotypic. Importantly, we did not detect any changes in the overall LSK population frequencies highlighting the heterogeneity of this phenotype. Furthermore, LSK cells from diseased mice were unable to engraft irradiated recipients or transfer disease suggesting a decrease in functional HSC/LIC frequency even within this population often described as a stem cell. These data emphasize that investigators should take care not interpret the LSK phenotype as a surrogate for HSC/LIC function.

We previously used a transplant assay to prove the persistence of LICs in the H/P;A/E mouse. We now describe the more clinically relevant situation of therapy interruption. As with CML patients who discontinue imatinib therapy, we have found that the H/P;A/E mouse MPD returns within 7 days of imatinib discontinuation[4,31]. The relapsed disease retains hematologic sensitivity to imatinib indicating that the persistent LICs are not drug resistant clones. Based on these data, and the incomplete transplantation of disease, we think that therapy withdrawal in mouse models is a gold standard for making qualitative (and perhaps quantitative) conclusions about the efficacy of LIC targeting.

Given the multiple lines of evidence for LIC persistence *in vivo*, we used the chimeric system to interrogate the frequency and behavior of these cells. *A priori*, our hypothesis was that imatinib would lead to near complete elimination of donor type cells and that only a rare cell population would remain. This rare population would be the primary suspect in our quest to identify the LIC. Moreover, we predicted that this would be a unique cell type which is suppressed from differentiating or self-renewing. This

hypothesis presumes that the active LIC is dependent upon H/P signaling for leukemogenesis and/or survival. To our surprise, the bone marrow of imatinib-responding mice contained very large numbers of donor type cells which express the H/P and A/E oncogenes. These cells were distributed across myeloid and lymphoid lineages similar to control mice. In fact, donor cells made up a larger component of the bone marrow than cells from control Cre^{neg};H/P;A/E mice which do not develop disease. Importantly, there was no unique population of mutant donor type cells that persisted (LSK were the only cells with statistically significant elevation above control type cells). In contrast, spleen donor chimerism dropped below levels in Cre^{neg} control mice suggesting effective clearance of disease from this peripheral collection tissue. The persistence of robust levels of cells in which the H/P and A/E oncogenes have been activated suggests to us that the LIC(s) in this system is capable of reverting to the functions of its normal counterpart, the HSC.

Despite reversion to HSC-like functions, we found that the LIC (or some other donor type cell) is still producing oncogenic transcript (A/E transcript actually increased) in the bone marrow. Our data indicate that H/P transcript is *not* upregulated in stem or progenitor cells during imatinib therapy. It is unclear whether this persistent transcript is ultimately translated into functional oncoprotein. We are currently testing the activation status of tyrosine kinase pathways in specific cell populations. Nonetheless, the maintenance of similar levels of H/P transcript suggests two things. First, LICs are not being "converted" into HSCs by complete shutdown of the oncogenes responsible for the initial myeloproliferation. Second, tyrosine kinase inhibitor refractoriness is not being

caused by amplification of fusion tyrosine kinase transcript in this H/P;A/E model of MPD.

Another possible mechanism of LIC persistence is evasion from immunosurveillance. Based on previous reports, the hematopoietic surface marker CD47 is upregulated in myeloid leukemias and, by binding its receptor SIRPα on macrophages, provides protection from phagocytosis[24]. In the H/P;A/E induced MPD, CD47 is globally upregulated on all hematopoietic cell types tested although most significantly on the LSK population. Importantly, surface CD47 returns to wildtype levels upon a response to imatinib. This data suggests that immune evasion via persistence of upregulated CD47 expression is not the principal mechanism of LIC persistence in this mouse model of MPD.

As further evidence of the HSC origin of disease in the H/P;A/E induced MPD, short-term BrdU incorporation data demonstrate that a cell or cells within the LSK compartment display increased proliferation. This hyper-proliferation is entirely dependent on H/P signaling and even minimal tyrosine kinase inhibition led to a return to normal. Despite this increased proliferation, we have not yet observed progression of the H/P;A/E MPD to blast crisis. This is in contrast to the JunB knockout mouse model of CML which progresses through the chronic, accelerated and blast crisis phases typically observed in humans[32]. We are conducting longer-term observation studies of H/P;A/E mice to determine if progression occurs. Furthermore, a retroviral insertional mutagenesis screen may identify cooperating mutations that induce progression from the indolent, treatable chronic phase of CML to the aggressive, less treatable blastic phase.

There is a wealth of data using cultured $CD34^+$ cells from human CML patients that demonstrate therapeutic concentrations of imatinib are principally cytostatic, inhibiting the proliferation of primitive progenitors without significantly inducing cytotoxicity via apoptosis[27,33]. Here, we corroborate that result *in vivo* using proliferation and cell death assays. More importantly, we demonstrate that this cytostatic rather than cytotoxic response to imatinib poses a challenge to achieving absolute elimination of the mutant cell populations, a likely source of disease relapse and progression. Here we show functional persistence of LICs and unexpectedly, phenotypic persistence of multiple cell types containing the H/P and A/E oncogenes. These data support the notion that an LIC is not addicted to activated tyrosine kinase signals and thereby is able to revert to essentially normal HSC function when under the influence of tyrosine kinase inhibition. This independence from oncogenic kinase signaling suggests that therapeutic advances will necessarily come from two possible approaches. First, ways to convert the LIC to an oncogene-addicted state might allow more effective targeting by imatinib. Second, discovery and inhibition of non-kinase pathways that are critical to LIC, but not HSC, survival and homeostasis would complement the cytostatic effect of imatinib.

It is well-established that the most quiescent leukemic cell populations in CML are insensitive to imatinib and recent studies have attempted to enhance cell cycle entry as a means of improving imatinib sensitivity *in vitro*[8-10]. This hypothesis was tested clinically in a small phase II trial published in 2009[34]. Imatinib-responding CML patients were randomized to three treatment arms: continuous imatinib (cIM), pulsed imatinib (pIM) and pulsed imatinib plus G-CSF (pIM/G). No significant difference in BCR-ABL/ABL transcript ratio was detected between pIM and pIM/G. Of note, 6 of 30

patients in the experimental arms (pIM, pIM/G) exhibited disease progression versus 1 of 15 in the control arm (not significant, progression defined as loss of cytogenetic/molecular remission). A followup study developed a novel mathematical model to simulate these clinical results[7]. This theoretical analysis predicted no added benefit of G-CSF to imatinib and in fact, an increased risk of mutations leading to IM resistance via an increased pool of cycling leukemic stem cells. *In vivo* validation of these limited human results in a clinically relevant mouse model is lacking. We used the imatinib-sensitive MPD induced by H/P and A/E to test whether induction of LIC cycling by cyclophosphamide/G-CSF enhances sensitivity to tyrosine kinase inhibition in vivo. Imatinib treatments were maintained during the mobilization regimen to minimize disease relapse. We did not observe any change in LIC sensitivity to imatinib following the cyclophosphamide/G-CSF mobilization protocol as determined by AnnexinV staining and donor chimerism levels. This result implies that mobilized LICs retain their independence from H/P signaling. We are currently conducting trials with other HSC/LIC mobilization regimens (arsenic trioxide, IFNγ) to confirm or refute our conclusion that induction of cell cycle entry does not alter the in vivo sensitivity of the H/P;A/E LIC to imatinib. It should be noted that none of the mobilized mice displayed re-emergence of disease or blastic progression when maintained on IM.

A recent study using human CML cells and the inducible Bcr/Abl transgenic model of CML demonstrated that the combination of imatinib and histone deacetylase inhibitors (HDACi) was effective at targeting LICs[35]. *In vitro* evidence strongly suggest that AML1/ETO recruit HDACs to the Aml1 promoter, thus inhibiting the normal transcriptional activity of this critical hematopoietic regulator[36-38]. We have tested the

HDACi suberoylanilide hydroxamic acid (SAHA) in the H/P;A/E mouse model of MPD and found no hematologic response (data not shown). Furthermore, the combination of SAHA and IM showed no added benefit of SAHA to the gross hematologic response evoked by IM. However, further evaluation of combination TKI/HDACi therapy on LICs is ongoing.

While the precise immunophenotype of the LIC in the H/P;A/E induced MPD is not yet known, we favor the notion that, in the absence of blastic transformation, HSCs are the only normal cells capable of self-renewal, and thus must be the ultimate cell of origin for the MPD. Surface markers or gene expression changes that distinguish normal HSCs from mutant LICs are of paramount importance in developing LIC targeted therapies. Because our data indicate that addition of HDAC inhibitors and cellular mobilization agents to the imatinib therapy was largely ineffective, we are currently studying the molecular differences between HSCs from imatinib treated H/P;A/E mice and imatinib treated Cre^{neg};H/P;A/E mice to discover new therapeutic targets. The inability to cure CML with imatinib, the toxicities of allogeneic bone marrow transplant and the expense and possible side effects of long term imatinib treatment are legitimate reasons to pursue novel therapies for elimination of this disease. Identification, characterization and targeting of the LICs in H/P;A/E mice will contribute to the identification of new molecular targets in CML.

Genotype	n	Age (yr)	Liver Tumor	Lethal Disease	Spleen >150mg	Thymus >100mg	Lymph Mass	Total w/disease
Wt	2	<1	0	0	0	0	0	0 (0%)
H/P-KI	16	<1	0	0	0	0	0	0 (0%)
Wt (ENU)	6	1	0	0	1	0	0	1 (17%)
H/P-KI (ENU)	18	1	0	1	2	1	0	5 (28%)

Genotype	n	Latency (wks)	Total diseased
Wildtype	2	-	0
H/P-KI;Mx1-Cre;Aml1$^{LSL-A/E}$	2	1-6	2

Genotype	n	Age (wk)	Total diseased
Wildtype	3	7	0
Vav1-Cre;H/P;A/E	3	7	3
Widltype	2	12	0
MRP8-Cre; H/P;A/E	2	12	0

Table 4.1: Development of MPD depends on expression of H/P and A/E in stem cells but not on the order of oncogene activation.
Top, Incidence and type of disease observed in germline H/P-KI and control mice. A cohort of age-matched littermate mice were mutagenized with ENU (+/- G-CSF pretreatment) and sacrificed at 1 year. *Middle,* Incidence and latency of MPD in H/P-KI;Mx1-Cre;Aml1$^{LSL-A/E}$ mice. *Bottom,* Incidence and latency of MPD induced by activation of H/P and A/E by Vav1Cre and MRP8-Cre transgenes.

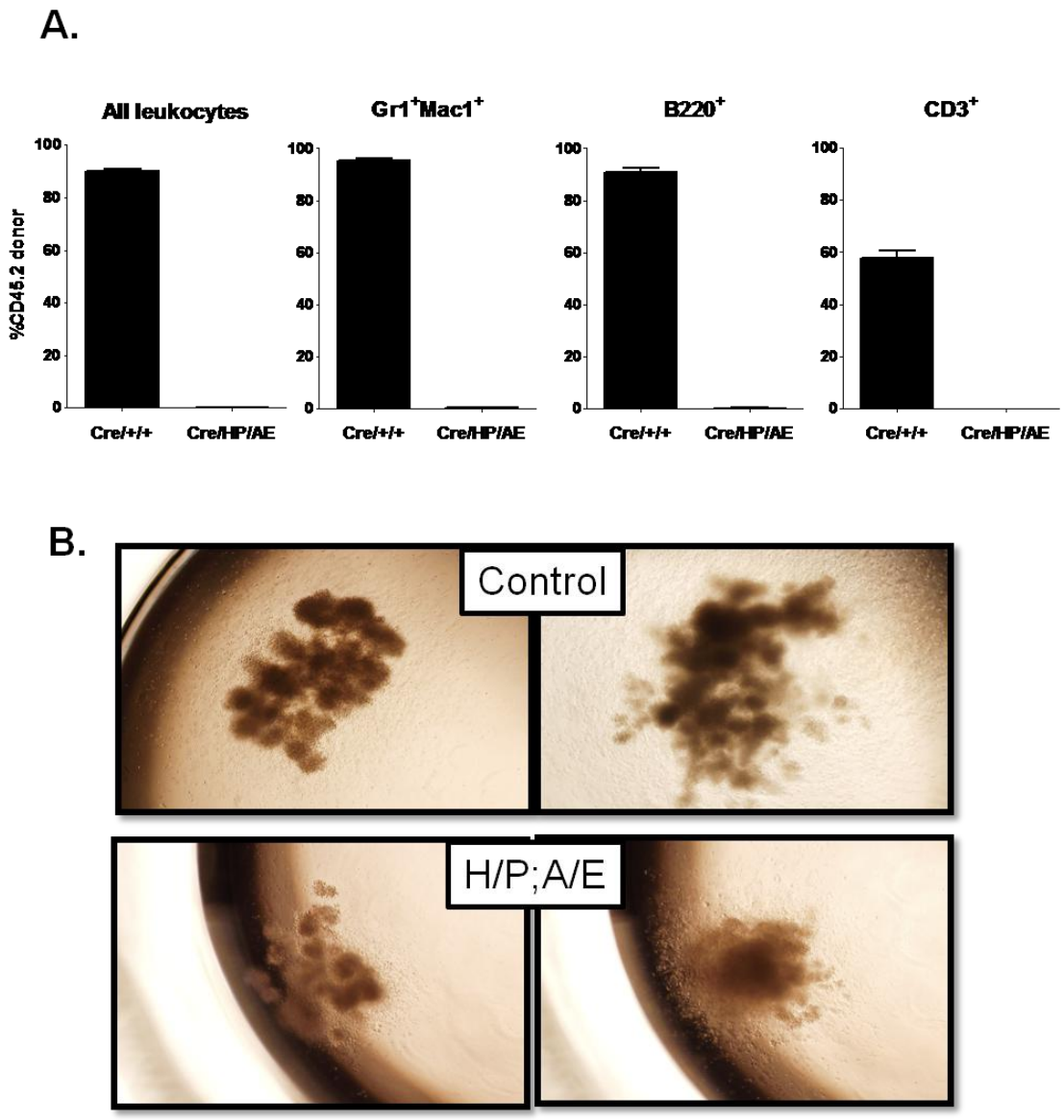

Figure 4.1: Stem cells from H/P;A/E mice have decreased reconstituting potential.
A, 3000 Lin-c-Kit+Sca1+ (LSK) cells were FACS sorted from control (Cre+;+/+;+/+, n=1) or diseased (Cre+;H/P;A/E, n=1) primary mice and transplanted into lethally irradiated syngenic recipients along with $3x10^5$ wildtype SJL bone marrow cells (5 recipients each). The average peripheral blood engraftment in various lineages was measured 15 weeks after transplant *B,* Single LT-HSCs (CD150+CD48-CD41-LSK) from control or diseased primary mice were directly sorted into cytokine-supplemented methylcellulose. Colony formation was assessed after 14 days. Top row, control. Bottom row, H/P;A/E diseased.

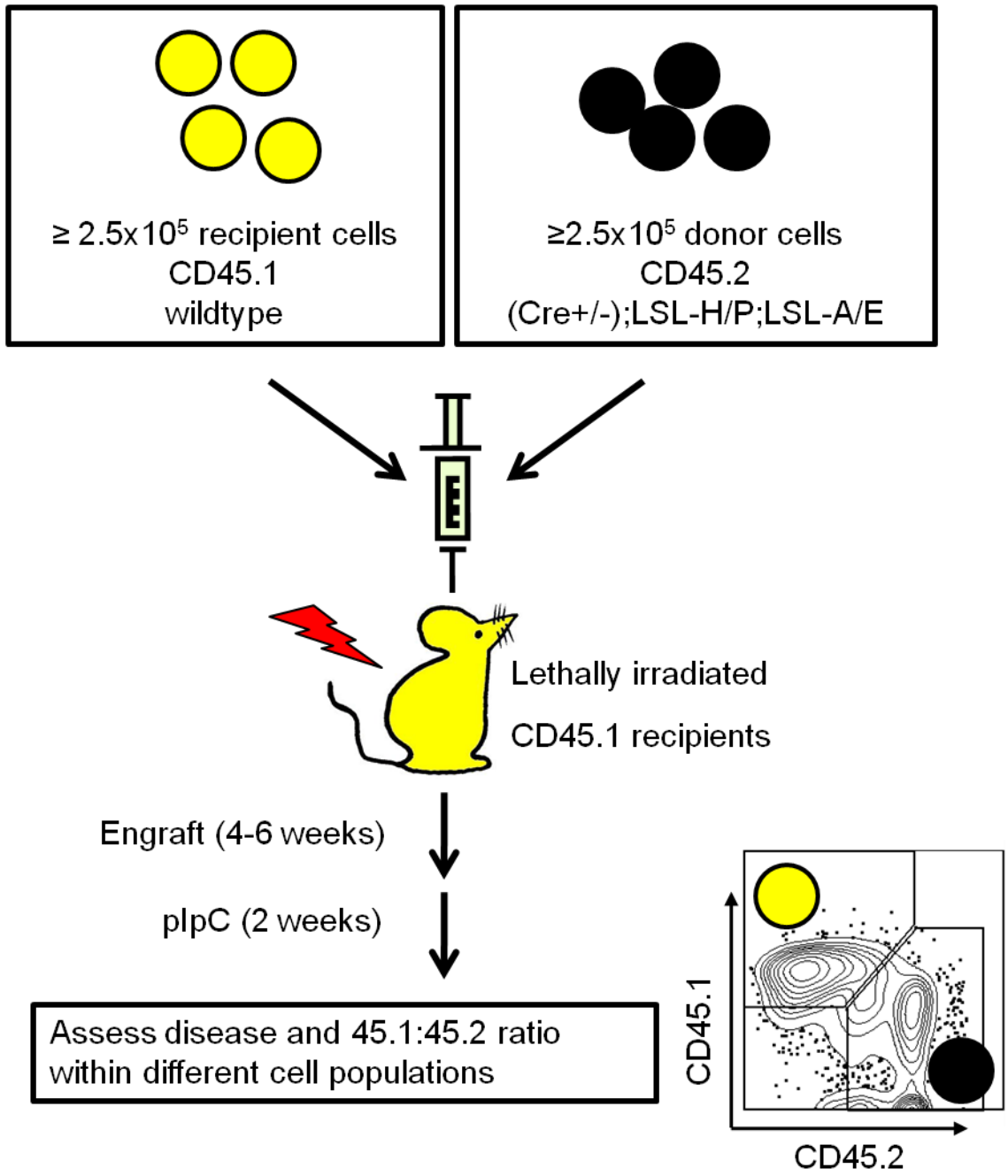

Figure 4.2: Schematic of competitive transplant system
Bone marrow cells from wildtype CD45.1 (yellow) and experimental CD45.2 (black) donor mice is transplanted at a specific ratio (depicted 1:1) into lethally irradiated CD45.1 recipients. Following 4-6 weeks of engraftment, mice are treated with pIpC for 2 weeks and then analyzed for disease and changes in donor chimerism.

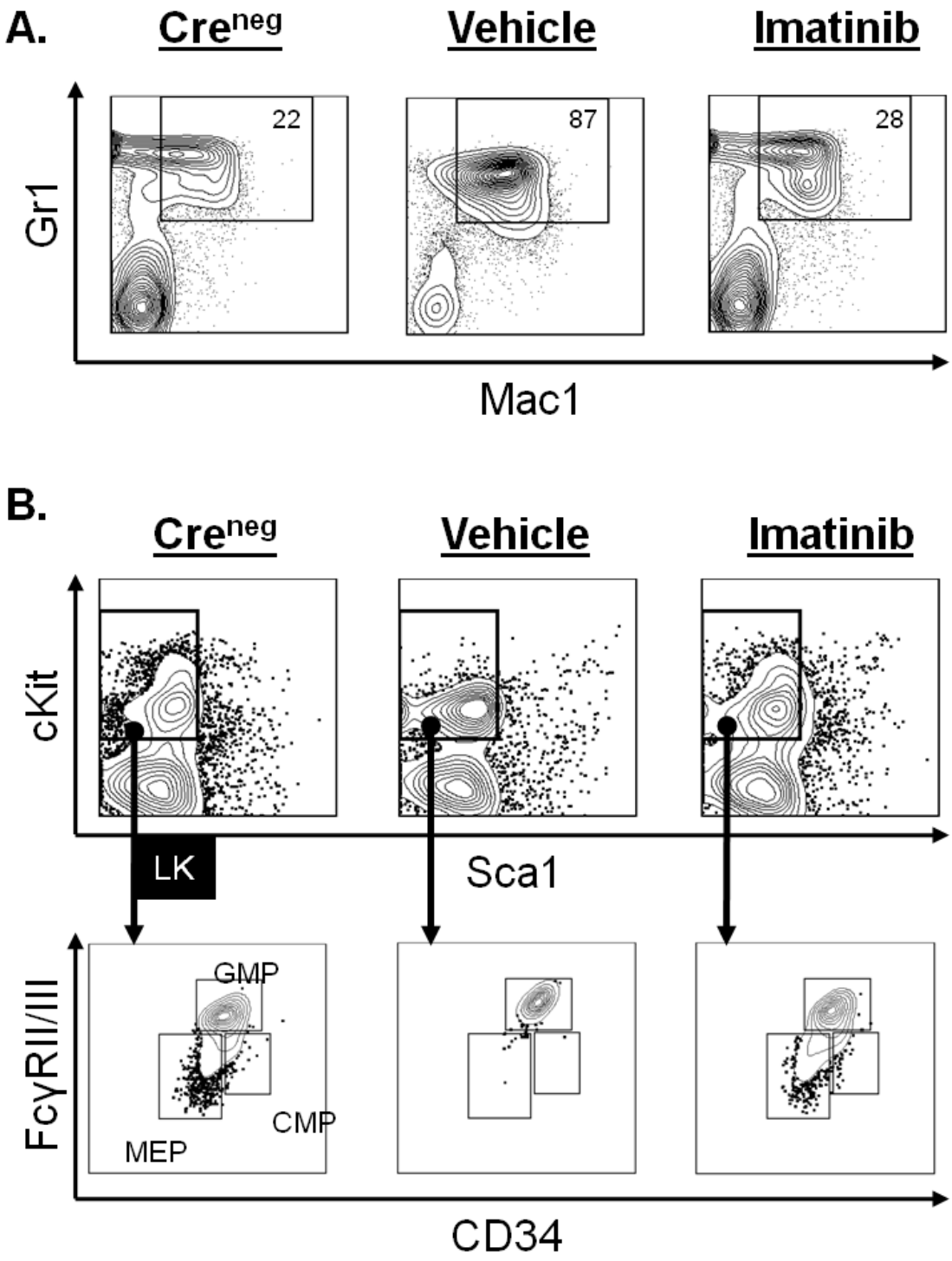
A.
Cre^neg
Vehicle
Imatinib
22
87
28
Gr1
Mac1
B.
Cre^neg
Vehicle
Imatinib
cKit
Sca1
LK
GMP
CMP
MEP
FcγRII/III
CD34

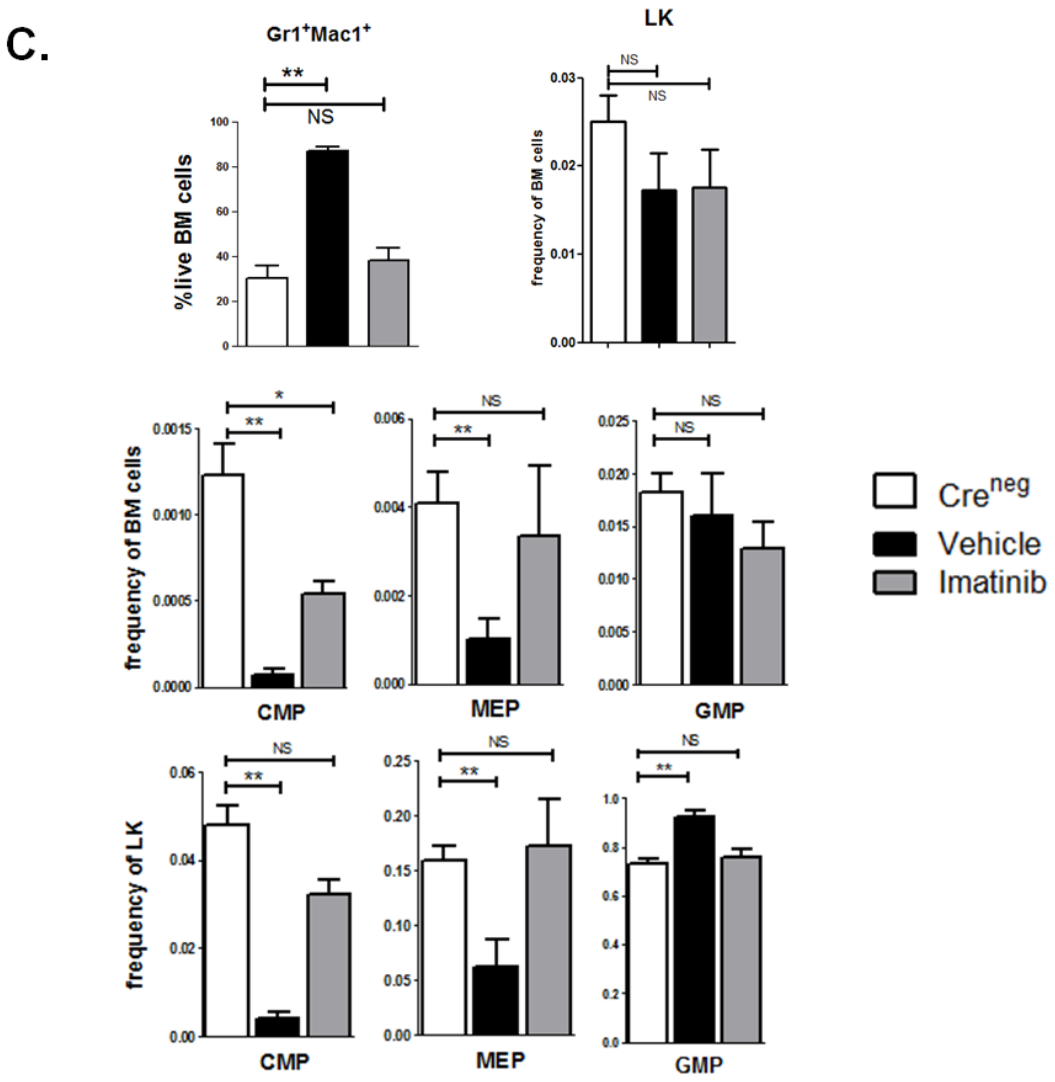

Figure 4.3: Hematopoietic progenitor cell alterations during H/P;A/E induced MPD and normalization with imatinib therapy.

Competitive transplants were performed as described in Figure 2 using Cre^{neg};H/P;A/E donor cells (Cre^{neg}, recipient n=6, no treatment) and Cre^{+};H/P;A/E donor cells (recipient n=10). Chimeric recipients were treated with pIpC and developed MPD within 4-6 weeks. Recipients of Cre^{+};H/P;A/E cells were then treated with vehicle (n=6) or imatinib (n=4) for 14-35 days. *(A)* FACS plots showing $Gr1^{+}Mac1^{+}$ expansion in bone marrow and response to imatinib. *(B)* FACS plots depicting gating for Lin^{-} myeloid progenitor cells. (C) Quantification of mature myeloid and progenitor cell alterations in H/P;A/E induced MPD. *Middle row,* myeloid progenitors frequency of live cells, *Bottom row,* myeloid progenitor frequency of LK population. $LK=Lin^{-}Sca1^{-}c\text{-}Kit^{+}$, GMP = Granulocyte/Macrophage progenitor, MEP = Megakaryocyte/Erythrocyte progenitor, CMP = common myeloid progenitor. *p<0.05, **p<0.005, NS=not significant. Data from one of two independent competitive transplants conducted.

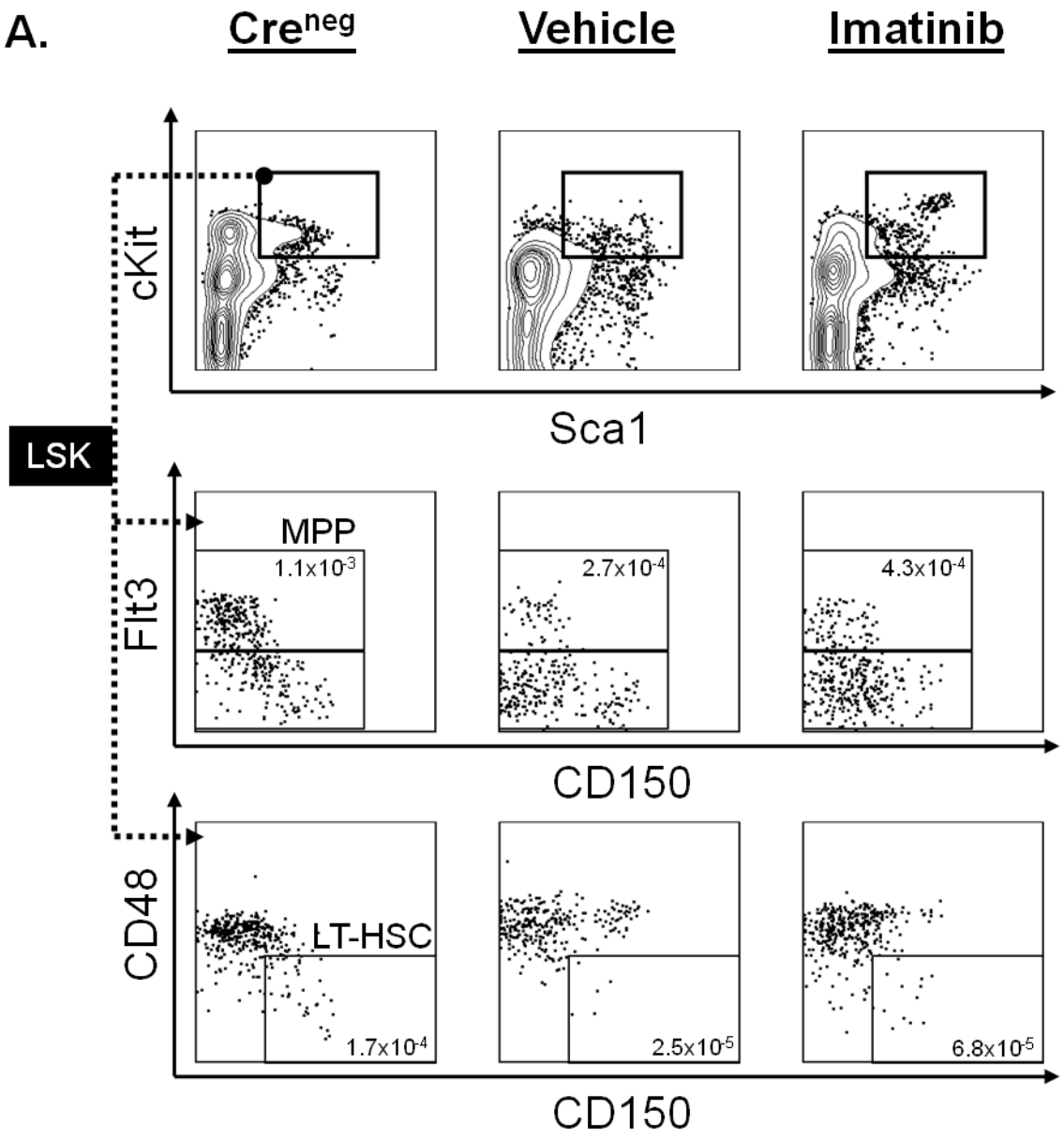
A.
Cre^neg
Vehicle
Imatinib
cKit
Sca1
LSK
MPP
1.1x10-3
2.7x10-4
4.3x10-4
Flt3
CD150
CD48
LT-HSC
1.7x10-4
2.5x10-5
6.8x10-5
CD150

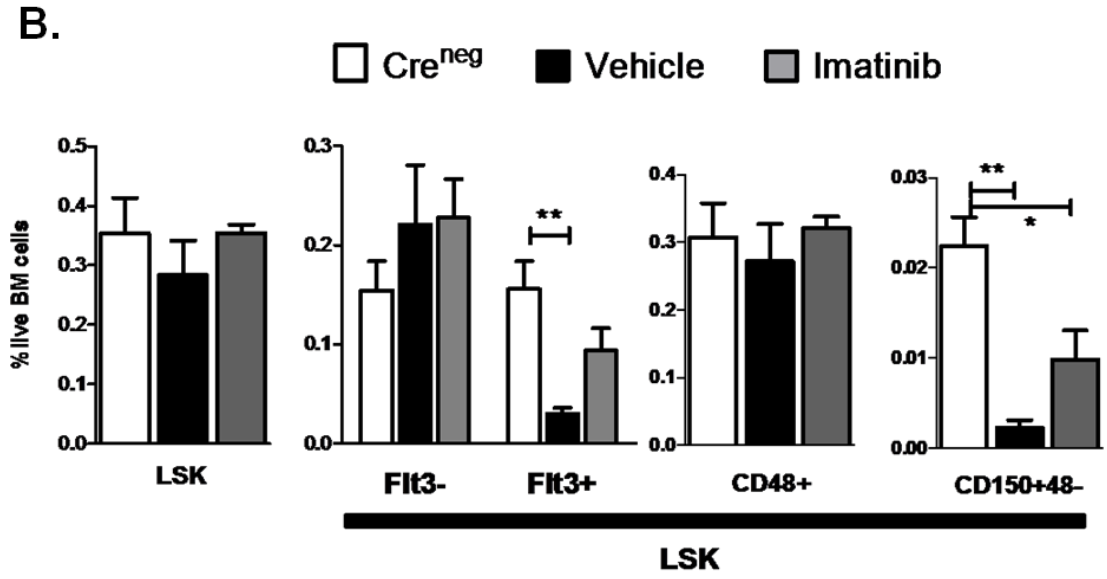

Figure 4.4: Hematopoietic stem cell phenotypic changes during H/P;A/E induced MPD and normalization with imatinib therapy.
Primary Cre^{neg} or H/P;A/E mice were induced with pIpC and treated with vehicle or imatinib for 7-14 days. (Untreated Cre^{neg} n=7, Vehicle n=7, Imatinib n=4). *(A)* FACS plots depicting initial gating for LSKs and subsequent gating for MPPs or LT-HSCs (*B)* Overall frequency of various HSC subpopulations. LSK=Lin-Sca1+c-Kit+, *$p<0.05$, **$p<0.005$.

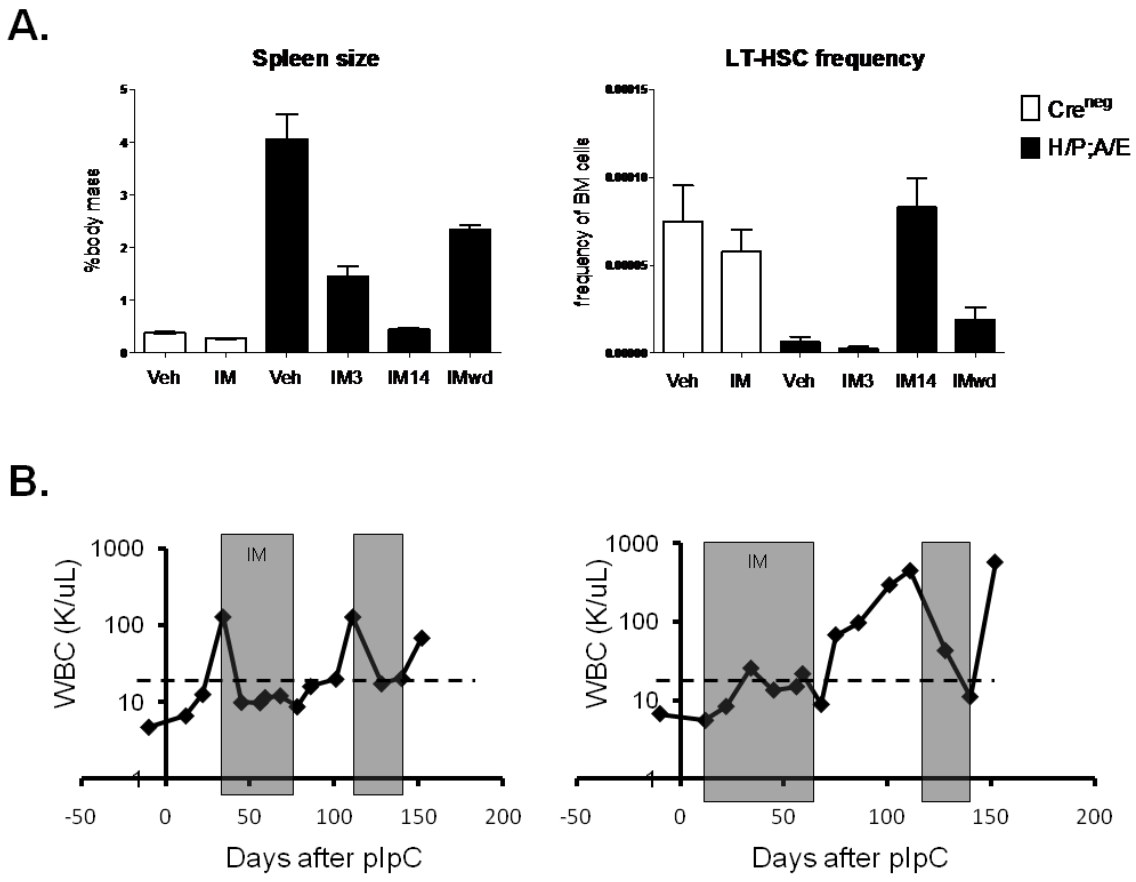

Figure 4.5: Functional evidence for persistence of MPD-initiating cells during imatinib therapy.
Cre^{neg};H/P;A/E recipients were treated with vehicle (n=12) or imatinib (n=3) for 3 days. Cre^{+};H/P;A/E recipients were treated with vehicle for 14-35 days (n=10) or imatinib for 3 days (IM3, n=8) or 14-21 days (IM14, n=9). One group of Cre^{+};H/P;A/E recipients was treated with imatinib for 14-35 days followed by 7 days with no treatments (IMwd, n=8). (*A) Left*, Spleen weight as percent of body mass. *Right*, Frequency of CD150+CD48-LSK (LT-HSC). (*B) Left*, Example of white blood cell trend upon interruption of imatinib therapy. *Right*, Example of white blood cell trend when imatinib therapy is initiated immediately after pIpC. Gray boxes indicate periods of imatinib treatments.

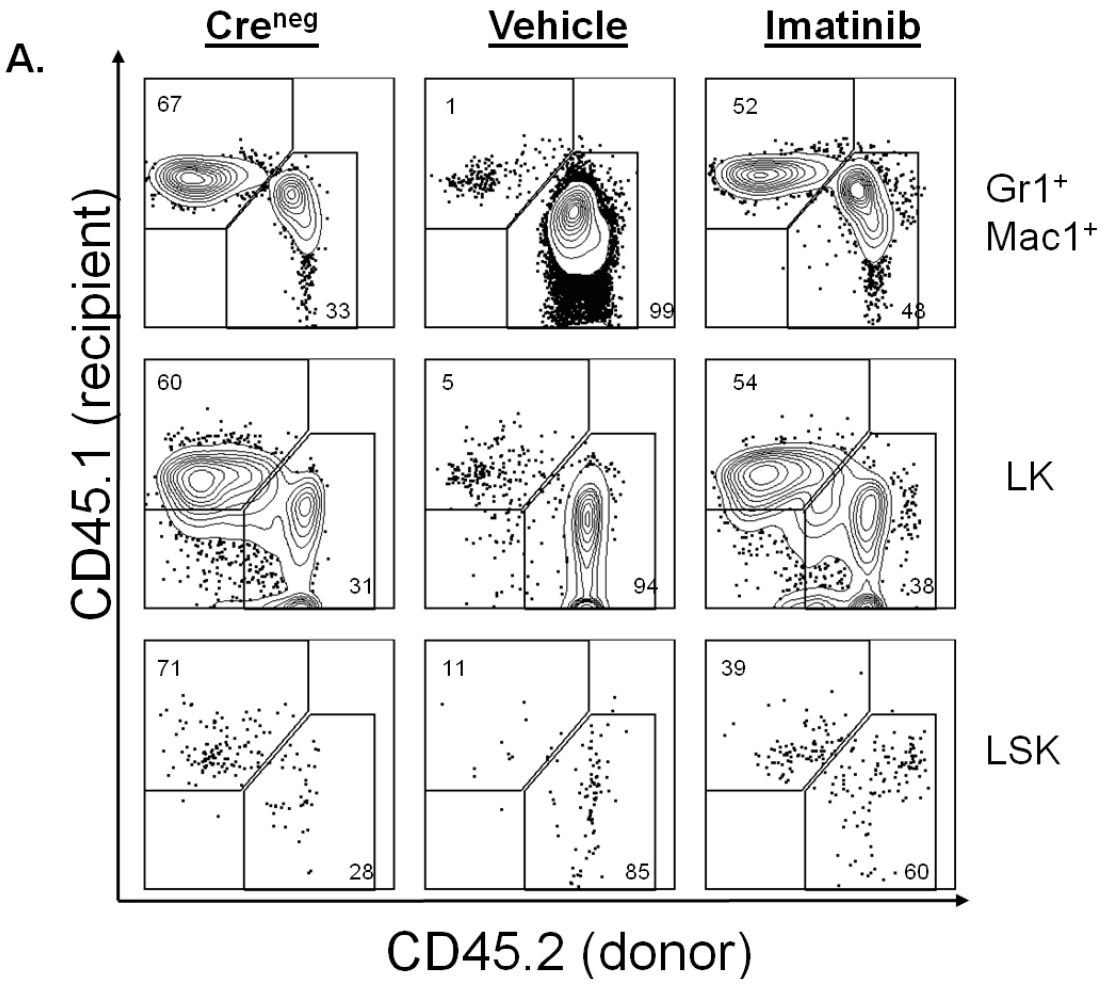
A.
Cre^neg
Vehicle
Imatinib
67
33
1
99
52
48
60
31
5
94
54
38
71
28
11
85
39
60
Gr1+
Mac1+
LK
LSK
CD45.1 (recipient)
CD45.2 (donor)

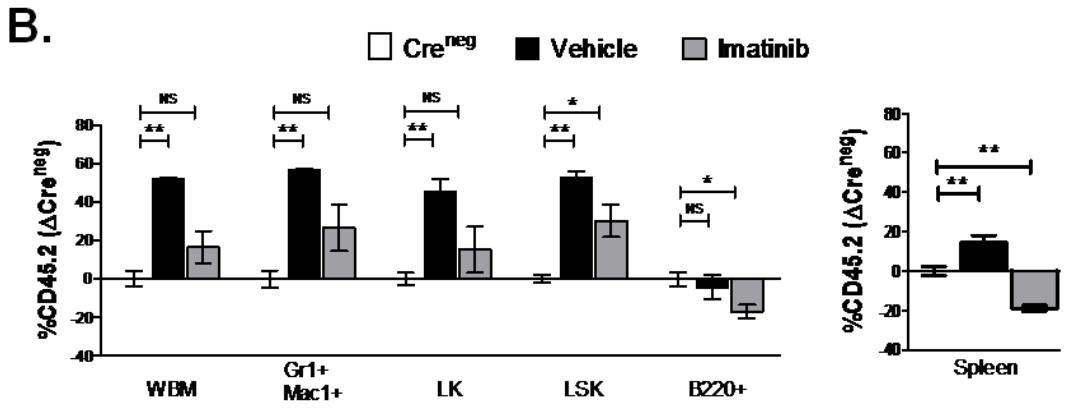

Figure 4.6: Phenotypic evidence for persistence of MPD-initiating cells during imatinib therapy.

Chimeric Cre^{neg};H/P;A/E recipients were treated with imatinib (n=4) for 3 days. Cre^{+};H/P;A/E recipients were treated with vehicle (n=3) or imatinib (n=5) for 14 days. (*A)* FACS plots of recipient (CD45.1, y-axis) and donor (CD45.2, x-axis) contributions to $Gr1^{+}Mac1^{+}$, LK and LSK populations. (*B)* The proportion of each cell population that is donor-derived (calculated as [CD45.2]/[CD45.1+CD45.2]). Bar graph represents difference between experimental groups and Cre^{neg} control chimerism. LSK=Lin-Sca1+c-Kit+, LK=Lin-Sca1-c-Kit+. *p<0.05, **p<0.005, NS=not significant Spleen data are from a 2:1 transplant ratio. WBM data are from a 1:4 transplant ratio.

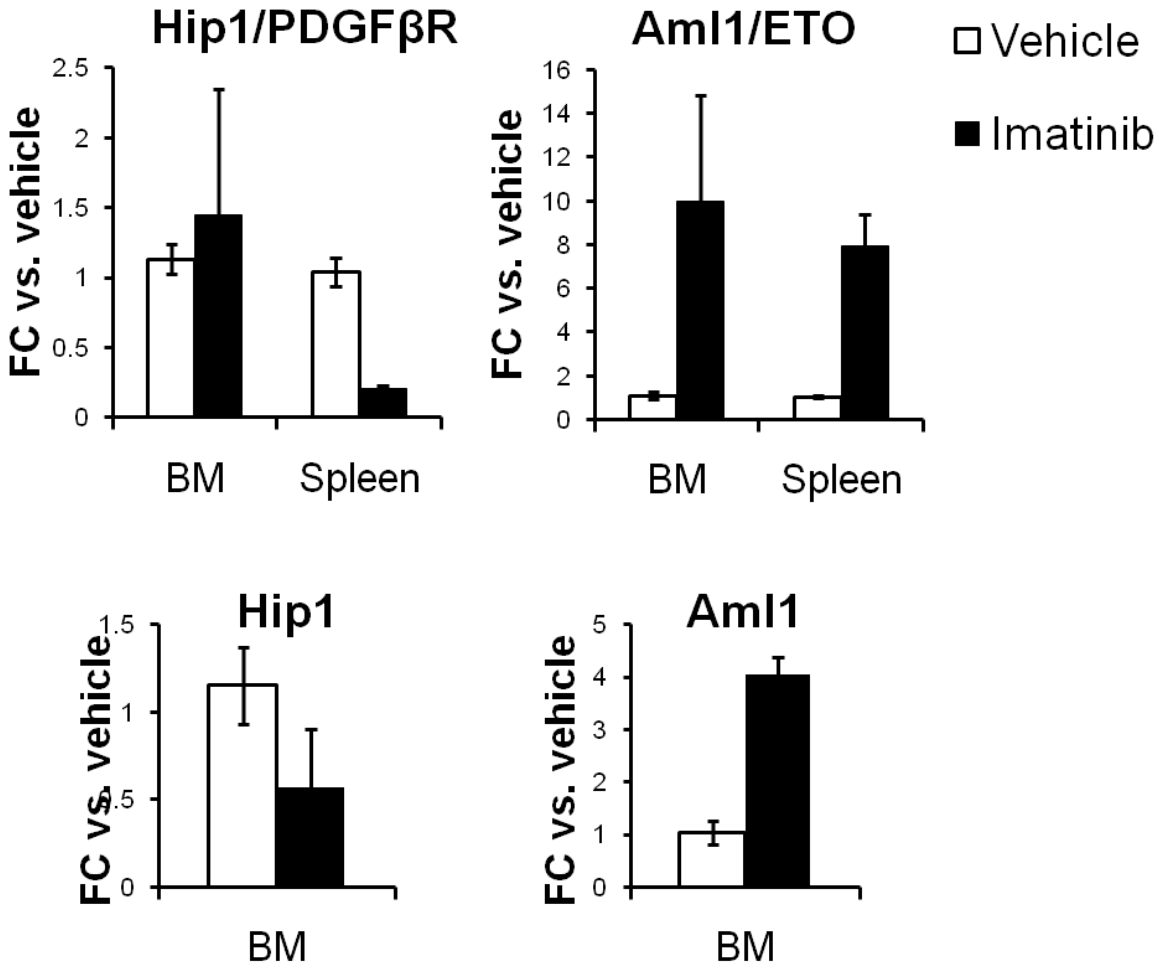

Figure 4.7: Oncogene transcription in response to imatinib.
Expression levels of *H/P*, A/E, *Hip1*, and *Aml1* were assessed by quantitative PCR in whole bone marrow (WBM) cells and splenocytes. The RNA content of samples was normalized based on *GAPDH* and fold-change comparisons were made between imatinib (n=3) and Cre^{neg} (n=3) cells (Cre^{neg} cells were set to 1 for purposes of the comparison). Data represent mean±SD.

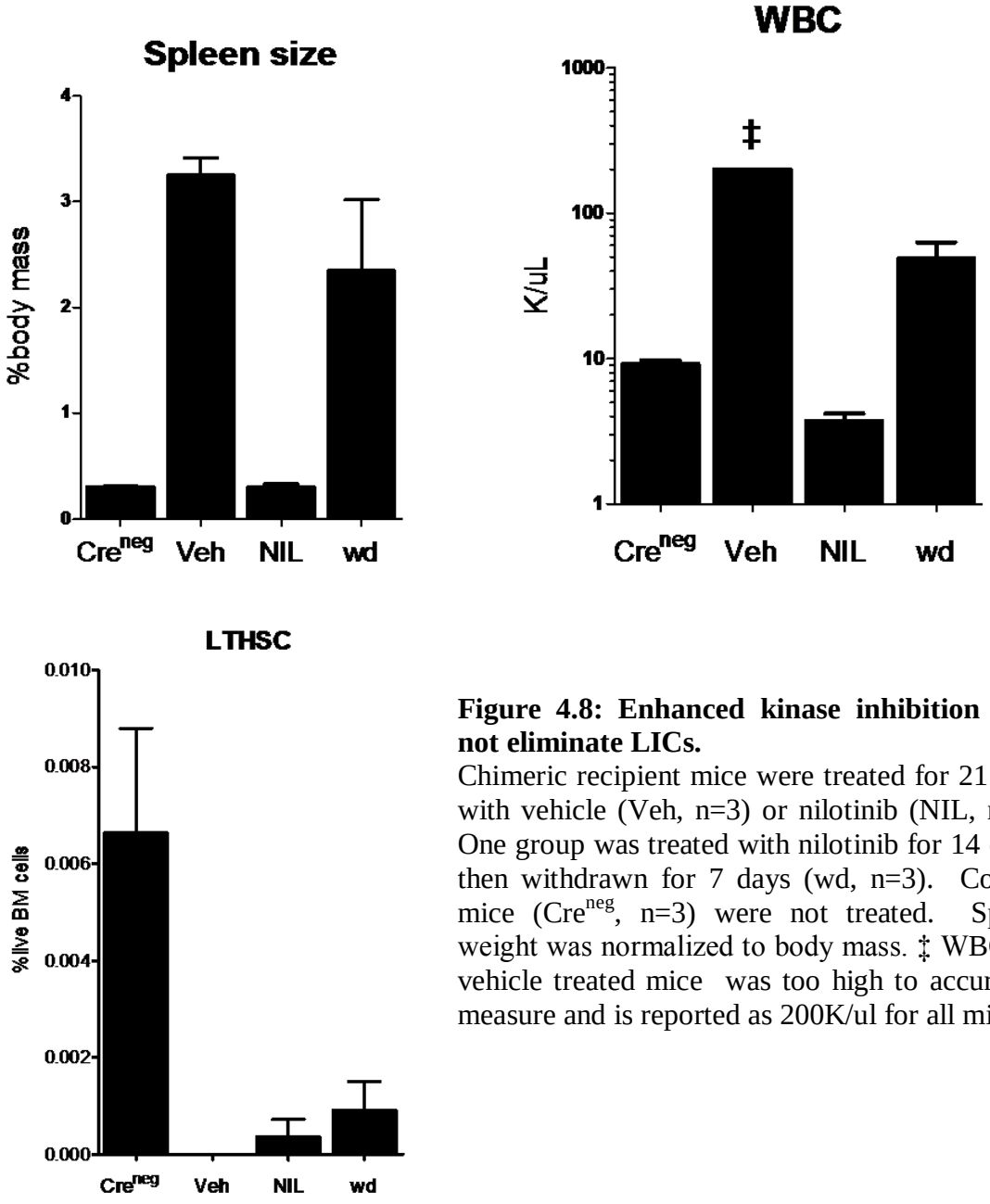

Figure 4.8: Enhanced kinase inhibition does not eliminate LICs.
Chimeric recipient mice were treated for 21 days with vehicle (Veh, n=3) or nilotinib (NIL, n=3). One group was treated with nilotinib for 14 days, then withdrawn for 7 days (wd, n=3). Control mice (Cre^{neg}, n=3) were not treated. Spleen weight was normalized to body mass. ‡ WBC for vehicle treated mice was too high to accurately measure and is reported as 200K/ul for all mice.

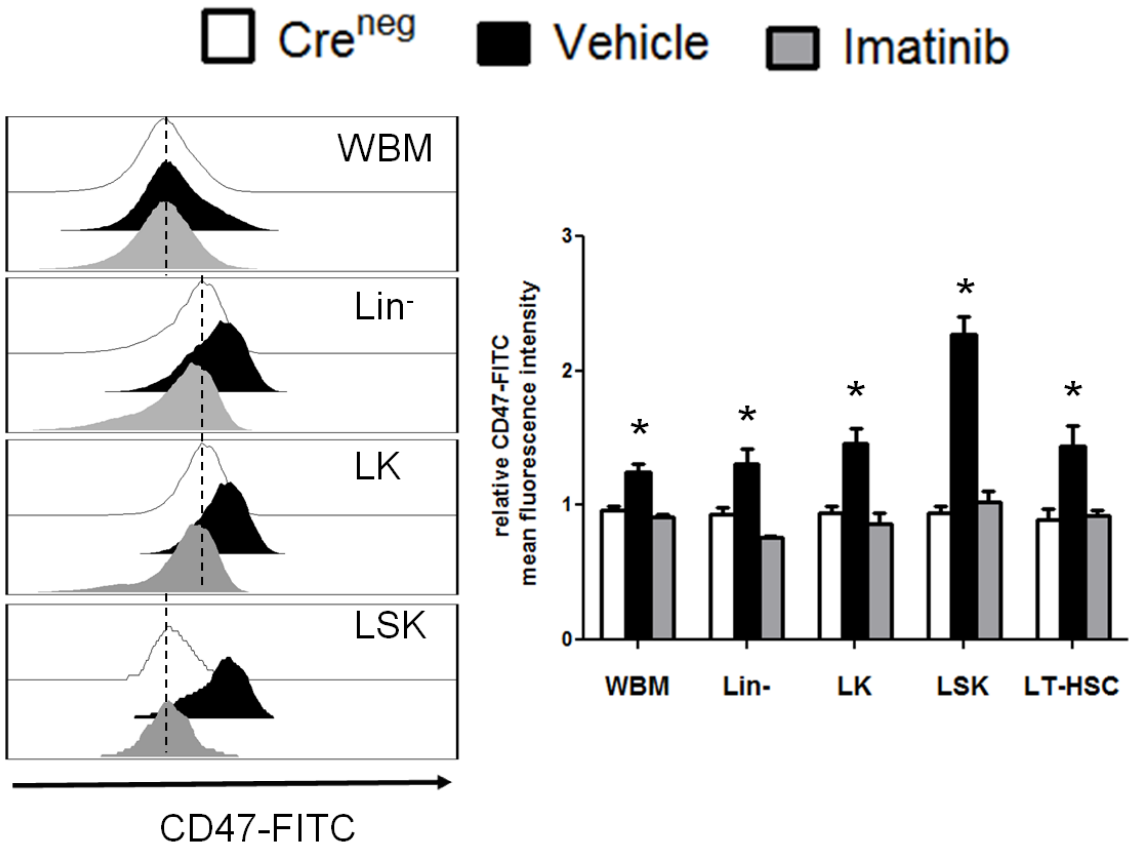

Figure 4.9: CD47 is upregulated in MPD but returns to baseline with imatinib response.

Chimeric recipients were treated with vehicle or imatinib for 14 days and bone marrow cells were stained with CD47-FITC. *Left*, sample histogram plots of CD47 fluorescence intensity within different bone marrow cell populations. Dotted line drawn at Cre^{neg} median. *Right*, quantification of mean fluorescence intensity for multiple cell populations (relative to Cre^{neg}). All vehicle values are significantly greater than Cre^{neg} (*$p<0.005$), but none of the imatinib values are significant. Cre^{neg} n=3, Vehicle n=3, Imatinib n=3. WBM = whole bone marrow, Lin^- = lineage negative, LK = $Lin^-c\text{-}Kit^+$, LSK = $Lin^-c\text{-}Kit^+Sca1^+$, LT-HSC = $CD150^+CD48^-CD41^-LSK$.

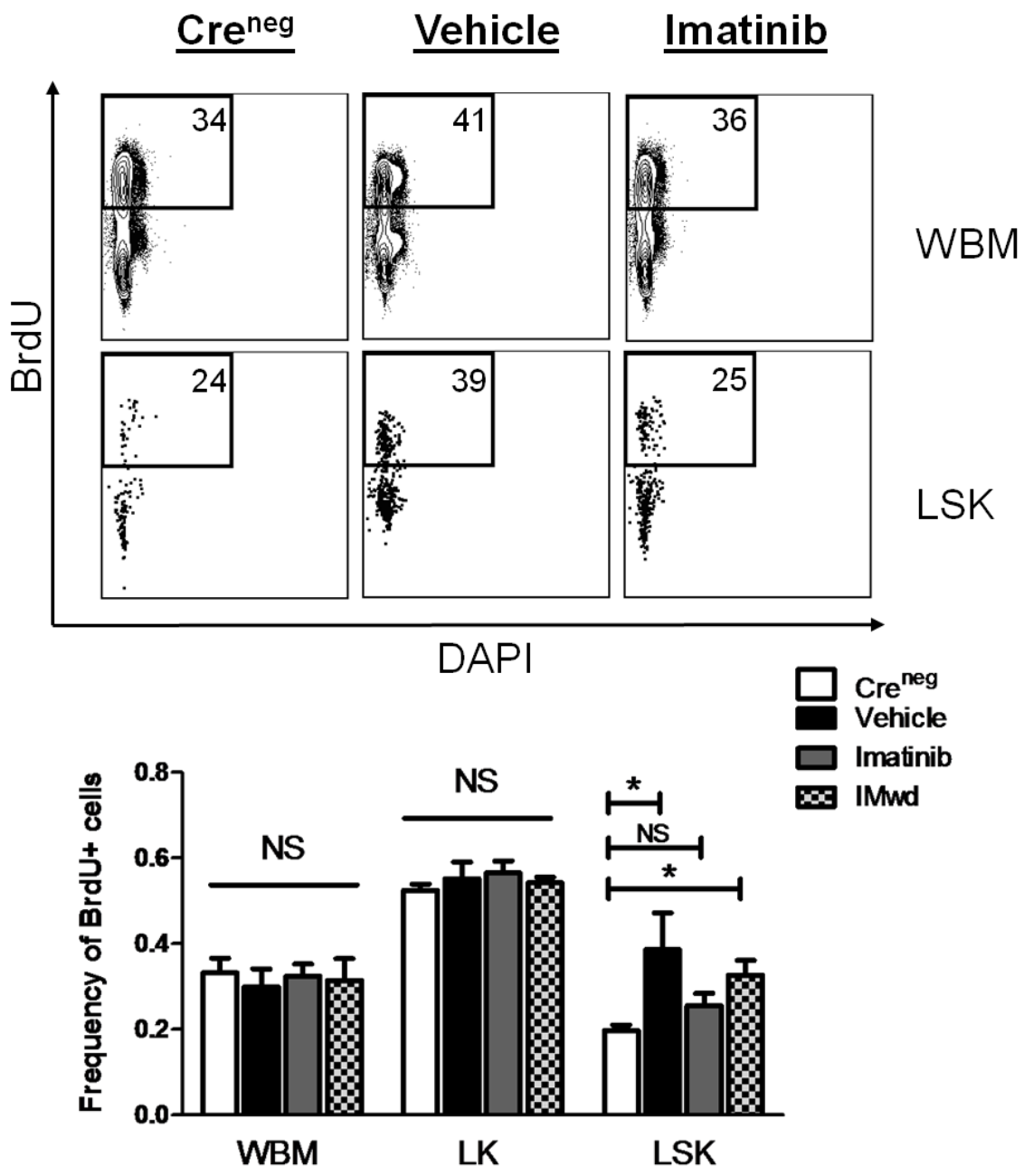

Figure 4.10: Imatinib inhibits LSK hyperproliferation in H/P;A/E MPD.
Chimeric recipients were treated with vehicle or imatinib for 14-35 days. 24 hours prior to sacrifice, mice were injected with 1mg of BrdU. *Top*, sample FACS plots of BrdU incorporation into WBM or LSK cells. *Bottom*, Quantification of BrdU incorporation into different populations. Creneg (n=5), Vehicle (n=7), Imatinib (n=6), Withdrawal (n=8). *$p<0.05$ compared to Cre^{neg}

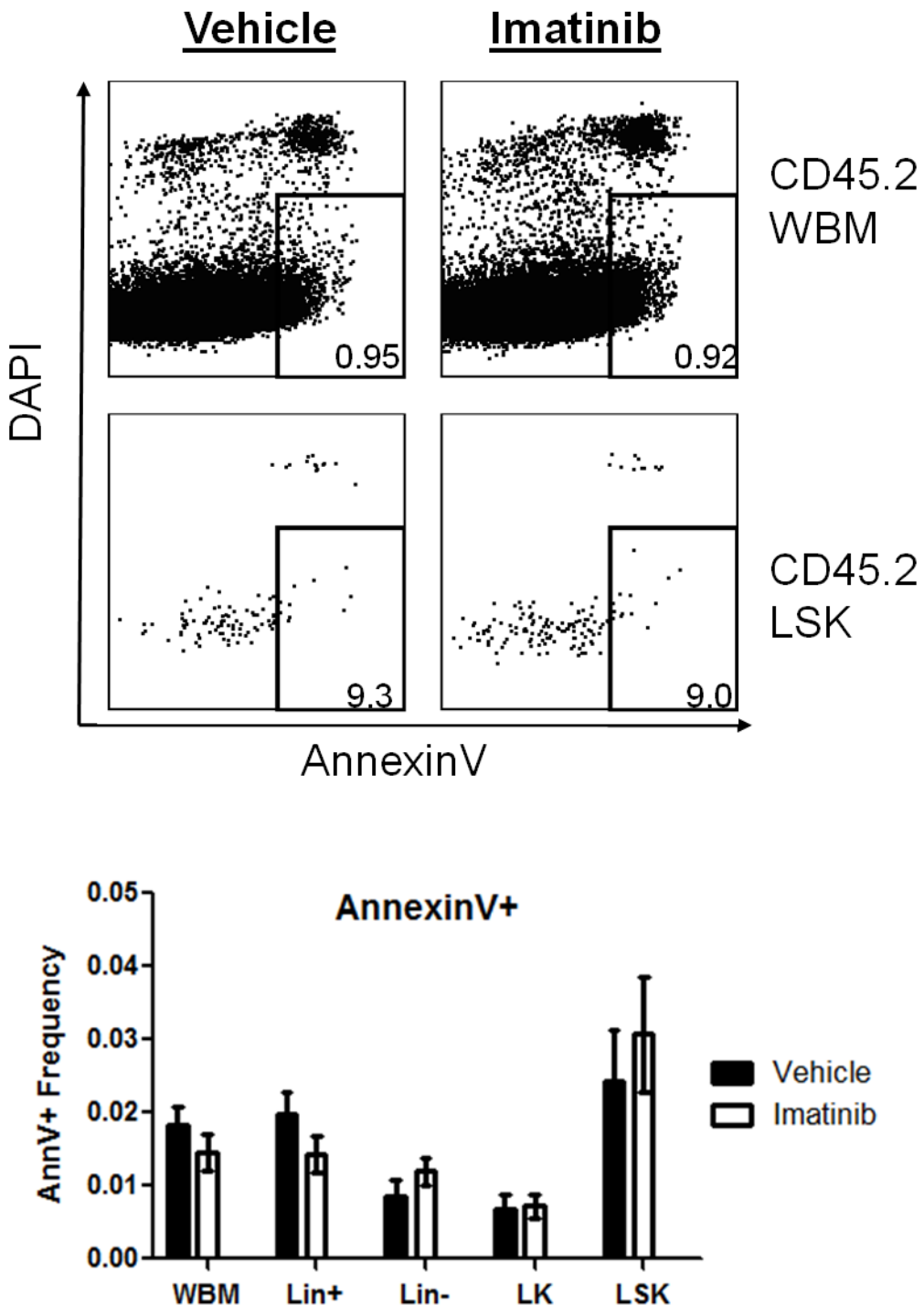

Figure 4.11: Imatinib does not induce an apoptotic response *in vivo*
Diseased recipient mice were treated with vehicle or imatinib for 3 days (6 doses). Bone marrow cells were analyzed for AnnexinV staining one hour after sacrifice. *Top*, Sample FACS plots of apoptotic cells. *Bottom*, Frequency of AnnexinV+ cells within given population. Vehicle n=3, Imatinib n=3.

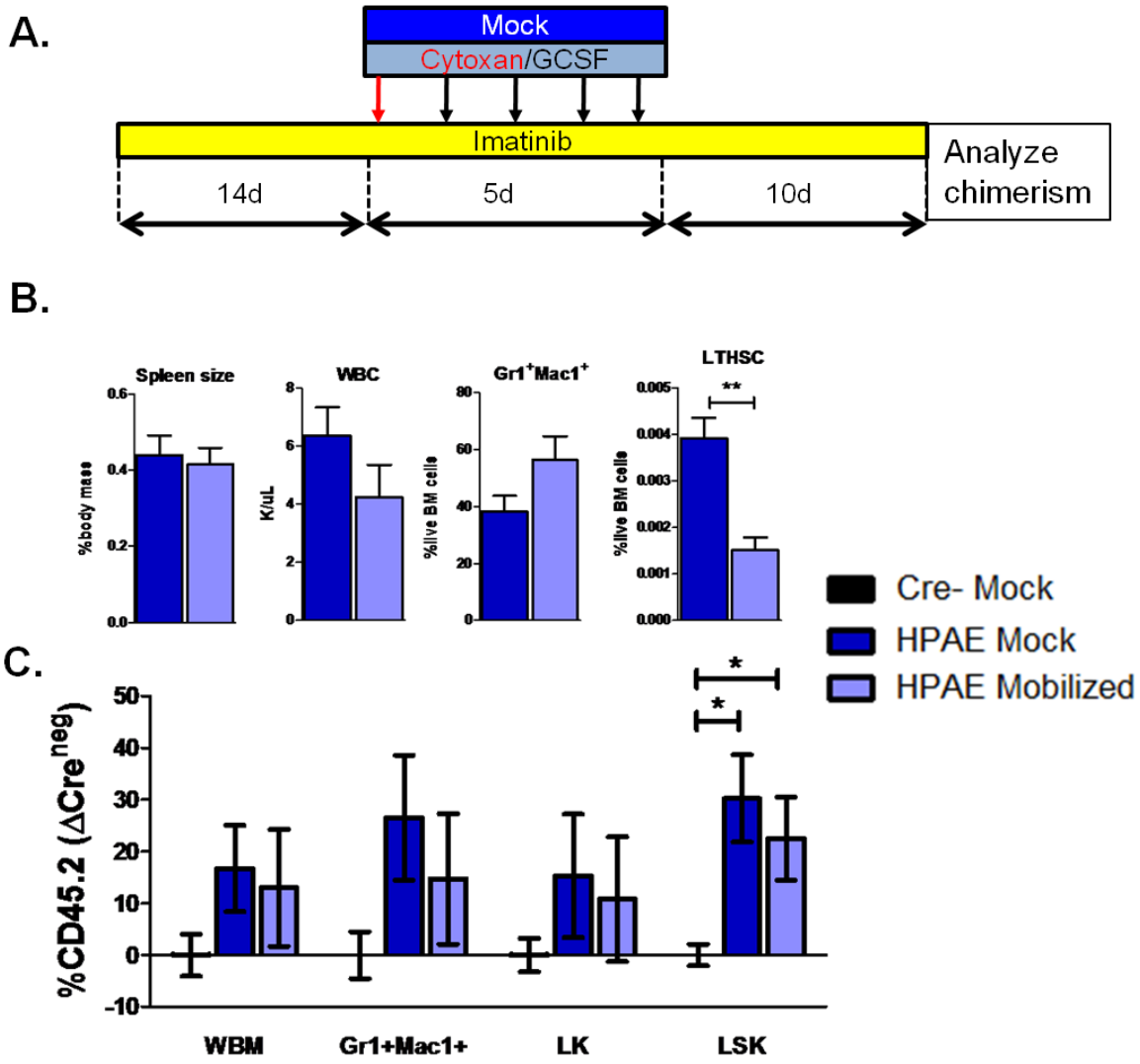

Figure 4.12: Mobilization of LICs does not enhance their sensitivity to imatinib
A. Treatment schedule for chimeric mice with MPD (Mock n=5, Mobilized n=5) *B,* Gross and cellular analysis of mock and mobilized (Cytoxan/G-CSF) mice: normalized spleen weight, WBC, Gr1+Mac1+ frequency, LTHSC frequency *C,* Donor chimerism of WBM and specific cell populations. The only population with significantly different donor chimerism was LSK (mock and mobilized). No differences were detectable between mock and mobilized mice, with the exception of bone marrow LTHSC frequency.

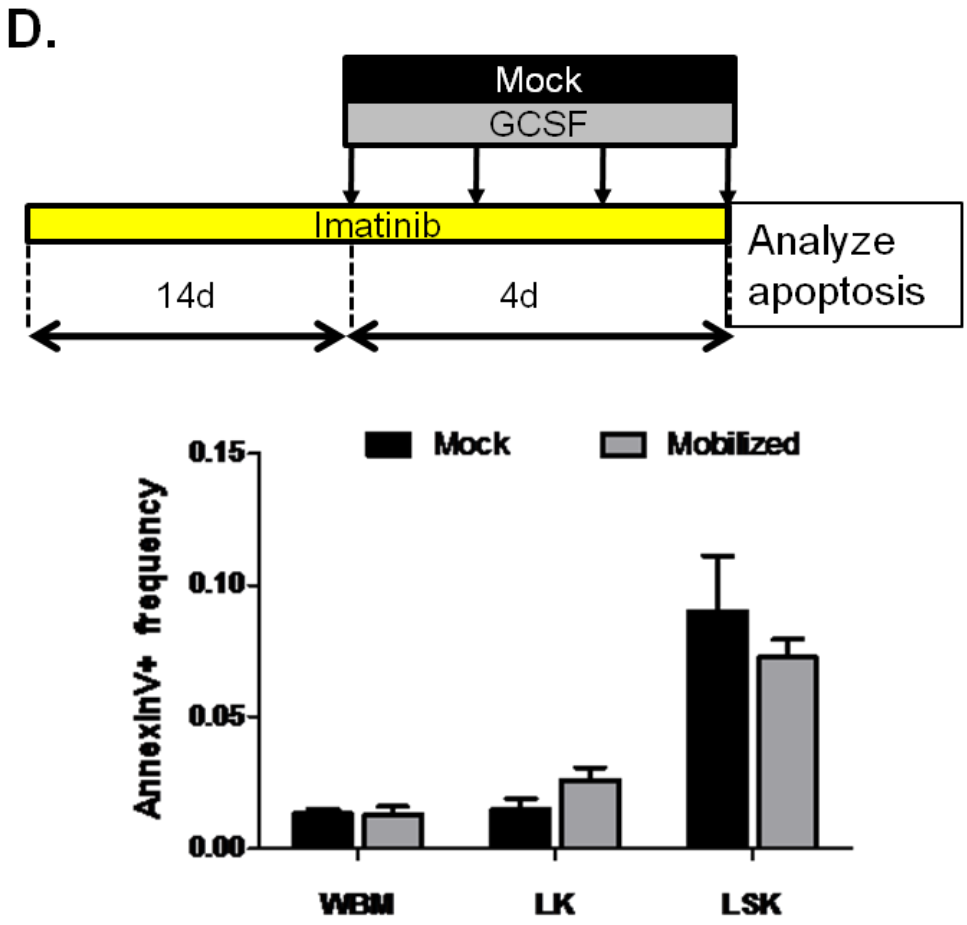

Figure 4.12 cont. Mobilization of LICs does not enhance their sensitivity to imatinib

D. In a different experiment, mice were analyzed for apoptosis 24 hours after the mobilization regimen (GCSF only). No difference in AnnexinV+ frequency was detected between mock and mobilized mice in any population.

References

1. Oravecz-Wilson, K. I. et al. Persistence of leukemia-initiating cells in a conditional knockin model of an imatinib-responsive myeloproliferative disorder. *Cancer Cell* 16, 137-48 (2009).
2. Savona, M. & Talpaz, M. Getting to the stem of chronic myeloid leukaemia. *Nat Rev Cancer* 8, 341-50 (2008).
3. Hughes, T. P. et al. Frequency of major molecular responses to imatinib or interferon alfa plus cytarabine in newly diagnosed chronic myeloid leukemia. *N Engl J Med* 349, 1423-32 (2003).
4. Cortes, J., O'Brien, S. & Kantarjian, H. Discontinuation of imatinib therapy after achieving a molecular response. *Blood* 104, 2204-5 (2004).
5. Higashi, T. et al. Imatinib mesylate-sensitive blast crisis immediately after discontinuation of imatinib mesylate therapy in chronic myelogenous leukemia: report of two cases. *Am J Hematol* 76, 275-8 (2004).
6. Mauro, M. J., Druker, B. J. & Maziarz, R. T. Divergent clinical outcome in two CML patients who discontinued imatinib therapy after achieving a molecular remission. *Leuk Res* 28 Suppl 1, S71-3 (2004).
7. Foo, J., Drummond, M. W., Clarkson, B., Holyoake, T. & Michor, F. Eradication of chronic myeloid leukemia stem cells: a novel mathematical model predicts no therapeutic benefit of adding G-CSF to imatinib. *PLoS Comput Biol* 5, e1000503 (2009).
8. Graham, S. M. et al. Primitive, quiescent, Philadelphia-positive stem cells from patients with chronic myeloid leukemia are insensitive to STI571 in vitro. *Blood* 99, 319-25 (2002).
9. Jorgensen, H. G. et al. Intermittent exposure of primitive quiescent chronic myeloid leukemia cells to granulocyte-colony stimulating factor in vitro promotes their elimination by imatinib mesylate. *Clin Cancer Res* 12, 626-33 (2006).
10. Holtz, M., Forman, S. J. & Bhatia, R. Growth factor stimulation reduces residual quiescent chronic myelogenous leukemia progenitors remaining after imatinib treatment. *Cancer Res* 67, 1113-20 (2007).
11. Yilmaz, O. H. et al. Pten dependence distinguishes haematopoietic stem cells from leukaemia-initiating cells. *Nature* 441, 475-82 (2006).
12. Morrison, S. J., Wright, D. E. & Weissman, I. L. Cyclophosphamide/granulocyte colony-stimulating factor induces hematopoietic stem cells to proliferate prior to mobilization. *Proc Natl Acad Sci U S A* 94, 1908-13 (1997).
13. Higuchi, M. et al. Expression of a conditional AML1-ETO oncogene bypasses embryonic lethality and establishes a murine model of human t(8;21) acute myeloid leukemia. *Cancer Cell* 1, 63-74 (2002).
14. Lakso, M. et al. Efficient in vivo manipulation of mouse genomic sequences at the zygote stage. *Proc Natl Acad Sci U S A* 93, 5860-5 (1996).
15. Kuhn, R., Schwenk, F., Aguet, M. & Rajewsky, K. Inducible gene targeting in mice. *Science* 269, 1427-9 (1995).
16. Georgiades, P. et al. VavCre transgenic mice: a tool for mutagenesis in hematopoietic and endothelial lineages. *Genesis* 34, 251-6 (2002).
17. de Boer, J. et al. Transgenic mice with hematopoietic and lymphoid specific expression of Cre. *Eur J Immunol* 33, 314-25 (2003).
18. Lagasse, E. & Weissman, I. L. bcl-2 inhibits apoptosis of neutrophils but not their engulfment by macrophages. *J Exp Med* 179, 1047-52 (1994).
19. Akashi, K., Traver, D., Miyamoto, T. & Weissman, I. L. A clonogenic common myeloid progenitor that gives rise to all myeloid lineages. *Nature* 404, 193-7 (2000).
20. Santos, F. P. & Ravandi, F. Advances in treatment of chronic myelogenous leukemia--new treatment options with tyrosine kinase inhibitors. *Leuk Lymphoma* 50 Suppl 2, 16-26 (2009).
21. Jorgensen, H. G., Allan, E. K., Jordanides, N. E., Mountford, J. C. & Holyoake, T. L. Nilotinib exerts equipotent antiproliferative effects to imatinib and does not induce apoptosis in CD34+ CML cells. *Blood* 109, 4016-9 (2007).
22. Chen, J. et al. Stable expression of small interfering RNA sensitizes TEL-PDGFbetaR to inhibition with imatinib or rapamycin. *J Clin Invest* 113, 1784-91 (2004).

23. Stover, E. H. et al. The small molecule tyrosine kinase inhibitor AMN107 inhibits TEL-PDGFRbeta and FIP1L1-PDGFRalpha in vitro and in vivo. *Blood* 106, 3206-13 (2005).
24. Jaiswal, S. et al. CD47 is upregulated on circulating hematopoietic stem cells and leukemia cells to avoid phagocytosis. *Cell* 138, 271-85 (2009).
25. Nicholson, E. & Holyoake, T. The chronic myeloid leukemia stem cell. *Clin Lymphoma Myeloma* 9 Suppl 4, S376-81 (2009).
26. Kiel, M. J. et al. Haematopoietic stem cells do not asymmetrically segregate chromosomes or retain BrdU. *Nature* 449, 238-42 (2007).
27. Holtz, M. S., Forman, S. J. & Bhatia, R. Nonproliferating CML CD34+ progenitors are resistant to apoptosis induced by a wide range of proapoptotic stimuli. *Leukemia* 19, 1034-41 (2005).
28. Passegue, E., Wagers, A. J., Giuriato, S., Anderson, W. C. & Weissman, I. L. Global analysis of proliferation and cell cycle gene expression in the regulation of hematopoietic stem and progenitor cell fates. *J Exp Med* 202, 1599-611 (2005).
29. Kondo, M., Weissman, I. L. & Akashi, K. Identification of clonogenic common lymphoid progenitors in mouse bone marrow. *Cell* 91, 661-72 (1997).
30. Jamieson, C. H. et al. Granulocyte-macrophage progenitors as candidate leukemic stem cells in blast-crisis CML. *N Engl J Med* 351, 657-67 (2004).
31. Usuki, K., Iijima, K., Iki, S. & Urabe, A. CML cytogenetic relapse after cessation of imatinib therapy. *Leuk Res* 29, 237-8 (2005).
32. Passegue, E., Jochum, W., Schorpp-Kistner, M., Mohle-Steinlein, U. & Wagner, E. F. Chronic myeloid leukemia with increased granulocyte progenitors in mice lacking junB expression in the myeloid lineage. *Cell* 104, 21-32 (2001).
33. Holtz, M. S. et al. Imatinib mesylate (STI571) inhibits growth of primitive malignant progenitors in chronic myelogenous leukemia through reversal of abnormally increased proliferation. *Blood* 99, 3792-800 (2002).
34. Drummond, M. W. et al. A pilot study of continuous imatinib vs pulsed imatinib with or without G-CSF in CML patients who have achieved a complete cytogenetic response. *Leukemia* 23, 1199-201 (2009).
35. Zhang, B. et al. Effective targeting of quiescent chronic myelogenous leukemia stem cells by histone deacetylase inhibitors in combination with imatinib mesylate. *Cancer Cell* 17, 427-42 (2010).
36. Downing, J. R., Higuchi, M., Lenny, N. & Yeoh, A. E. Alterations of the AML1 transcription factor in human leukemia. *Semin Cell Dev Biol* 11, 347-60 (2000).
37. Downing, J. R. The AML1-ETO chimaeric transcription factor in acute myeloid leukaemia: biology and clinical significance. *Br J Haematol* 106, 296-308 (1999).
38. Speck, N. A. et al. Core-binding factor: a central player in hematopoiesis and leukemia. *Cancer Res* 59, 1789s-1793s (1999).

CHAPTER 5

CONCLUSION

A cryptic splicing event partially rescues a targeted knockout of *Hip1*

The focus of this thesis has been investigating the role of the oncogenic fusion protein HIP1/PDGFβR in mouse leukemogenesis. Prior to beginning this investigation, I participated in the characterization of a *Hip1* knockout allele termed $Hip1^{\Delta 3\text{-}5}$, which is described in chapter 2. Previously, germline *Hip1* and *Hip1/Hip1r* knockout mice generated in our laboratory exhibited severe degenerative phenotypes characterized by spinal deformities, weight loss, shortened lifespan and testicular degeneration. This data, together with other *in vitro* data suggests that the HIP1 family plays a critical role in cellular survival and homeostasis. The previous knockout mice also exhibited decreased tumor formation (number and severity) in the TRAMP mouse model of prostate tumorigenesis, suggesting that HIP1 may be necessary for tumor initiation and/or progression. This was also suggested by earlier findings of HIP1 overexpression in prostate cancer that was predictive of a bad outcome. However, these germline mouse findings are difficult to interpret because of the deficiency of HIP1 in all tissues and cell types, the severe degenerative phenotypes of affected mice and the possible effects of the complex targeting vector on expression of neighboring genes.

To resolve these issues, we attempted to generate a conditional *Hip1* knockout allele. Our approach was to delete the ANTH-coding domain known to be necessary for normal HIP1 function *in vitro*, while simultaneously inducing a nonsense frameshift mutation that would lead to a truncated non-functional protein product. Following germline recombination of the loxP sites using CMV-Cre transgenic allele, the $Hip1^{\Delta 3\text{-}5/\Delta 3\text{-}5}$ mouse was predicted to recapitulate most (if not all) aspects of the previously described $Hip1^{null/null}$ mouse. As expected, $Hip1^{\Delta 3\text{-}5/\Delta 3\text{-}5}$ mice did display spinal defects and male infertility secondary to testicular degeneration, similar to the gross phenotype of $Hip1^{null/null}$ mice. However, these mice did not exhibit ophthalmic abnormalities and the spinal defects were less severe than the prior knockout. We initially hypothesized that these differences might be due to absence of neighboring gene effects of the $Hip1^{null}$ allele.

To our surprise, $Hip1^{\Delta 3\text{-}5/\Delta 3\text{-}5}$ mice displayed breast and prostate tumor susceptibility more comparable to $Hip1^{+/+}$ than to $Hip1^{null/null}$ mice. This striking difference, as well as the detection of a truncated protein product in cultured tumor tissue, suggested that the $Hip1^{\Delta 3\text{-}5}$ allele was more complex than originally thought. Further DNA, RNA and protein analysis demonstrated the presence of a cryptic U12-dependent splicing event that inserted an AG dinucleotide to restore the wildtype reading frame and produce a nearly full-length HIP1 protein product. We demonstrated that this HIP1Δ3-5insAG protein product retains clathrin, AP2, lipid and EGFR binding capacity *in vitro*. The expression of this truncated protein was detected in brain, lung, embryonic fibroblasts and neoplastic tissue and was notably not detected in other adult tissues that normally express HIP1. It remains unclear how expression of the HIP1Δ3-5insAG protein

is insufficient to prevent the adult degenerative phenotype but sufficient to restore breast and prostate tumorigenesis. One possibility is that the altered tissue expression profile includes loss of functional protein product in a critical tissue type. Testing various tissue-specific Cre alleles should allow dissection of the location and timing of HIP1 necessity in cellular homeostasis. Another possibility is that an unknown function of HIP1 is lost in the HIP1Δ3-5insAG protein and this function is necessary for normal cellular processes but not tumorigenesis. Characterization of the *Hip1*$^{\Delta 3\text{-}5}$ allele has provided insight into the complexity of the *Hip1* genetic structure and shed light on one potential mechanism (U12 splicing) by which a gene targeting event to knockout a protein may be thwarted. Future generation of a true conditional knockout of *Hip1* will add to the understanding of this gene in normal and cancer biology.

Modeling the HIP1/PDGFβR oncogene in mice

Mouse models of human cancers are a critical tool for understanding the biology of tumorigenesis. Some aspects of tumor biology such as niche effects, immunosurveillance and metastasis can only be evaluated in the intact organism. Given the scarcity of accurate mouse models of CML, as well as the relative inefficiency of CML xenotransplantation, we sought to model H/P-induced human CMML in mice. In chapter 3 of this thesis, we describe a conditional knockin of human H/P into the mouse *Hip1* locus. Unlike the retroviral transduction and transplantation method (BTT), which led to a fatal myeloproliferative disorder, endogenous expression of H/P in adult hematopoietic cells was insufficient for leukemogenesis. This striking contrast between BTT and genetically engineered mouse models has been appreciated for multiple other

human oncogenes including Flt3-ITD, AML1/ETO, BCR/ABL and MLL/AF9[1-4]. Chen and colleagues attributed this difference to gene dosage and target cell specificity[4]. Endogenous expression of Mll-AF9 from the mouse *Mll* promoter was able to transform LSK cells but not GMPs. However, both LSKs and GMPs were susceptible to transformation by high-level Mll-AF9 retroviral transduction. The phenotypic variability associated with the various methods of oncogene expression is likely due to a combination of the differences in expression level, cell specificity and cooperating mutations. Future work with the H/P knockin mouse will elucidate the precise cell types that express the fusion oncogene (mRNA and protein) and whether gene dosage is critical for MPD. While frank leukemias were not observed in the H/P knockin mouse, it is possible that sub-threshold kinase signaling induces subtle hematopoietic changes. More sensitive functional assays such as HSC transplants and methylcellulose re-plating assays may uncover these subtleties and help identify the mechanism of cooperation with A/E. Retroviral insertional mutagenesis (potentially coupled to introduction of Cre) may also lead to identification of other cooperating mutations for induction of MPD.

The failure of conditional H/P knockin mice to develop disease could be due to any of the reasons outlined above, but we favor the notion that additional transforming mutations are required for myeloid transformation. Gilliland and others have proposed a "2-hit" model of myeloid leukemia in which a mutation in each of two broad classes of genes are required: (1) Mutations which confer survival and/or proliferative advantages to hematopoietic stem/progenitors and (2) Mutations which interfere with normal hematopoietic differentiation[5]. Neoplastic cells from most patients with de novo AML express only one mutation from each class, providing indirect epidemiologic evidence for

this 2-hit hypothesis[6]. The first class of mutations includes the X/P fusions as well as activating mutations in *Flt3, N-ras, K-ras* and *cKit*. The second class includes gene rearrangements such as CBFβ/SMMHC, PML/RARα, and AML1/ETO (A/E). Extensive *in vitro* and *in vivo* work has shown that A/E exerts its oncogenic activity by impairing the normal function of the hematopoietic transcription factor AML1 (Runx1)[7-10].

Given the lack of a striking phenotype in the H/P knockin mouse (as compared to the H/P or T/P retroviral system), we tested the ability of the A/E mutation to cooperate with H/P *in vivo*. BTT studies have shown that co-expression of A/E transforms the myeloproliferative disorder induced by T/P or activated FLT3 into blastic leukemia[11,12]. To improve upon and compare with this retroviral cooperation, we chose to cross our H/P knockin mice with a conditional knockin of A/E which also fails to develop myeloid neoplasms in isolation[2,11]. Co-expression of H/P and A/E from their respective mouse promoters in the adult hematopoietic system rapidly led to an aggressive MPD, validating the cooperation observed in the BTT assay. Two important findings stand out from this result. First, the disease induced by H/P and A/E endogenous co-expression is a fully differentiated, mature myeloid neoplasm, unlike the immature, blastic T/P;A/E retroviral disease. It is possible that this is due to differences between H/P and T/P kinase signaling, although it is more likely secondary to the fundamental differences between the model systems (direct testing of this will require H/P;A/E retroviral co-transduction). Second, the extremely short latency of the disease suggests complete sufficiency of H/P and A/E cooperation. Importantly, we have not yet observed blastic transformation in these double knockin mice, suggesting that endogenous expression of A/E in stem cells does not inhibit hematopoietic differentiation. While this result seems to run contrary to the

premise of the 2-hit hypothesis, clearly A/E must induce changes at the cellular or molecular level that cooperate with the mitogenic signaling of H/P to induce myeloproliferation. In the original report of the A/E conditional knockin, the authors describe an enhanced methylcellulose re-plating capacity for A/E expressing cells[2]. It is unclear how (or if) this gain of self-renewal occurs *in vivo* and if it contributes to the H/P;A/E disease. Another possibility is that A/E expression potentiates H/P signaling by increasing H/P levels or by enhancing expression of downstream targets. Data to support this would include cell-specific detection of activated PDGFβR signaling pathways. Yet another possibility is that A/E somehow shifts the balance between myeloid and lymphoid differentiation. To address these possibilities, we plan to isolate hematopoietic stem and progenitor cells from single and double knockin mice after pIpC induction to conduct gene expression microarrays and competitive transplants. Further studies of the signaling expression patterns in H/P and A/E single knockin mice and the H/P;A/E double knockin mouse will hopefully elucidate the mechanism of cooperation between these oncogenes.

Characterization of the H/P;A/E mouse model of MPD

Chapters 3 and 4 describe the gross and cellular phenotype of the MPD induced by H/P and A/E. Similar to human myeloproliferative disorders, the H/P;A/E induced MPD is characterized principally by splenomegaly and neutrophilia. This expansion of normal appearing neutrophils is a hallmark of MPD and distinguishes it from the more aggressive dysplastic forms of acute leukemia. We show that the disease is made up principally of $Gr1^{+}Mac1^{+}$ granulocytes which completely take over the bone marrow

space and spleen. As with other mouse models of MPD, we observed extramedullary myelopoiesis in the liver and spleen.

We examined the proportions of hematopoietic stem and progenitor cells in the H/P;A/E induced MPD and found significant myeloid progenitor alterations. There was a near absence of CMPs and MEPs but no changes in GMP frequency. This suggests a shift in myeloid differentiation that favors granulocyte production. We also found a profound decrease in MPP and LT-HSC frequency. Importantly, chimeric analysis of diseased H/P;A/E and wildtype cells demonstrated that the decrease in phenotypic LT-HSCs was not restricted to the donor population, suggesting that the chaos caused by rampant myeloproliferation has a negative regulatory effect on wildtype HSC survival. This extrinsic LT-HSC depletion (phenotypic) will need to be confirmed functionally by secondary transplants of the CD45.1 and CD45.2 fractions. Regardless, this non cell-autonomous HSC depletion is an important aspect of CML that must be accounted for when monitoring response to therapy. Using the chimeric transplant system, we confirmed donor expansion of all myeloid lineage cells but not lymphoid cells, consistent with an MPD.

Targeting the LIC in CML

Imatinib has been hailed as the poster-drug of targeted therapy in cancer. However, persistence of a CML-initiating cell or cells suggests that imatinib is acting to suppress, rather than eliminate disease[13]. Using the H/P;A/E mouse model of MPD, we have confirmed the presence of a persistent LIC despite a robust hematologic response to tyrosine kinase inhibition. Our data suggest that the mutant HSC is a candidate LIC, but

further studies of tumor-initiating capacity are needed to verify this. The imatinib sensitive MPD induced by H/P;A/E provides a unique animal model for testing the many hypotheses regarding LIC persistence.

Figure 5.1 depicts a model of LIC persistence in MPD. At the top is shown a simplified hierarchy of normal myeloid development, with dark blue HSCs (cycling between quiescent and activated states) differentiating into light blue myeloid progenitors which divide into lighter blue terminally differentiated mature myeloid cells. In MPD, an LIC (depicted as a dark orange mutant HSC) leads to hyperproduction of light orange myeloid progenitors and lighter orange mature myeloid cells. Three possibilities are presented for what a response to tyrosine kinase inhibition by imatinib might look like at the cellular level. Situation I assumes that myeloid progenitors with the oncogenic kinase are the only cells sensitive to elimination by imatinib (mature myeloid cells have a very short half-life and are rapidly cleared from the system). In this scenario, LICs circumvent (or remain unaffected by) kinase inhibition and continue to aberrantly differentiate and self-renew. However, the continued presence of imatinib summarily dispatches the overproduced myeloid progenitors, leaving behind a relatively rare (but active) population of LICs. Situation II assumes that LICs are sensitive to elimination by imatinib (i.e. addicted to oncogenic kinase signaling) when actively cycling, but not while quiescent. Thus, imatinib eliminates all cells containing the oncogenic kinase except a relatively rare, quiescent population of LICs. In situation III, the LIC and mutant progenitors are dependent upon oncogenic kinase signaling for leukemogenesis, but not survival. In this scenario, kinase inhibition by imatinib causes reversion to relatively normal HSC behavior. The end result is a hematopoietic compartment with a

mixed population of wildtype and mutant cells. In all three of these scenarios, a persistent LIC serves as a reservoir for disease relapse upon discontinuation of imatinib.

While clearly a gross simplification of the complexity of CML and LIC persistence, this model provides a framework for understanding the H/P;A/E response to imatinib therapy. We have demonstrated that the H/P;A/E-LIC does not persist secondary to insufficient kinase inhibition as use of the more potent TKI nilotinib does not improve elimination of the LIC. We have also shown that the LIC does not maintain upregulation of the phagocytosis inhibitor CD47 as a means toward immuno-protection. These mechanisms can be classified as kinase-dependent and most likely fall into category I of LIC persistence. Another kinase-dependent mechanism of LIC refractoriness worthy of investigation will be determining if decreased intracellular imatinib concentration, via increased efflux or plasma sequestration of the drug is occurring.

Scenario II is an intriguing possibility that is supported by some *in vitro* data [14-16]. This scenario lends itself to the hypothesis that cell cycle induction and concomitant TKI therapy may lead to enhanced LIC elimination. We have shown that HSC-mobilizing agents (cyclophosphamide + GCSF) do not enhance H/P;A/E-LIC sensitivity to imatinib *in vivo*. This result is consistent with the limited human data available[16] as well as mathematical modeling of CML kinetics[17,18]. One explanation for our observed data is that LICs are resistant to cell cycle induction agents that mobilize wildtype HSCs. Another possibility is that mobilized LICs are not addicted to oncogenic H/P signaling. Further testing of the combination of imatinib and other mobilization agents is warranted, especially the drugs IFNα and arsenic trioxide which have been shown to enhance LIC elimination by chemotherapeutic drugs[19,20].

Using the chimeric transplant system, we have demonstrated that after clearance of bulk disease by imatinib, large populations of mutant donor cells persist. These include myeloid and lymphoid cells in wildtype ratios, suggesting that the LIC has reverted to normal HSC functionality (scenario III). It is unclear if this *in vivo* response to imatinib occurs in human patients with CML. An important inference from these data is that targeting of the H/P pathway might be insufficient for elimination of the LIC. Numerous other pathways and genes have been implicated in maintenance of the CML-LIC including: Pten, PML, Alox5, TGFβ/FoxO, HDACs, Hedgehog, Wnt/β-catenin and autophagy[20-27]. Further analysis of the H/P;A/E mouse model of MPD should focus on identifying non-kinase pathways that distinguish LICs from HSCs. An unbiased approach to this that is in progress is analysis of gene expression profiles of specific stem and progenitor cell populations isolated from imatinib-responding mice.

This thesis has focused on understanding the role of HIP1 in tumorigenesis and modeling the HIP1/PDGFβR human oncogene in mice. We have established a clinically relevant model of myeloproliferative disease that is driven by constitutive kinase signaling in hematopoietic stem cells. This model will serve as an excellent tool for understanding the basic biology of mouse hematopoiesis and tyrosine kinase signaling. Furthermore, this mouse provides a platform for analysis of drug responses in both the mutant and surrounding non-mutant hematopoietic and niche cells.

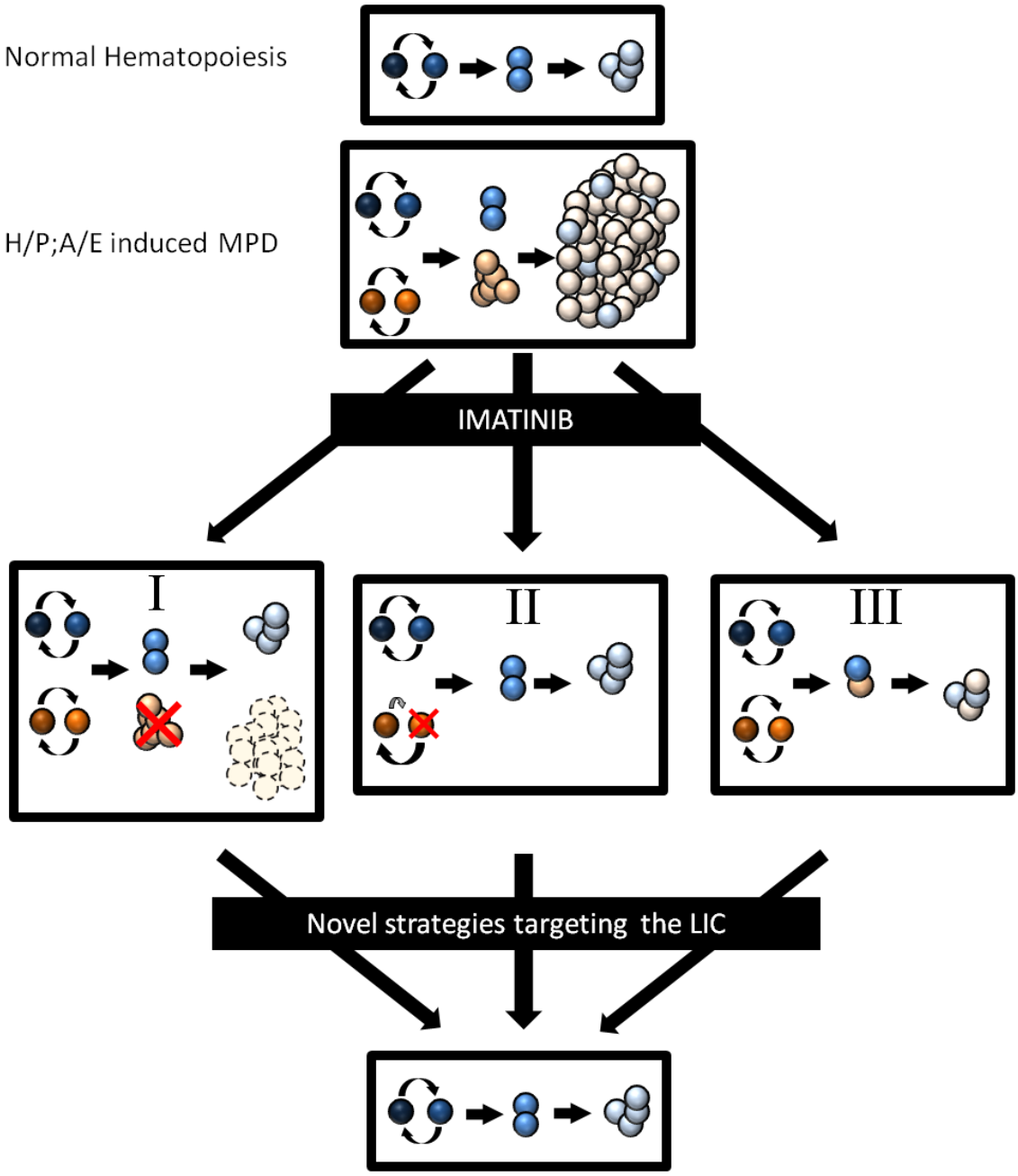

Figure 5.1: Proposed model for LIC persistence *in vivo*
See text for description

References

1. Lee, B. H. et al. FLT3 mutations confer enhanced proliferation and survival properties to multipotent progenitors in a murine model of chronic myelomonocytic leukemia. *Cancer Cell* **12**, 367-80 (2007).
2. Higuchi, M. et al. Expression of a conditional AML1-ETO oncogene bypasses embryonic lethality and establishes a murine model of human t(8;21) acute myeloid leukemia. *Cancer Cell* **1**, 63-74 (2002).
3. Castellanos, A. et al. A BCR-ABL(p190) fusion gene made by homologous recombination causes B-cell acute lymphoblastic leukemias in chimeric mice with independence of the endogenous bcr product. *Blood* **90**, 2168-74 (1997).
4. Chen, W. et al. Malignant transformation initiated by Mll-AF9: gene dosage and critical target cells. *Cancer Cell* **13**, 432-40 (2008).
5. Gilliland, D. G. & Griffin, J. D. Role of FLT3 in leukemia. *Curr Opin Hematol* **9**, 274-81 (2002).
6. Ishikawa, Y. et al. Comprehensive analysis of cooperative gene mutations between class I and class II in de novo acute myeloid leukemia. *Eur J Haematol* **83**, 90-8 (2009).
7. Okuda, T. et al. Expression of a knocked-in AML1-ETO leukemia gene inhibits the establishment of normal definitive hematopoiesis and directly generates dysplastic hematopoietic progenitors. *Blood* **91**, 3134-43 (1998).
8. Westendorf, J. J. et al. The t(8;21) fusion product, AML-1-ETO, associates with C/EBP-alpha, inhibits C/EBP-alpha-dependent transcription, and blocks granulocytic differentiation. *Mol Cell Biol* **18**, 322-33 (1998).
9. Yergeau, D. A. et al. Embryonic lethality and impairment of haematopoiesis in mice heterozygous for an AML1-ETO fusion gene. *Nat Genet* **15**, 303-6 (1997).
10. Castilla, L. H. et al. Failure of embryonic hematopoiesis and lethal hemorrhages in mouse embryos heterozygous for a knocked-in leukemia gene CBFB-MYH11. *Cell* **87**, 687-96 (1996).
11. Grisolano, J. L., O'Neal, J., Cain, J. & Tomasson, M. H. An activated receptor tyrosine kinase, TEL/PDGFbetaR, cooperates with AML1/ETO to induce acute myeloid leukemia in mice. *Proc Natl Acad Sci U S A* **100**, 9506-11 (2003).
12. Schessl, C. et al. The AML1-ETO fusion gene and the FLT3 length mutation collaborate in inducing acute leukemia in mice. *J Clin Invest* **115**, 2159-68 (2005).
13. Savona, M. & Talpaz, M. Getting to the stem of chronic myeloid leukaemia. *Nat Rev Cancer* **8**, 341-50 (2008).
14. Holtz, M., Forman, S. J. & Bhatia, R. Growth factor stimulation reduces residual quiescent chronic myelogenous leukemia progenitors remaining after imatinib treatment. *Cancer Res* **67**, 1113-20 (2007).
15. Holtz, M. S., Forman, S. J. & Bhatia, R. Nonproliferating CML CD34+ progenitors are resistant to apoptosis induced by a wide range of proapoptotic stimuli. *Leukemia* **19**, 1034-41 (2005).
16. Jorgensen, H. G. et al. Intermittent exposure of primitive quiescent chronic myeloid leukemia cells to granulocyte-colony stimulating factor in vitro promotes their elimination by imatinib mesylate. *Clin Cancer Res* **12**, 626-33 (2006).
17. Drummond, M. W. et al. A pilot study of continuous imatinib vs pulsed imatinib with or without G-CSF in CML patients who have achieved a complete cytogenetic response. *Leukemia* **23**, 1199-201 (2009).
18. Foo, J., Drummond, M. W., Clarkson, B., Holyoake, T. & Michor, F. Eradication of chronic myeloid leukemia stem cells: a novel mathematical model predicts no therapeutic benefit of adding G-CSF to imatinib. *PLoS Comput Biol* **5**, e1000503 (2009).
19. Burchert, A. et al. Sustained molecular response with interferon alfa maintenance after induction therapy with imatinib plus interferon alfa in patients with chronic myeloid leukemia. *J Clin Oncol* **28**, 1429-35 (2010).
20. Nasr, R. et al. Eradication of acute promyelocytic leukemia-initiating cells through PML-RARA degradation. *Nat Med* **14**, 1333-42 (2008).
21. Peng, C. et al. PTEN is a tumor suppressor in CML stem cells and BCR-ABL-induced leukemias in mice. *Blood* **115**, 626-35 (2010).
22. Chen, Y., Hu, Y., Zhang, H., Peng, C. & Li, S. Loss of the Alox5 gene impairs leukemia stem cells and prevents chronic myeloid leukemia. *Nat Genet* **41**, 783-92 (2009).

23. Naka, K. et al. TGF-beta-FOXO signalling maintains leukaemia-initiating cells in chronic myeloid leukaemia. *Nature* **463**, 676-80 (2010).
24. Zhang, B. et al. Effective targeting of quiescent chronic myelogenous leukemia stem cells by histone deacetylase inhibitors in combination with imatinib mesylate. *Cancer Cell* **17**, 427-42 (2010).
25. Zhao, C. et al. Hedgehog signalling is essential for maintenance of cancer stem cells in myeloid leukaemia. *Nature* **458**, 776-9 (2009).
26. Hu, Y., Chen, Y., Douglas, L. & Li, S. beta-Catenin is essential for survival of leukemic stem cells insensitive to kinase inhibition in mice with BCR-ABL-induced chronic myeloid leukemia. *Leukemia* **23**, 109-16 (2009).
27. Bellodi, C. et al. Targeting autophagy potentiates tyrosine kinase inhibitor-induced cell death in Philadelphia chromosome-positive cells, including primary CML stem cells. *J Clin Invest* **119**, 1109-23 (2009).